

NASA Contractor Report 179510

A Design Study of Hydrazine and Biowaste Resistojets

Russell J. Page, Willis A. Stoner,
and Larry Barker

*The R. J. Page Company
Santa Ana, California*

September 1986

Prepared for
Lewis Research Center
Under Contract NAS3-23863

(NASA-CR-179510) A DESIGN STUDY OF
HYDRAZINE AND BIOWASTE RESISTOJETS Final
Report (Page (R. J.) Co.) 149 p CSCL 21H

N87-14425

G3/20 Unclas
43786



National Aeronautics and
Space Administration

TABLE OF CONTENTS

| | Page |
|---|------|
| SUMMARY | 1 |
| INTRODUCTION | 3 |
| STUDY MODELS | 4 |
| Biowaste Resistojets | 5 |
| Hydrazine Electrothermal Augmenters | 7 |
| ANALYTICAL PROCEDURE | 8 |
| Heater Performance | 8 |
| Nozzle Performance | 9 |
| Overall Performance Calculations | 11 |
| Life and Reliability Criteria | 12 |
| Overall Rating Criteria | 12 |
| MATERIALS | 12 |
| Propellants | 12 |
| Thruster | 15 |
| Structure | 16 |
| Electric Heaters | 20 |
| Thermal Insulation | 20 |
| Electric Insulators | 21 |
| RESULTS AND DISCUSSION | 22 |
| Biowaste Resistojets | 22 |
| Concept 1 | 24 |
| Concept 2 | 26 |
| Concept 3 | 26 |
| Concept 4 | 27 |
| Hydrazine Augmenters | 28 |
| Concept 5 | 29 |
| Concept 6 | 29 |
| MANUFACTURING | 30 |
| Joining methods | 31 |
| SUMMARY OF RESULTS | 32 |
| APPENDIX A: CONCEPT 1 - ELECTRICALLY CONDUCTING CERAMIC | |
| HEATER WITH EXPOSED INTERNAL FLOW | 33 |
| Description | 34 |
| Performance | 36 |
| Thermal Analysis | 38 |

| | |
|---|-----|
| Gas Dynamic Analysis | 52 |
| Mechanical Design | 53 |
| Chemical Corrosion, Sublimation and Deposition | 53 |
| Rating | 54 |
| APPENDIX B: CONCEPT 2 - EXPOSED METALLIC TRUSS HEATER IN | |
| EXTERNAL CROSS FLOW | 55 |
| Description | 56 |
| Performance | 63 |
| Thermal Analysis | 64 |
| Gas Dynamic Analysis | 72 |
| Structural and Other Mechanical Effects | 74 |
| Chemical | 75 |
| Rating | 76 |
| APPENDIX C - CONCEPT 3 - EXPOSED METALLIC BICOIL TUBULAR | |
| HEATER IN INTERNAL FLOW | 77 |
| Description | 78 |
| Performance | 80 |
| Thermal Analysis | 81 |
| Gas Dynamic Analysis | 85 |
| Mechanical Design | 86 |
| Chemical Corrosion, Sublimation and Deposition | 87 |
| Rating | 87 |
| APPENDIX D - CONCEPT 4 - NONEXPOSED RADIANT HEATER WITH | |
| FLOW IN THE SURROUNDING CASE PASSAGE (BIOWASTE) | 89 |
| Description | 90 |
| Performance | 92 |
| Thermal Analysis | 96 |
| Gas Dynamic Analysis | 101 |
| Mechanical Design | 101 |
| Chemical Corrosion, Sublimation and Deposition | 101 |
| Rating | 101 |
| APPENDIX E - CONCEPT 5 - EXPOSED METALLIC BICOIL HEATER | |
| WITH INTERNAL FLOW | 103 |
| Description | 104 |
| Performance | 107 |
| Thermal Analysis | 108 |
| Gas Dynamic Analysis | 113 |
| Mechanical Design | 113 |
| Chemical Corrosion, Sublimation and Deposition | 115 |
| Rating | 116 |
| APPENDIX F - NONEXPOSED RADIANT HEATER WITH FLOW IN | |
| SURROUNDING CASE SPIRAL PASSAGE (HYDRAZINE) | 117 |
| Description | 118 |
| Performance | 121 |
| Thermal Analysis | 122 |
| Gas Dynamic Analysis | 125 |

| | |
|--|-----|
| Mechanical Design | 125 |
| Chemical Corrosion, Sublimation and Deposition | 126 |
| Rating | 126 |
| APPENDIX G - DEFINITION OF PERFORMANCE PARAMETERS | 128 |
| APPENDIX H - BASIS OF MATHEMATICAL COMPUTATIONAL MODEL | 129 |
| APPENDIX I - THERMOPHYSICAL PROPERTIES USED IN MATHEMATICAL MODELING PROGRAMS | 135 |
| REFERENCES | 143 |

SUMMARY

A generalized mathematical modeling program is used to project the best performance of four types of biowaste resistojets and two hydrazine augmenters. Its use with a personal computer and Basic programming language permits the designer to obtain results which have been found to approximate closely experimental results. The biowaste designs are analyzed for best design separately on carbon dioxide or steam at 1573°K heater temperature. Designs of augmenters of decomposed products of hydrazine were also evaluated at heater temperatures of 2073°K. System adequacy in terms of such variables as response are verified also, where necessary.

The first design, Concept 1, uses a compact electric heater-convective heat exchanger made of an electrically conductive ceramic, cubic phase stabilized zirconia (mp 2860°K). It is already an oxide itself and, thus, has the highest growth potential with the oxidizing biowaste gases studied. At 2000°K, 70% of its melting temperature, the specific impulse is projected to be 192.5 and 269 seconds for CO₂ and H₂O (steam), respectively. An auxiliary starting heater is required which, operating by itself, produces 133 seconds (CO₂) and satisfies the study specific impulse criteria, giving a redundant reliability. The time for the starting cycle is shown as acceptable if cold starts are required. Its standby heated mode is of low power consumption of 22 watts.

Of the biowaste resistant metal-oxide grain stabilized platinum heaters, Concept 3 is the next recommended candidate of those studied. The specific impulse is 170 and 240 for CO₂ and H₂O (steam) in turn. The overall power efficiency is .79 and .78 for each. The bicoil consists of two platinum coils of precisely the same tubular heating length and cross-sectional diameter coiled in opposite rotation, one closely fitting within the other directly exposed to the biowaste gases. The pressure drop and flow of each passage and the resistance heating length are the same. The cross over points are at the same voltage potential and the two coils are physically bonded to one another there. As a result, the bicoil design is found by stress analysis using numerical methods to be stable and transversely rigid yet accommodating for axial thermal expansion compensation. The gas flow in passing through the tubes of the bicoil closely approaches the wall in temperature. The design has the favorable features of a low temperature outer pressure case. No electrical insulation is used in the high temperature zones.

Concept 4 is a radiant non-exposed heater design. It physically separates the heat exchanger function, which may be made more massive, from that of the ohmic heater, which may be separately designed for higher voltage. Used as a biowaste resistor, the heat exchanger may be made of grain stabilized platinum with a thickness to insure its structural integrity. The ohmic heater, not being exposed to the biowaste bases, may be made of grain stabilized rhenium, the highest temperature capability of available conductive ductile materials. The heater temperature of the study of the hydrazine augmenters of 2073°K is used as logical as it is not exposed to the biowastes.

Two variations of the radiant design studied are of the pressurized and unpressurized heater cavity types. A pressurized cavity, though, shows a significant improvement, particularly with a high emissivity surface incorporated into the radiation heat transfer link. The pressurized type design requires a metal to ceramic seal and an inert pressurant line to the cavity. The notable characteristic of this type design is the much larger temperature difference required between heater and gas than all the other designs for the same specific impulse.

Because its exchanger thermal mass is ten times higher than the direct convective exchanger - heater design, it has a slower response to reach its specific impulse from rest on short firings.

The radiant heater design must be specifically sized with regard to power required for a specific propellant. There is a much wider variation in resultant gas temperature when various propellants are run in a fixed design.

The bicoil heater-convective-exchanger and radiant type designs are again compared, specifically redesigned for use as a hydrazine augments.

Concept 5, the bicoil, produces the highest gas temperature of 2007°K, hence specific impulse of 317 seconds for a given maximum heater temperature of 2073°K compared to 1727°K for the gas temperature for the best radiant design, giving a specific impulse of 295 seconds. The overall efficiencies are comparable, .73 vs .72, respectively. A pressurizing inert gas is used in the case of the best of the radiant designs.

The detailed heat transfer with resultant temperature profile results of each design are shown, as well as the construction details of the designs. The scaled layout drawings of each concept are presented with materials and recommended fabrication methods.

INTRODUCTION

The early development of resistojets started at Lewis Research Center with Jack (ref. 1) in 1960. Similar development was concurrently undertaken in industry by Howard (ref. 2) who used some early mathematical modeling of the heat transfer process by means of a computer. This work focused on a 30 kW level of power with a goal of 6.67 N (1.5 lb_r) of thrust and specific impulse goal of up to 1000 seconds on hydrogen. As the expectations for availability of these levels of power diminished, Page (ref. 3) reported a 3 kW, .67 N (150 mlb_r) of thrust at a measured specific impulse of 840 seconds on hydrogen. Subsequently, Page (ref. 4) reported resistojets of .045 N (10 mlb_r) for hydrogen or ammonia, achieving a specific impulse of 668 and 320 seconds, respectively. Life tests of >8000 hours were demonstrated on these thrusters (ref. 5). These showed promise on the MORL studies (ref. 6) for use on manned space stations, particularly when made of biowaste resistant materials.

Approximately 26 flight experiments and operational propulsion systems using resistojets were developed by many groups from 1965 to 1984. About 40 hydrazine resistojets are performing North/South station keeping functions on Intelsat V and RCA spacecraft. At present, NASA is pursuing the development of a permanent facility in space. This facility is comprised of a manned Space Station core, platforms and free-flying spacecraft which require propulsion systems for orbit maintenance, maneuvering, and possibly attitude control. The resistojet system is a strong candidate to satisfy these auxiliary propulsion requirements which are more demanding and variable than those of present space systems. Resistojet systems provide benefits which include, 1) the ability to operate on many candidate propellants including station fluids, 2) the use of gaseous, nontoxic propellants which can ease the problems of distribution, maintenance and contamination, 3) low variable thrust which produces accelerations below those of concern to users and provides the options of precision acceleration and ephemeris control, and 4) growth potential to high specific impulse for evolutionary stations and performance driven advanced free-flyers.

The advent of the personal computer gives the design engineer the opportunity to rapidly model resistojet configurations to provide development guidance. In this study, a generalized axisymmetrical model diagram has been developed which may have dimensions of its elements prescribed so as to closely resemble the shape of the thruster being studied and the thermal relationship between elements assigned via subroutines. The use of the IBM PC and the Basic programming language allows the designer to quickly debug his program. When compiled, the code has much

faster execution. The few numbers of runs required justifies the somewhat long run times of several hours to come to a solution as a trade against significant reduction of programming time.

Four biowaste resistojet designs and two hydrazine augmenters are analyzed and numerical results compared for recommendations of designs for performance and qualitatively for reliability to give guidance to future resistojet designs.

STUDY MODELS

The following study models were used to define the concepts. These thruster concepts were guided by the input and output performance goals of table 1.

TABLE 1
RESISTOJET PERFORMANCE GOALS

| Gas | Carbon Dioxide | Water (Steam) | Hydrazine |
|--|-------------------|------------------|-------------|
| Thrust, N (lb) | .222 (.050) | .222 (.050) | .222 (.050) |
| Specific impulse, s | 130 | 200 | 300 |
| Nominal heater temp., °C | 1300 | 1300 | 1800 |
| Feed system abs. pressure | | | |
| Maximum kPa(psia) | 2068 (300) | 2068 (300) | 2068 (300) |
| Minimum kPa(psia) | 690 (100) | 690 (100) | 690 (100) |
| Terminal voltage, V | 7-28 | 7-28 | 7-28 |
| Max. power/thrust, W/mN (W/mlb) | 1.35 (6) | 1.35 (6) | 1.12 (5) |
| Propellant water content, % by weight | - | 100 | 1 (max.) |
| Thruster Power Interruptions | 1000 | 1000 | 1000 |
| Minimum design life goal, hrs. | 10,000 | 10,000 | 10,000 |

The detailed descriptions of each of these concepts as to geometry, materials, fabrication and the supporting design study analyses are covered in the respective appendices, A through F. Included there are the results from each model by a mathematical modeling program using a generalized node diagram for heat transfer, gas and electric flow. The latter is described under Analytical Procedure. It permits solution of the steady state and transient equations. The gas dynamics analysis also includes pressure drop calculations. The pertinent structural and other mechanical effects are treated separately as are chemical corrosion, sublimation and deposition effects.

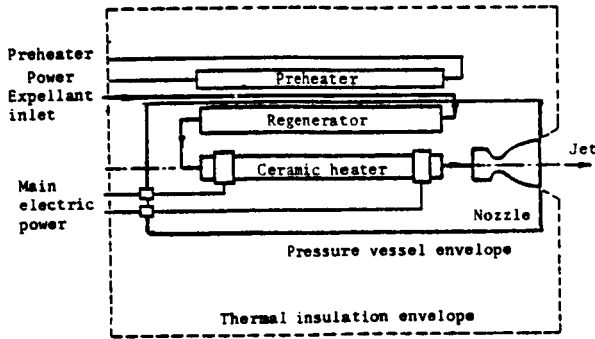
The study models are shown in conceptual form in figures 1 and 2. Their concepts are described below. Note that all designs employ regenerators which are favorably configured in each case for maximum efficiency.

Biowaste Resistojets

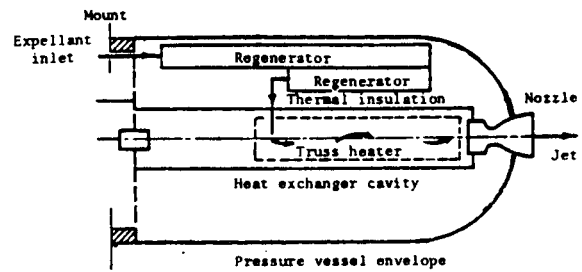
Concept 1 uses an electrically conducting heater exchanger of cubic phase stabilized zirconia capable of directly heating the biowaste gas reliably to more than 2000°K. Stabilized zirconia, itself an oxide, is highly resistant to oxidizing gases. It has a high melting point of 2860°K compared to its nearest metallic counterpart of grain stabilized platinum of 2047°K. The high electric resistance allows generous structural heater cross sections and a high terminal voltage. Because zirconia is an electric insulator effectively below 1000°K, a starter heater must be provided which is shown. The preheater is located outside the pressure case. Since it is therefore unexposed to biowaste gases, it can be made of grain stabilized rhenium (mp 3453°K). Operation on the preheater alone achieves the goal specific impulse and, hence contributes further to reliability.

Concept 2 is based upon two novel features, the radially inverted functional design and the truss heater. This biowaste resistojet uses the metal-oxide grain stabilized platinum for the heater as well as the highest temperature components. The pressure case is its outermost member. The wide passages regenerators are adjacent and interior to the pressure case. All thermal insulation is contained within these. Functionally it is radially "inverted" from all others studied except Concept 3. Consequently, it is one of implied higher structural reliability and thermal efficiency. No pressure balancing considerations are required within the design to prevent creep of the critical inner elements. The truss heater is a wire type heater using an external cross flow heat exchanger which is structurally designed for high transverse strength yet axial compliance and high electric resistance. This design eliminates the need for electrical insulators in the high temperature zone.

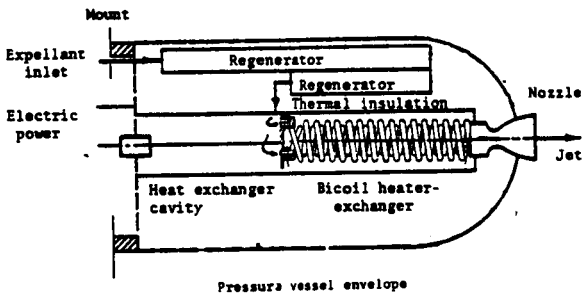
Concept 3 introduces a new type heater, a heat exchanger using internal forced convection which is best described as two coils of opposite rotation of precisely the same tubular heating length and cross sectional diameter. One coil is located within the other and is of tighter pitch. The two coils are physically bonded to one another at the crossover points. The pressure drop of each passage is the same. The cross over points are at the same voltage potential. Hence they are metallurgically bonded there for transverse structural rigidity, yet remain axially compliant. The radial inverted geometry of Concept 2 is used, hence it also has the features of a low temperature reliable outer pressure case and high overall thermal efficiency.



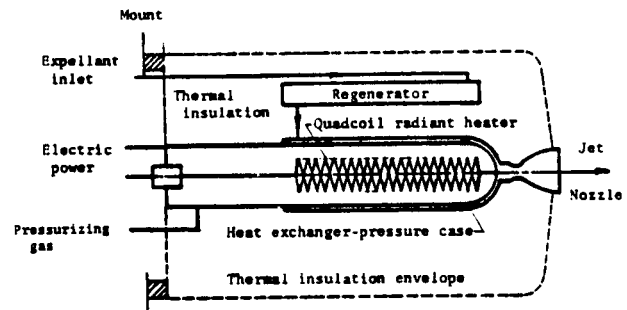
a) Concept 1 (Appendix A)



b) Concept 2 (Appendix B)

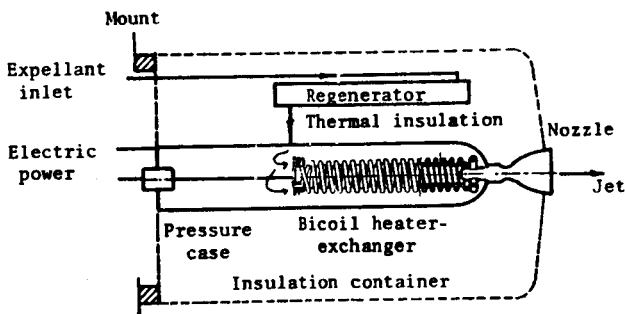


b) Concept 3 (Appendix C)

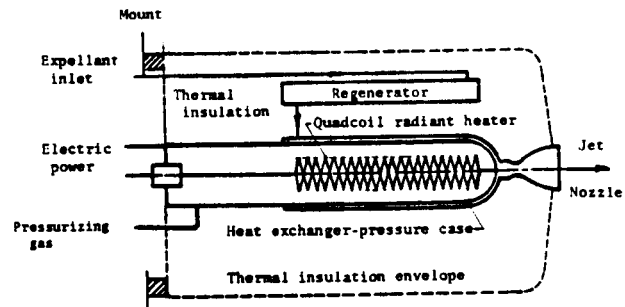


d) Concept 4 (Appendix C)

Figure 1. - Functional description of the bio-waste resistojets study models.



a) Concept 5 (Appendix E)



b) Concept 6 (Appendix F)

Figure 2. - Functional description of hydrazine augments study models.

Concept 4 physically separates the heat exchanger function from that of the ohmic heater. It has an indirect radiant heater in an inert gas pressurized central cavity radiating and conducting to a heat exchanger in the pressure case flowing the biowaste expellants. The inert gas suppresses sublimation of the heater. A high emissivity surface incorporated in the radiation heat transfer link makes a notable further improvement over unpressurized designs. The radial order of components is contemporary. A rhenium (mp 3453°K) heater suitably protected by inert gas in the cavity may operate at a significantly higher temperature than grain stabilized platinum (mp 2047°K) which are exposed to the biowaste gases. The platinum members are within goal temperatures.

Hydrazine Electrothermal Augmenters

Concept 5, like Concept 3 presented earlier as a biowaste resistojet, uses the bicoil configuration as an integrated tubular ohmic heater and gas heat exchanger for a hydrazine augments. The philosophy of the design is to achieve the lowest material temperature operation for the goal specific impulse. This promotes reliability and longer life. Primarily because of the high temperature inlet gases from the decomposition chamber, a high temperature central pressure case design is used. The inlet temperature is 866°K if the ammonia is fully dissociated and higher if not. A higher heater thermal efficiency is found from this choice. This is unlike Concept 3 which has a cool inlet of biowaste gases of low thermal conductivity. All high temperature parts are fabricated of grain stabilized rhenium. No electric insulation is used in the high temperature zones. Propellant flow deters backstreaming of any sublimed metallic vapors onto the metal to ceramic seal.

Concept 6 is geometrically identical to Concept 4 but is of rhenium. It physically separates the heater and exchanger function from that of the ohmic heater. The heater and exchanger may thus be each made of different materials, each favorable to its own design. The figure illustrates the concept schematically. Because of the decoupling of the designs, the voltage of the heater may be made higher and the walls of the gas exchanger thicker than if the design were an integral one. The design here, as a hydrazine augments, has all high temperature parts fabricated of the same material, grain stabilized rhenium. A unique feature of the design is the use of a sturdy quad-coil, described functionally earlier for the bicoil model, to give more reliability against touching. The heater cavity again uses a high emissivity receiving surface and a pressurized cavity.

ANALYTICAL PROCEDURE

The performance parameters of the study are defined in appendix G with the terms used for a common baseline of comparison between concepts.

The inlet conditions of the propellant in the analysis are given in the table below.

TABLE 2
PROPELLANT INLET CONDITIONS

| Propellant | Temperature, °K |
|--|-----------------|
| Carbon dioxide (CO ₂) | 300 |
| Steam (H ₂ O) | 442 |
| Hydrazine (N ₂ H ₄) | 866 |

For steam operation a separate evaporator design is shown as required to insure vapor injection into the resistojet. For hydrazine operation the input gas is from a first stage reactor.

The supply pressure is that necessary to provide a pressure at the nozzle of 3 atmospheres in all cases. This was chosen as a reasonable value to use in order to give an acceptable throat diameter at the 50 mlb (.22 N) thrust level.

Heater Performance

The gas flow and heat transfer analysis of the heater component of each thruster has been undertaken by a generalized numerical modeling technique described in appendix H. The specific transformation of the generalized model is shown graphically under each concept. It closely resembles the shape of the engine under study. Design drawings of the layout drawings of each concept are seen to closely compare with their models.

The mathematical computational model employed here was used for this study in order to make rapid detailed studies of a number of resistojet concepts. Such calculations were necessary to make meaningful heater recommendations. The numerical values in the performance tables were derived directly from these analyses and the following one described for the nozzles. The former is presented herein in appendix H in synoptic form. The program was written in basic and executed on an ordinary IBM PC machine.

The nodal positional indices for a cylindrical coordinate system are presented in array format. The array indices keep the

same relationship to the functional physical member independent of adjustment of the overall dimensions of the thruster under study. By assignment of specific dimensional multipliers both axially and radially to each of the generalized nodes, the shapes of each configuration can be approximated. This makes it convenient to compare temperatures, for instance, versus functional locations between similar designs. For example, a longer design can be compared to a shorter one.

In order to keep within the initial memory constraints, the computational model assumed an initial mass flow close to the anticipated value. During the course of the relaxation to the temperature distribution, the actual resulting mass flows are noted and adjustments made in mass flow. These were made manually because of the time allowed during reaching equilibrium amounted to approximately six hours. The convenience of setting up the model in compiled Basic was that it can be checked out in the interpretive mode for fast check out. The code was then compiled. The use of Basic was not a penalty as the number of cases run were small and the penalty of run time was not significant. A thrust check is shown to compare the the closeness to the 50 mlb condition.

Nozzle Performance

The overall total power efficiency of the resistojet is the product of the nozzle and heater efficiencies. See Appendix G. The heater efficiency is derived from the particular heat exchanger analysis for the configuration under study. It is the primary variable exercised in this investigation. The basis of the performance of the nozzle is the same for all those studied here and is a function of Reynolds number, defined below. The thermal analysis then delineates the major differences between designs.

Specific Impulse.- Based upon a study of reported experimental measurements of low thrust, pure gas rockets and their correlation with viscous nozzle theory, a nozzle design prediction method was developed as part of the program of reference 4 and reported as an appendix to reference 7 of the same series. Based upon this method which accounts for losses due to frozen flow, incomplete expansion, divergence, and viscous effects, the specific performance is summarized in figure 3. Shown is the projected performance for CO_2 , H_2O and decomposed hydrazine over the temperature range of interest for the 50 millipounds thrust class resistojet. The total gas temperature cited is at inlet to the nozzle.

Efficiency.- The geometries of the conical nozzles based upon a 150 mlb, and a 1.5 lb, resistojet were measured and found to have excellent nozzle efficiencies (ref. 3). See table 3 for

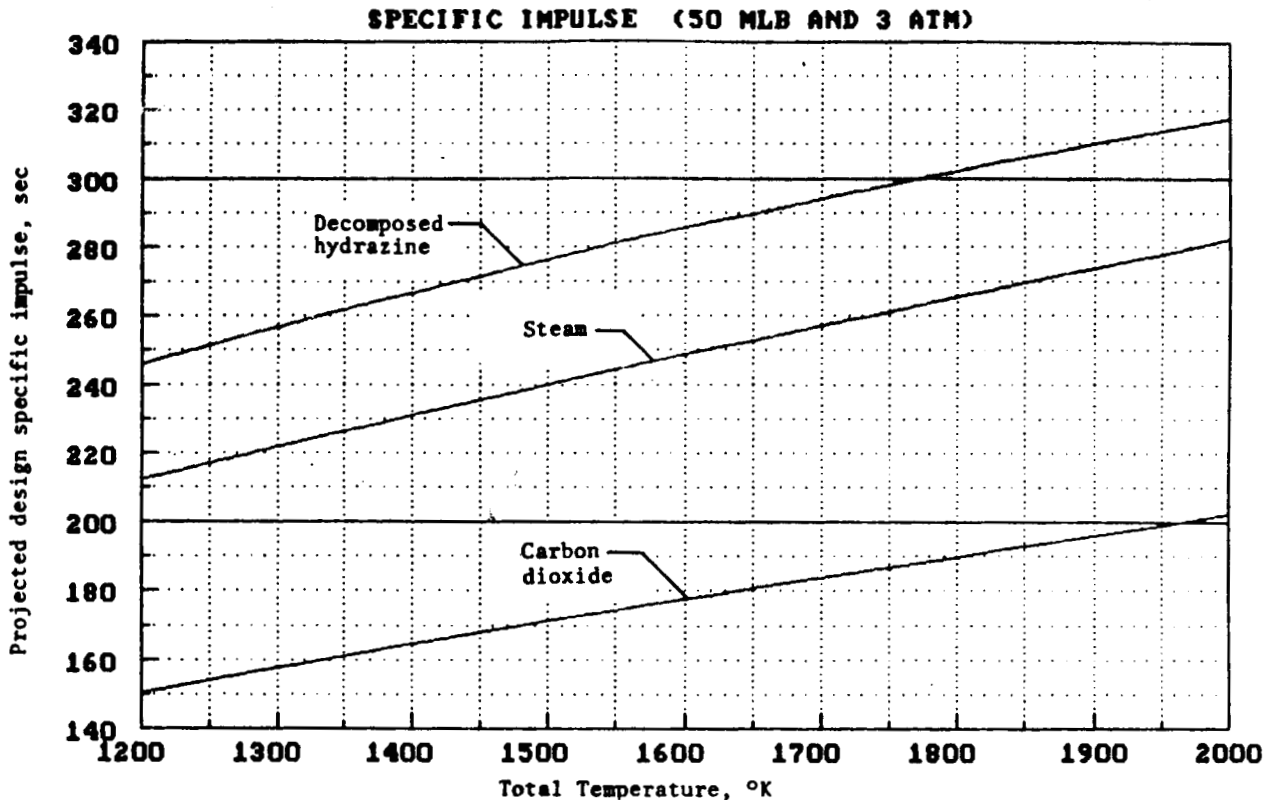


Figure 3.- Projected design specific impulse as a function of nozzle entrance total gas temperature for CO₂, H₂O, and decomposed N₂H₄ at a total pressure of 3 atmospheres.

typical geometry used. Note the nozzle power efficiencies used in the study are consistently derived from reference 7 with the physical properties of the propellants reported herein. The geometry and performance of this nozzle is expected to be close to that indicated based on the reference 3 results.

TABLE 3
CONICAL NOZZLE DESCRIPTIONS

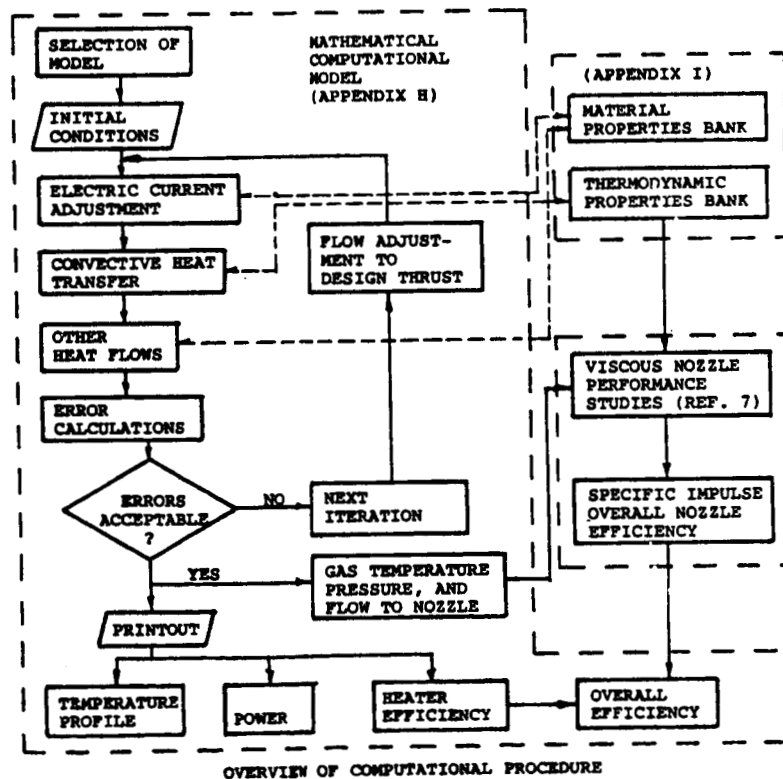
| | Concept 3 | Concept 5 |
|---------------------------------------|------------------------------|-------------------------------|
| Gas | CO ₂ ¹ | N ₂ H ₄ |
| Total temperature, °K | 1486 | 2007 |
| Total pressure, atm | 3 | 3 |
| Throat diameter, mm | 0.70 | 0.76 |
| Reynolds number | 4816 | 2356 |
| Discharge coefficient, C _d | .974 | .969 |
| Expansion half angle, deg | 17.5 | 17.5 |
| Geometric area ratio | 190 | 190 |

¹The results for H₂O (steam) are similar. The flow parameters for the six designs are given in each appendix.

Note that fully dissociated hydrazine, which is one mole of N_2 and two of H_2 , was selected in the study as the desired input gas to the augments. The expected frozen flow losses are experienced in the preceding decomposition chamber component. Since this chamber was not part of the design study, it prevents reporting the overall efficiency of the overall decomposition chamber-augmenter system. The efficiencies reported are of the augmenters alone. Note from figure 5 that for both the hydrazine augments and the biowaste resistojet, no further dissociation occurs over the inlet conditions and the frozen flow component, η_F , of overall nozzle efficiency, η_N , of all cases studied is unity. See appendix G for definitions.

Overall Performance Calculations

The flow diagram for the overall analysis is shown in the adjacent diagram. The results of the Mathematical Computational Model (Appendix H), which is primarily an evaluation of the temperature profile and heater efficiency, is input into the viscous nozzle study results. This is the gas temperature, pressure and mass flow to the nozzle chamber. Based upon these specific gas properties from the thermodynamics properties bank (Appendix I) and the viscous nozzle study, the specific impulse, overall nozzle efficiency, and hence, the overall efficiency result.



Life and Reliability Criteria

No mathematical analysis was made with regard to reliability as there was no basic life data in this field with which to establish it. The comments on reliability generally are practical ones where redundancy is observed or where functional designs can be considered qualitatively more reliable than others.

All analyses are based upon extrapolation of test data for the determination of life as no full term data are known.

Overall Rating Criteria

The overall rating criteria are based upon the requirements of table 1, Resistojet Performance Goals, in the main. The following notions were used:

- 1) Did the design, under the operating condition constraints, meet the goal conditions required?
- 2) What was the relative order of potential performance achievement relative to the baseline goals? The greater performance potential of one design over another can imply more reliability at the goal condition, other conditions being equal.
- 3) Does the design have redundant features? What are the implications on reliability?

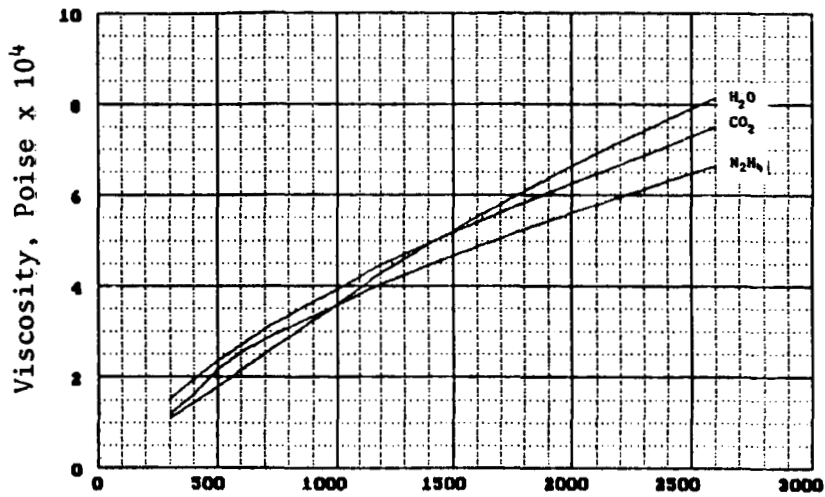
MATERIALS

Propellants

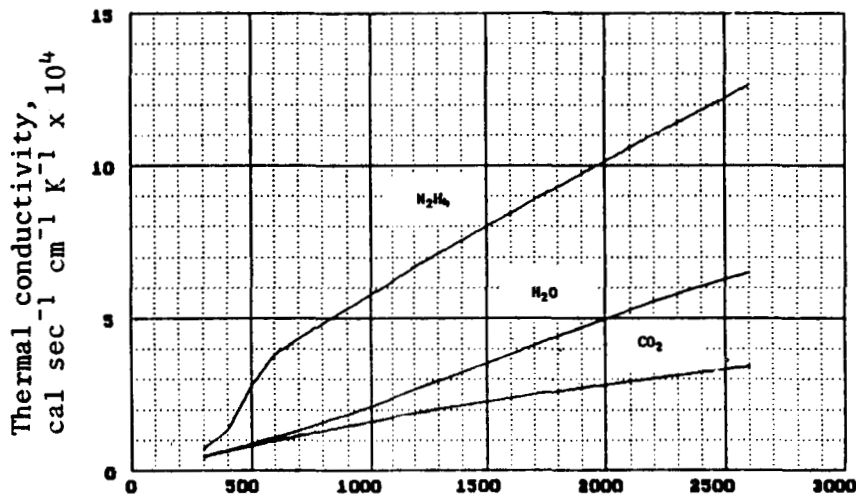
For the mathematical modeling, the thermodynamic and transport properties of the pure propellants were needed. The three propellants are carbon dioxide and water vapor for the biowaste resistojets and hydrazine for the augmenters. The three properties, specific heat, viscosity and thermal conductivity, of equilibrium mixtures derived from each pure substance were calculated for a pressure of three atmospheres and a temperature range of 300 to 2600°K. These are presented in figure 4. The data are tabulated in appendix I.

The equilibrium compositions were calculated using a method of Gibbs free energy minimization described in reference 8. Data for this method was obtained from reference 9.

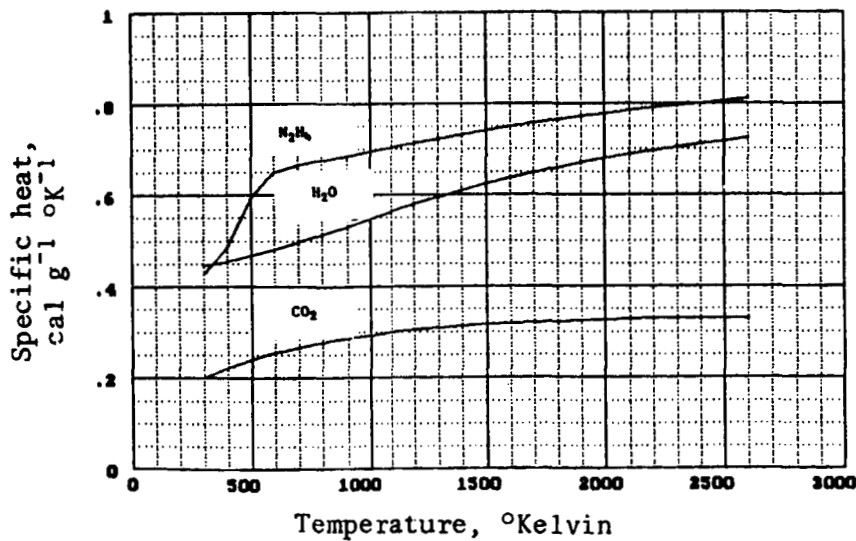
Thermodynamic properties for the sixteen resultant components were obtained from reference 10, except for the thermal



a) Viscosity



b) Thermal conductivity



c) Specific heat

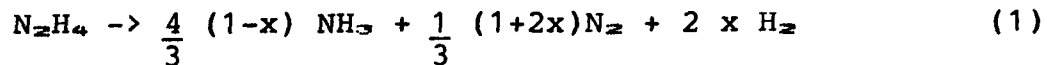
Figure 4. - Physical properties used for expellants

conductivity of water vapor. In this reference, thermal conductivity was calculated using an equation which, according to the author, shows poor correlations to experimental data for polar molecules. As the values are about 30% higher than those of three other sources at temperatures for which they were available, thermal conductivity of water vapor was instead taken from reference 11.

Properties of the equilibrium mixtures thus determined were calculated using the equations described in reference 12.

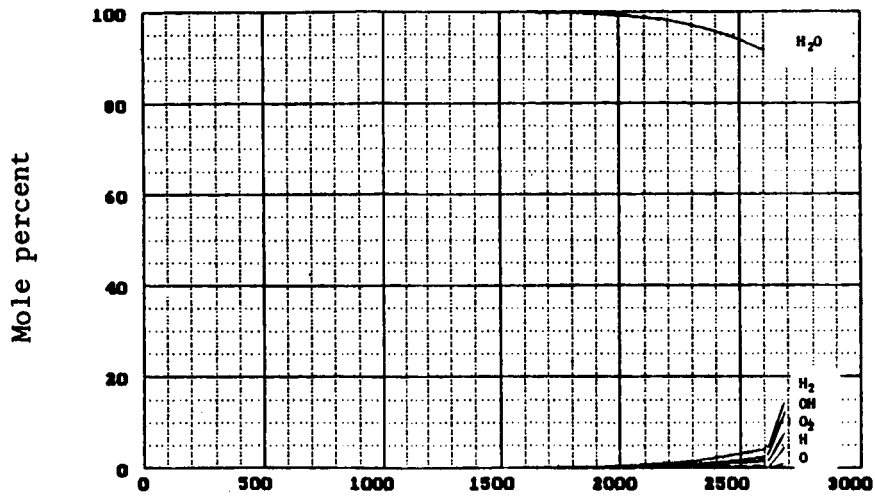
As a practical matter, the propellants supplied would most probably contain other chemical species which are indigenous from their production source. These must be addressed in any practical design.

The hydrazine augments receives its propellant from the first stage decomposition chamber. The decomposition reactant from this chamber is given by the reaction equation (1):

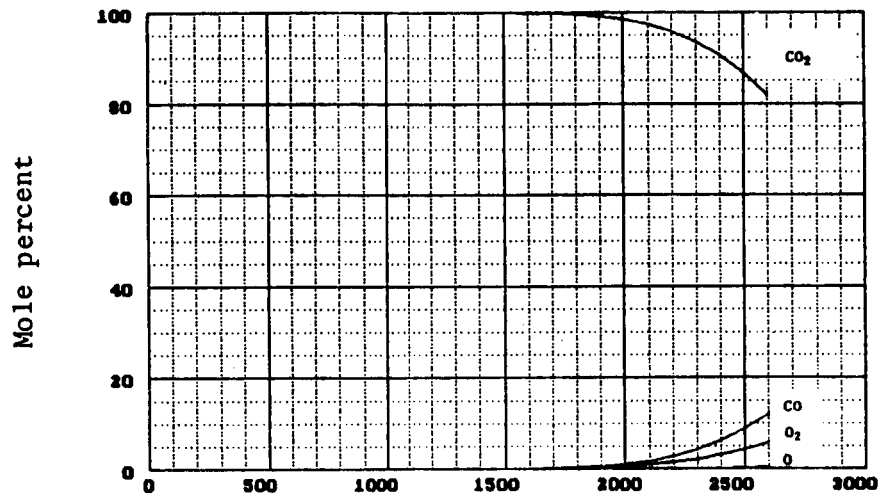


The temperature and properties of the gas can vary widely depending on x , the degree of reaction. The propellant description chosen here is that of full decomposition ($x = 1$) for definition, resulting in a gas temperature of 866.5°K. The gas then consists of one mole of nitrogen and two moles of hydrogen with no ammonia. This is the most favorable input for several reasons. This condition represents the lowest interstage transfer temperature, hence, minimizes interstage heat loss. Too, it simplifies the analysis of the augments in that no chemical kinetics assumptions must be made as is described under the thermal analysis of the augments presented. This assumption has small impact on the final augments power performance figures presented, only the thermal profile.

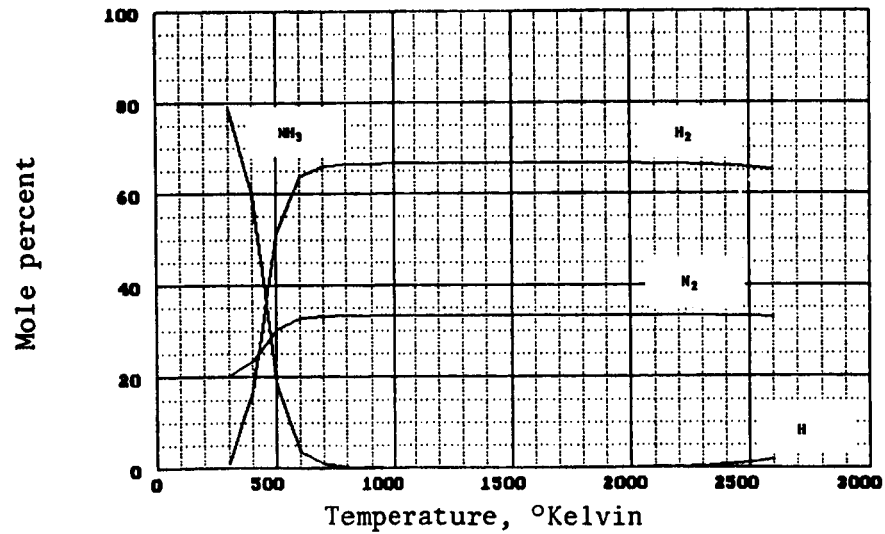
The temperature range of this study did not encounter the need for consideration of dissociation of the expellants other than the hydrazine which was considered fully decomposed. Neither the hydrogen nor the nitrogen significantly dissociates in the temperature range of interest. See figure 5.



a) Steam



b) Carbon dioxide



c) Hydrazine

Figure 5. - Composition of expellants at 3 atmospheres

Thruster

The material finally selected for each function depended upon its ability to withstand the combined effects of temperature, pressure and gas atmospheres to which they were subjected in the design. The candidates selected have evolved over a long development period for each propellant classification from a number of experimental studies and experiences of the authors and others with resistojets (refs. 4, 5, 13, 14, 15). Table 4 compares the endurance characteristics of the critical materials used.

TABLE 4
ENDURANCE CHARACTERISTICS OF CRITICAL
STRUCTURAL MATERIALS USED

| | Rhenium | Platinum | Platinum, grain stabilized w/zirconia | Zirconia, phase stabilized w/10% yttria |
|--|----------------------|--------------|--|--|
| Melting point, °K | 3459 | 2047 | 2047 | 2858 |
| Density, gm cm ⁻³ | 21.04 | 21.45 | 21.38 | 5.65 |
| Surface recession in a vacuum in 10 ⁴ h, μm | | | | |
| @ 1573°K | 5.2x10 ⁻³ | 5.3 | 5.3 | .36 |
| @ 2073°K | .033 | - | - | 1.8 |
| Linear thermal expansion % change | | | | |
| @ 298 | 0 | 0 | 0 | 0 |
| @ 1573°K | 0.875 | 1.380 | n.a. | 1.53 |
| @ 2073°K | 1.278 | - | - | 2.36 |
| Endurance strength, kPa (psi) for 10 ⁴ h | | | | |
| @ 1573°K | 41,301 (5990) | 970 (140) | 5808 (842) | 3450 (500) |
| @ 2073 | 12,424 (1802) | - - | - - | 207 (30) |
| Oxidation recession in air, μm in 10 ⁴ hr | | | | |
| @ 1573°K | 6.7x10 ³ | 18.65 | 18 | nil |
| @ 2073°K | 2x10 ³ | - | - | - |

Structure.- For the biowaste, the metal selected was grain stabilized platinum, based upon the extensive experimental studies of references 14, 15, and particularly, 16. Recent developments in the grain stabilization are discussed in the latter reference.

As the strength of platinum is low, the use of grain stabilization is extremely attractive for improving its high temperature endurance strength. As a guide, the ultimate strength of zirconia grain stabilized platinum at 1573°K is four to five times greater than pure platinum alone.

Concept 1 uses a metal oxide, cubic phase stabilized zirconia, which is capable of withstanding the biowaste gases and other oxides to significantly higher temperatures than platinum, that is approximately 600°C higher! Concept 4 chooses the refractory metal, rhenium, for its heater with a similar high temperature capability using radiative transfer in a separate cavity with an inert environment. Therefore, the consideration of the materials, zirconia and rhenium, also are applicable to the biowaste thrusters. The properties of these three candidates structurally are reviewed.

Because of its (a) superb ductile behavior, (b) high strength at temperature, (c) weldability, and (d) successful prior experience with thruster design in electric propulsion, grain stabilized rhenium was chosen for the entire hot structure of the hydrazine augments.

Mechanical Properties: Data for 10,000 hours, if they exist at all, were not possible to obtain at this time. Therefore, extrapolation from existing data is necessary. Based on reference 16, a supplier of grain stabilized platinum, the following endurance stress design line for grain stabilized platinum was generated. The endurance stress, σ , in kilopascals at 10,000 hours was calculated at each temperature, T , in °K for grain stabilized platinum by,

$$\log_{10} \sigma = -2.13 \times 10^{-3} T + 7.115 \quad (2)$$

As the strength of pure platinum, is low, the use of grain stabilization is extremely attractive for improving its high temperature endurance strength. As a guide, the ultimate strength of zirconia grain stabilized platinum at 1753°K is four to five times greater than pure platinum alone.

Values of endurance stress for ZrO_2 may be found in reference 17. The allowable stress for ZrO_2 values are small and the applied stresses in designs using these heaters must be kept small. This is done by designing low pressure drops in the exchanger which are in turn pressure balanced externally so as to be in slight compression.

The physical structural properties of grain stabilized rhenium are as yet unknown, but are anticipated to be significantly better in endurance stress rupture capability as has been demonstrated for the other refractory metals (refs. 18 and 19). For the structural analysis of this study, however, pure rhenium data were used because of its availability, which are expected to have greater reliability. The endurance strength of rhenium, for a 10,000 hour design line, was chosen based upon a Larson-Miller correlation with the data of reference 20 and is shown in equation 3.

$$\log_{10} \sigma = -1.043 \times 10^{-3} T + 6.257 \quad (3)$$

Recently the addition of grain stabilizing metal oxides to rhenium has been found possible in the refined shapes required here (ref. 21). No stress design data is as yet available.

Physical Properties: The thermophysical properties of the material used in the study for each of the functional elements of the resistojet are tabulated in appendix I. These tabulated data were generated from the polynomials used in the mathematical computational model, which are in turn based on the best recommended values from the Thermophysical Properties of Matter from the Purdue Series (ref. 22).

Sublimation: The process of a material passing directly from a solid to a vapor state from a surface causing its recession, either under vacuum or with a suppressant gas, is an important factor in determining the service life of a device operating at high temperature. The surface recession rate is greatest in the vacuum. It can be suppressed by many orders of magnitude by adding an inert atmosphere. Key references used for vacuum were Dushman (ref. 23), and for zirconia specifically (ref. 24). The sublimation recession rates for a number of very high temperature materials in vacuum are shown in figure 6.

The surface recession rate under forced convection mass transfer uses the methods of Zima (ref. 25) and Dushman (ref. 23).

Chemical corrosion resistance: The chemical corrosion processes at high temperature are very complex. Interactions between all of the components of the system can occur. This involves a) members which are in contact, namely heater elements, electric insulators, thermal insulators; b) all three of these in propellant gases and trace species; and c) significant trace species in the peripheral elements such as brazes, insulations and components. The study here is strictly first order. Oxidation recession rates are based upon Phillips, (ref. 26). See figure 7 for a summary of these rates.

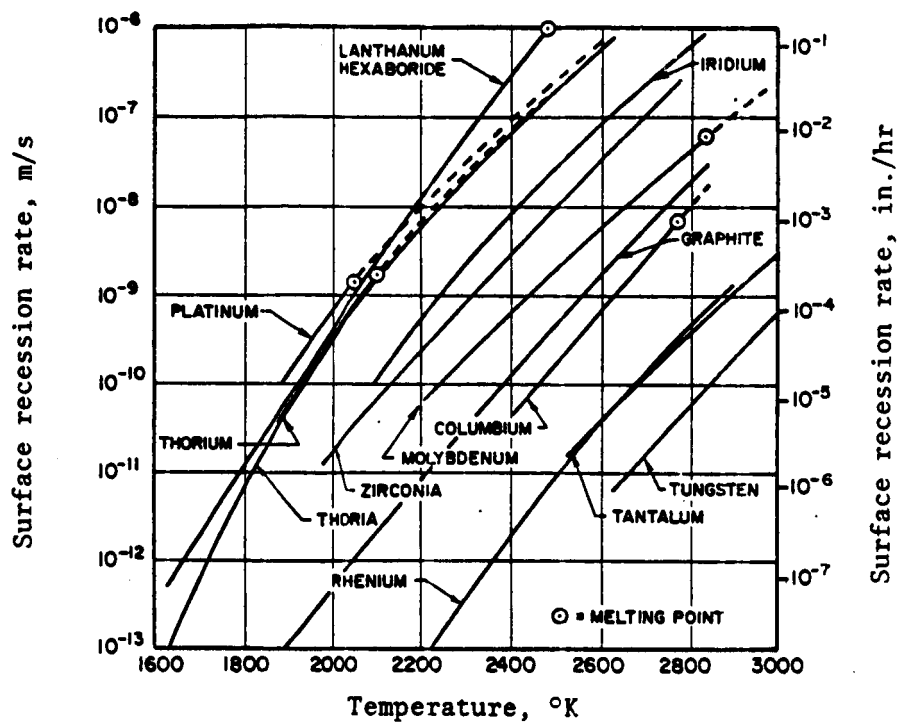


Figure 6. - Sublimation data of various materials in a vacuum.

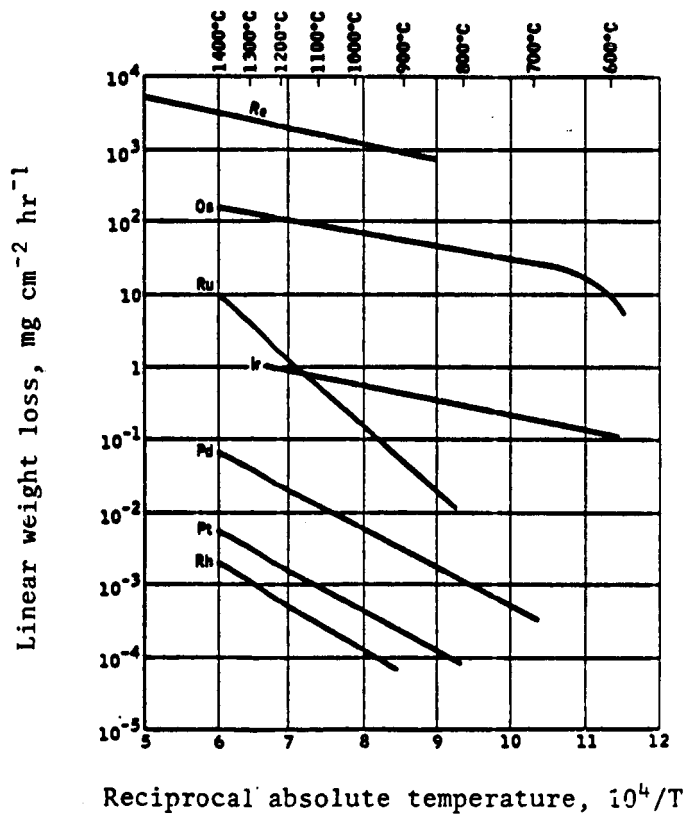


Figure 7. - Linear metal loss constants in air.

In Concepts 2 and 3 the intimate contact of the heater with biowaste gases, as well as the critical structural elements at high temperatures, suggested the use of a noble metal. The studies of reference 14 showed experimentally that platinum, while one of the lowest temperature and strength members of that family, must be considered because of chemistry.

Rhodium forms a carbonyl. Iridium has a very high oxidation rate with even small amounts of oxygen present (ref. 26). See figure 7.

Rhenium is not oxidation resistant. It does have a high resistance to small amounts of water vapor at high temperature. Unpublished test data of the authors found the erosion rate at 2400°K to be negligible in the presence of 1% H₂O vapor, where at 2000°K, it was 5 x 10⁻⁶ centimeters per hour. The higher the temperature above 2000°K, the more resistant it becomes to H₂O vapor.

Specific values for sublimation and corrosion life factors above are reported with each concept.

Electric Heaters.- Figure 8 compares the electric resistivity of the candidate materials. Table 37 tabularizes the values versus temperatures.

Thermal insulation.- The insulation systems used in the study were all of the porous or fibrous ceramic type.

In the high temperature regions (above 1000°K) it can be shown that the effective thermal conductivity of a reasonably practical radiation shield configuration is no better than the better fibrous ceramic oxide insulations. The trade-off then involves many other factors such as having to support the shields without excessive thermal losses through the shielding, and in the case of fibrous insulation, having to handle a possible dusting problem and considering the launch environment.

Zirconia fiber is an especially good high temperature insulation. It was selected for use here. Its thermal conductivity in a vacuum values are tabulated in appendix I.

A factor considered with fibrous insulation was the effect of gaseous environment. Its thermal conductivity changes from its value in air, argon, etc., and vacuum and was taken into account.

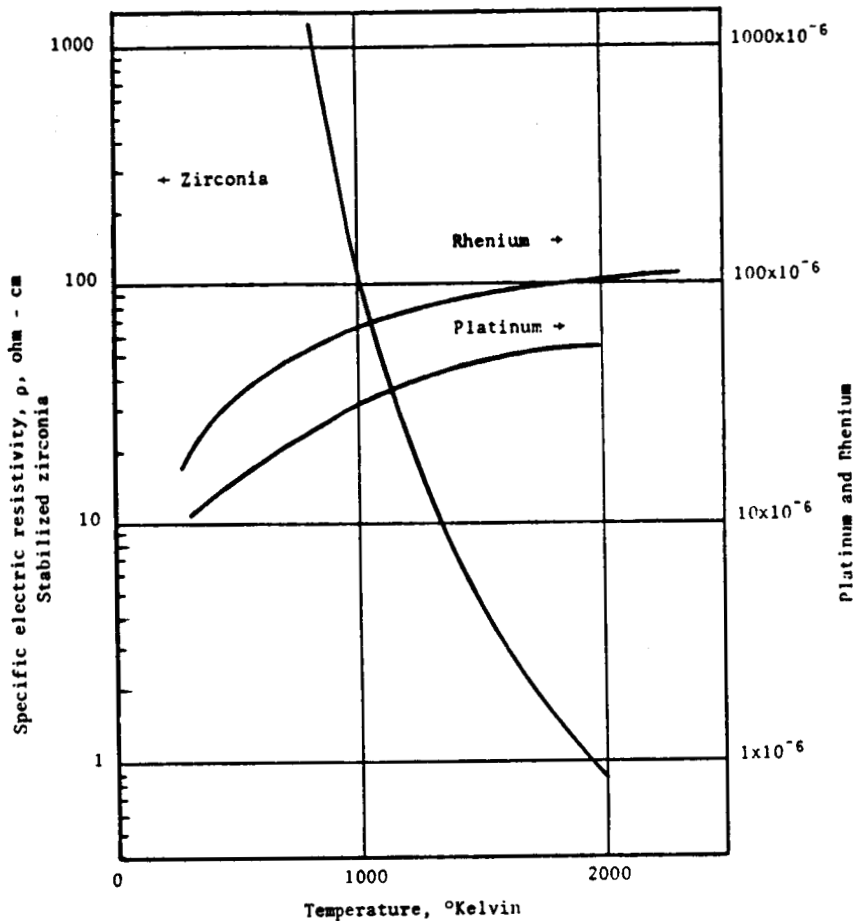


Figure 8. - Comparison of electric resistivity of platinum, rhenium and stabilized zirconia.

Electric insulators.- The thermal requirements of the electric insulators as found from the thermal analysis are very modest.

For the purposes of these designs, in light of the temperature and chemistries involved, very high purity (99.98%) alumina (Al_2O_3) is perfectly adequate. The temperatures where insulators are used is less than $625^\circ K$. The properties of alumina are given in appendix I.

Electrothermal designers have used boron nitride for electric insulation because of the relative ease of machining. The thermal conductivity, however, of boron nitride, like beryllium oxide is almost that of a metal. For this reason, the design philosophy employed was not to use it.

RESULTS AND DISCUSSION

The results of each of the thruster designs studied are presented in detail in the appendices A through F. Each stands as a complete, separate report of its concept. These are all organized the same. The Table of Contents identifies, for each concept, the specific page of the following:

1. Description
2. Performance
3. Thermal analysis
4. Gas dynamic analysis
5. Structural and other mechanical effects
6. Chemical corrosion, sublimation and deposition
7. Rating

The results and discussion here synopsise the main points. The designs are compared and recommendations made. The concepts are simply summarized under Study Models.

Biowaste Resistojets

The results of the thermal analysis by mathematical modeling studies for the four biowaste designs studied are summarized for operation separately on carbon monoxide and on steam in tables 5a and 5b. The performance at the design goal heater temperature of 1573°K, chamber pressure of 3 atmospheres and a thrust level of .22 Newtons (50 mlb_r) are shown.

The performance figures for Concepts 1 and 4 are shown in table 6 also for an advanced heater temperature of 2000°K and 2073°K, respectively, selected because of the unique features and the different heater materials of each of these designs. In these cases the other grain stabilized platinum components were limited to 1573°K resulting from this operation, the same value as the study goal temperature for the platinum heater.

All of the designs presented use a separate evaporator to insure that vapor is supplied to the biowaste thruster. The thruster is charged with the inlet steam power in its performance assessment. The performance of the evaporator is not considered part of the thruster.

Similar thermal insulation and electric insulator mounting standoffs are used for each concept to reduce power loss and so that thruster grounds are insulated from spacecraft grounds, respectively. This is to avoid ground loops.

TABLE 5a
 DESIGN PERFORMANCE SUMMARY
 CARBON DIOXIDE - 3 ATMOSPHERES

| Concept Version | 1 D2 | 2 A | 3 A | 4 ^a F | 4 ^b C |
|---------------------------|---------|--------|--------|---------------------|---------------------|
| Max. heater temp., °K | 1573 | 1573 | 1573 | 1573 | 1573 |
| Specific impulse, s | 167.5 | 164.0 | 170.2 | 138 | 92.6 |
| Electric power, W | 181.3 | 181.0 | 203.0 | 146.2 | 55.01 |
| Nozzle total temp., °K | 1448.0 | 1384.1 | 1486.1 | 1045.1 | 555.8 |
| Maximum gas temp., °K | 1468.4 | 1413.8 | 1510.3 | 1052.3 | 557.4 |
| Max. pres. case temp., °K | 777.2 | 553.4 | 592 | 1060.2 | 560.2 |
| Heater voltage, V | 153.33 | 7.38 | 6.83 | 18.07 | 11.19 |
| Heater current, A | 1.182 | 24.51 | 29.71 | 8.09 | 4.92 |
| Power efficiencies | | | | | |
| Overall, η_o | .849 | .815 | .793 | .816 | .870 |
| Heater, η_H | .932 | .901 | .882 | .909 | .971 |
| Nozzle, η_N | .910 | .904 | .899 | .898 | .891 |

TABLE 5b
 DESIGN PERFORMANCE SUMMARY
 STEAM (H₂O) - 3 ATMOSPHERES

| Concept Version | 1 D2 | 2 A | 3 A | 4 ^a D | 4 ^b C |
|---------------------------|---------|--------|--------|---------------------|---------------------|
| Max. heater temp., °K | 1573 | 1573 | 1573 | 1573 | 1573 |
| Specific impulse, s | 236 | 230.4 | 240 | 171 | 148 |
| Electric power, W | 222.7 | 223.5 | 255.3 | 108.1 | 56.08 |
| Nozzle total temp., °K | 1459 | 1391.2 | 1501.9 | 812.7 | 616.2 |
| Maximum gas temp., °K | 1472.2 | 1418.4 | 1518.9 | 815.5 | 617.4 |
| Max. pres. case temp., °K | 791.2 | 588.5 | 628.1 | 820.4 | 620.3 |
| Heater voltage, V | 173.74 | 8.24 | 7.76 | 15.65 | 11.30 |
| Heater current, A | 1.282 | 27.12 | 32.83 | 6.91 | 4.96 |
| Power efficiencies | | | | | |
| Overall, η_o | .840 | .799 | .784 | .850 | .873 |
| Heater, η_H | .930 | .899 | .884 | .956 | .970 |
| Nozzle, η_N | .903 | .889 | .887 | .889 | .900 |

1. Heater cavity in a vacuum.
2. The best case is shown with the heater cavity pressurized with N₂ at 3 atmospheres and the use of an emissive coating enhancement of cavity wall.
3. Case shown with heater cavity pressurized with N₂ at 3 atmospheres. Version 4F was not computed for steam. It would be better than the 4D shown.

TABLE 6
 PERFORMANCE SUMMARY
 AT ADVANCED BIOWASTE HEATER TEMPERATURE OPERATION
 3 ATMOSPHERES

| Expellent gas | CO ₂ | H ₂ O | CO ₂ | H ₂ O |
|------------------------------|-----------------|------------------|-----------------|------------------|
| Concept | 1 | 1 | 4 ¹ | 4 ¹ |
| Version | D2 | D2 | D | D |
| Maximum heater temp., °K | 2000 | 2000 | 2073 | 2073 |
| Specific impulse, s | 192.5 | 269 | 171 | 232 |
| Electric power, W | 254.9 | 310 | 222.4 | 244.4 |
| Nozzle total temp., °K | 1839.8 | 1841.9 | 1495.5 | 1405.8 |
| Maximum gas temp., °K | 1876.7 | 1872 | 1507.3 | 1413.5 |
| Max. pressure case temp., °K | 1257.1 | 1207.3 | 1530.6 | 1435.9 |
| Heater voltage, V | 85.31 | 98.3 | 24.04 | 25.24 |
| Heater current, A | 2.988 | 3.155 | 9.25 | 9.68 |
| Power efficiencies | | | | |
| Overall, η_o | .745 | .770 | .744 | .780 |
| Heater, η_H | .830 | .845 | .882 | .887 |
| Nozzle, η_n | .897 | .910 | .844 | .879 |

1. Pressurized heater cavity with N₂ at 3 atmospheres.

In general, the few design iterations in each of the configurations that were permitted by the study effort sought to maximize specific impulse performance with due regard for reasonable overall efficiency and reliability considerations. The spacecraft designer must prescribe the relative importance of these output parameters for his mission for design guidance.

The gas dynamic, structural, chemical corrosion, sublimation and deposition factors were kept within the limits of the study criteria during the course of configuring each concept design.

Concept 1.- The use of the electrically conductive ceramic, cubic phase stabilized zirconia, for its heating element permits a much higher than goal temperature of 1573°K of the study. It has the highest growth in specific impulse capability of the biowaste designs studied. It can achieve 192.5 and 269 seconds on carbon dioxide and steam, as shown in table 6. At the design goal condition, Concepts 1, 2 and 3 have nearly the same specific impulse and overall efficiency values. Since the propulsion characteristics for the Space Station core is not performance driven, the design choice between these concepts would have to be made on other trade-off considerations. Reliability is the major consideration.

Zirconia has not been developed as a miniature gas heater-exchanger. However, its use as heater elements at high temperature ($>2000^{\circ}\text{C}$) in air in commercial ARTCOR research furnaces have greatly advanced the technology of this material since its early consideration for a biowaste resistojet (ref. 13).

Electric characteristics: Figure 8 shows the marked difference in electric characteristics of the conducting ceramic designs as compared to the metallic ones. Tables 5 and 6 show a resulting higher operating voltage than the other designs of 153 to 173 V at operating conditions for CO_2 and H_2O , respectively. The current levels are of the order of an ampere. These characteristics are most favorable for power loss reduction in transmission on the power bus of the spacecraft. A special electric consideration is that the ionic nature of the conducting ceramics require alternating current to avoid polarizing the ZrO_2 . This is essentially the driving of the negative oxygen ions to one end and altering the stoichiometry if operation on D.C. is attempted. In addition, conducting ceramics, because of their negative electric characteristic with increasing temperature, a constant current type power control is required for stable operation. The latter eliminates any need for ballast resistors.

Starting: Since zirconia does not conduct electricity essentially below 800°K , it requires preheating. Only for this reason was the starting problem studied for Concept 1. The various modes of operation were evaluated by means of transient studies using the computational mathematical model. These are presented in detail in the appendix. There it is shown that the time from a cold start (state 1) to design condition (state 4) is approximately 3 minutes. It is shown that a holding state (state 3) at 1250°K with no flow requires only 22.6 watts of main heater power. Its thrust response is immediate but it is approximately 5 seconds away from full value of specific impulse.

Where the duty cycle is high and fast response in thrust cannot be readily anticipated as to schedule, the condition of holding at a no flow design and temperature state (state 3) is recommended. Power losses are low, the thrust and specific impulse response are high.

Where firing times are long and separated by long periods of no thrust, the power up mode from rest (state 1) to design (state 4 or 5) is recommended. When firing times are long and only separated by short inactive periods, a holding state at 1250°K (no propellant flow) is recommended. Overall reliability will be enhanced by the avoidance of heavy thermal cycling of ceramic materials. It is concluded with regard to starting that the systems engineer must ultimately make the final selection as to the best overall operating schedule.

Reliability by means of redundancy: Note that the inclusion of a preheater permits an additional powered mode (state 6) at 1250°K as a fully redundant reliability feature of the design. This powered mode will produce a specific impulse of 133 seconds (CO₂). This alone meets contractual goals! The preheater, because of the high temperature capability of rhenium, operating in the vacuum exterior to the pressure case as it is here, is limited in temperature only by the resultant temperature of the platinum pressure case. It represents a totally independent alternative means of powering Concept 1 for redundancy which could be from even a different power bus.

Concept 2.- This design (figure 1) is a new one based on novel features of a radially inverted functional design and a truss heater. The first feature results in the pressure case being its outermost member, which is the coolest of all the designs considered. Hence, it can be made of lower temperature stainless steel. The truss heater has high transverse strength, yet axial compliance and high electric resistance. The heater design does prove to be complex and Concept 3 which uses the same outer shell is somewhat superior in performance and easier to fabricate. Using radially broad regenerators is advantageous when cool expellant inlet gas of low thermal conductivity is used. This provides better thermal insulation and cooler cases than the traditional design order.

Concept 3.- This, like Concept 2, uses the radially inverted functional design in the biowaste configuration, but the bicoil heater as described in the Study Model. There are a number of advantages to Concept 3 besides the fact that the gas approaches the wall temperature very closely. This design has the highest specific impulse of all the biowastes at the goal temperature. It achieves 170.2 seconds on carbon dioxide and 240 on steam. It is perhaps the most thermally responsive in that the low mass coil is the first to heat during start up and the last to interact directly with the gas before it exits through the nozzle. Its overall thermal efficiency is approximately 5 percentage points less than Concept 1. The reason for the efficiency difference is primarily the difference in the axial lengths required of the two designs as discussed in the corresponding studies in the appendix. No electric insulation is used in the high temperature zones. Propellant flow deters backstreaming of any sublimed metallic vapors onto electric insulators at the mount end which contains the power service.

In respect to electric characteristics, the voltage of Concept 3 is the lowest of the designs studied and the current the highest. While the electric characteristic of the design was studied for voltage increase, a factor of perhaps two times that shown was considered the maximum. By means of pulsed mode control operation off a 28 volt bus is possible without transformation with a suitably designed power conditioner.

Concept 3 gives the highest specific impulse for any given wall temperature limit of those concepts studied. Because the cavity pressure surrounding the heater tube can be designed to be only slightly greater than within by use of its low mach number, a failure mode due to heater wall rupture by hoop stress is reduced. The design is pressure balanced internally with no appreciable creep load for all operating conditions. The thermal expansion compensation is inherent in the bicoil principal in that it is axially very compliant, yet the heater is structurally sturdy transversely because the coils are metallurgically bonded along the transverse length about every half turn at equipotential points. Since the heater coil is surrounded by expellant, any small leakage is inconsequential with time. The pressure case is cool and can be made of less expensive materials and, in addition, bring high reliability to the pressure integrity of the design.

Concept 4.- The nonexposed radiant heater concept is already in use. The design physically separating the heat exchanger function from that of the ohmic heater allows the heater to be independently designed and a material used which need not be biowaste resistant. A rhenium heater can be chosen to operate at significantly higher temperatures.

The power transfer link between the radiant wire heater and the heat exchanger pressure case is relatively fixed in value for a given temperature and radiant transfer heater. This power is mainly proportional to the heater temperature to the fourth power and transfer area. The lower temperature of the receiving surface is of much less influence. This somewhat limits its use as the variable thrust or multiexpellant design. By increasing chamber pressure, flow is increased. With a fixed amount of power, the gas temperature reduces and a noticeably lower specific impulse high thrust unit results. Its use as a multi-propellant design is difficult. A propellant with a significantly higher specific heat than the propellant for which it was designed cannot be run to achieve the same gas temperature for the same heater temperature limit. This is unlike a convective design where the gas is in intimate contact with the heater, itself, and the temperature difference between gas and heater is small. Using the same size thruster housing as Concept 3 and same heater temperature goal of 1573°K, the goal specific impulse could not be achieved with the cavity in a vacuum. This means larger designs are required to increase the transfer surfaces and more heat loss surface, hence lower efficiency. The answer here was to improve the radiation link by offering a pressurizing inert gas in the cavity to add a parallel conduction mode and high emissivity surfaces to promote better radiant heat transfer exchange. With these the goal specific impulses can be achieved. With CO₂ a specific impulse of 138 seconds was achieved with an efficiency of .816. In the same size design and heater temperature, Concept 3 produces 170 seconds with an efficiency of .793.

The heat exchanger is a more massive structure. It is a pressure vessel. The thermal mass is a factor of ten times that of the heater of Concept 3, the bicoil. The heat-up time transient is substantially longer than Concept 3. Conversely, Concept 4 is less sensitive to erosion.

In electrical characteristics the heater voltage is 18 to 15.6 volts for CO₂ and steam, respectively, are achieved by the quadcoil design.

Hydrazine Augmenters

Two designs, the convective and radiation type resistojet thruster designs, were studied by mathematical modeling their performance for operation on decomposed hydrazine (fully dissociated) with the inlet condition at 866°K. The complete study reports of these are found in Appendices E and F. The performance is abstracted in table 7. The philosophies employed in both designs were kept comparable, consistent with appropriateness in order to insure an accurate comparison.

TABLE 7
PERFORMANCE SUMMARY OF AUGMENTER DESIGNS
DECOMPOSED HYDRAZINE - 3 ATMOSPHERES

| Concept Version | 5 E | 6 ¹ A | 6 ² B |
|------------------------------|--------|---------------------|---------------------|
| Maximum heater temp., °K | 2073 | 2073 | 2073 |
| Specific impulse, s | 317 | 278.2 | 295.2 |
| Electric power, W | 295.32 | 181.32 | 239.91 |
| Nozzle total temp., °K | 1994.2 | 1512.8 | 1726.7 |
| Maximum gas temp., °K | 2058.7 | 1551.8 | 1773.9 |
| Max. pressure case temp., °K | 1758.7 | 1557.9 | 1780.9 |
| Heater voltage, V | 8.94 | 21.77 | 24.70 |
| Heater current, A | 33.04 | 8.33 | 9.71 |
| Power efficiencies | | | |
| Overall, η_o | .732 | .749 | .722 |
| Heater, η_h | .889 | .877 | .866 |
| Nozzle, η_n | .823 | .854 | .834 |

1. Vacuum in cavity.
2. Pressurized heater cavity with 3 atmospheres N₂ gas.

Concept 5.- Based on the maximum heater goal heater temperature of 2073°K, the specific impulse capability of Concept 5E is clearly superior, 317 seconds as compared to the radiative one of 295 seconds. The maximum gas temperature in the bicoil design reached 2059°K, only 14 degrees from the maximum wall temperature limit while in the radiative one was 300°K different because of the large temperature difference required by the radiative link. For this reason alone, Concept 5 will have a higher growth potential for operation on hydrazine and comparable propellants such as ammonia, hydrogen, nitrogen and the reducing gases in general. The overall power efficiency is approximately 1.5 percentage points greater than Concept 6B because of the heater efficiency as radiative type design is longer.

The voltage of the 5E design is 8.94 volts with a current of 33.04 amperes. It is estimated that the terminal voltage of Concept 5 can be increased by a maximum factor of two by design changes.

The thermal energy required to raise the heat exchanger mass to its design temperature during starting is relatively small, approximately one-tenth the radiative type. The specific impulse should respond faster after starting as compared with the more massive pressure case heat exchanger structure of Concept 6. For long term steady firing, this is not a factor. A heavier case of the latter has an advantage over the thinner surfaces of the bicoil heater from a long term erosion viewpoint. From a study of the sublimation enforced evaporation, Concept 5 meets the design objective of 10,000 hours. Since the bicoil is immersed in the expellant in the cavity, there is not a problem should small amounts of leakage occur.

Concept 6.- The performance of the nonexposed radiant heater type resistojet augmentor is improved by augmenting the radiant heat transfer link by the addition of an inert gas around the heater from a 278.2 seconds to 295.2. Further improvement could be expected with the addition of emissive surfaces on the cavity side of the case. The pressure case temperature, since it is also the heat exchanger member, is governing the maximum gas temperature and, hence, specific impulse. If anything, the pressure case temperature will be slightly higher than the pressure case of the bicoil type convective design of Concept 5.

The favorable feature of the radiant design is the independence of the radiant heater element to a greater extent than in the convective one. Adequate radiative heater transfer surface area, though, must still be provided. A higher voltage, in this case 24.7 volts in the 6B design, is achieved with a lower current of 9.7 amps. The radiant design, for best performance, does require an additional pressurization connection of the inert gas to the cavity and another pressure supply.

MANUFACTURING

The most critical elements in either the biowaste resistojet designs or the hydrazine augmenters must generally be supplied to near finished form by specialists in these fields. In the case of the biowaste designs, the exposed high temperature structure is of grain stabilized platinum, of which there are two suppliers (refs. 16 and 27). For pure rhenium, shaped resistojet parts may be obtained by the chemical vapor deposition process from a few suppliers in the United States. There are few suppliers of grain stabilized rhenium material in shaped resistojet parts. In the case of platinum, the high cost of the material makes material recovery methods important when machining final shapes. For this reason this is usually left to the suppliers of such material. The difficulty in the machining of the necessary shapes in rhenium causes the number of sources to be small. This is either done by the chemical vapor deposition method or a new method for grain stabilized rhenium described in reference 21.

Cubic phase stabilized zirconia is available from a number of suppliers. The combination of alumina and nickel for the insulator/seal assembly was chosen because that technology has been well developed for the high frequency cable terminal industry. The two materials have similar thermal expansion characteristics and are, therefore, easily joined. Examples of such seals are given in references 4 and 5, which successfully passed year long life tests. The finishing adjustment of mating parts for brazing processes and metallurgical bonds for platinum to platinum may be undertaken by ordinary machining methods similar to those used for the machining of A-200 nickel.

The machining of grain stabilized rhenium may be done by a number of techniques. The best method for finishing parts is grinding with tools having cutting surfaces coated with fine diamond abrasive particles. These tools can be obtained in almost any shape including drills, core drills, cutting wheels and grinding wheels. Curved surfaces can be obtained by the use of special tools with shapes corresponding to those of the desired parts. A second method used is the electro discharged machining method (EDM), which has been quite successfully employed. Rhenium parts should be annealed frequently during fabrication. This seems to relieve many problems. They should be annealed if made by vapor deposition and after other operations preceding welding. One-half hour at a temperature of 1925°K was sufficient in previous work.

The machining of zirconia is generally again by diamond tool grinding. The forming to final shape can be by any number of methods familiar to the ceramic industry depending upon the shape. Hot pressing, isostatic pressing, extrusion, slip casting, cold pressing followed by sintering.

Joining Methods

Considerable care must be exercised in joining grain stabilized platinum components. If the joints of the materials are heated above the melting point, as in the fusion welding, the oxide dispersion is lost in the weld area. Sometimes rhodium rich filler metal is added to the weld pool. This usually provides sufficient solution hardening to the platinum interface to compensate for the local loss of the oxide dispersion. However, for this resistojet application, the use of rhodium in high temperature areas should be avoided because of carbonyl reaction during operation with CO₂ (ref. 15).

The preferred practice is to design the components such that any welds are made away from any critically stressed areas. The preferred method for joining the grain stabilized platinum to itself is the diffusion bonding technique. The diffusion bonding is conducted in a vacuum furnace at 1575°K for two hours. This requirement is well within the capabilities of most vacuum furnaces. Brazing and/or electron beam welding can be used in joining the grain stabilized platinum to itself in the lower temperature areas where several brazing techniques are available as well, depending upon the mating part material and joint design.

Rhenium.- This is easily welded to itself either by the electron beam process or the tungsten inert gas process. With small parts, however, the more precise electron beam welding is superior. The following points should be observed for easy welding. The parts should be clean and free of oxidation and fit tightly with no gaps. It is much easier to weld parts of similar thickness than a thin part to a thick one. This is due to heat transfer considerations. Weld schedules should be determined by practice with sample parts, having thicknesses and geometry similar to the parts they represent.

The same observations apply to electron beam welding of stainless steel parts and of nickel to stainless steel.

Rhenium is readily brazed to many other metals with a brazing alloy consisting of 82% gold and 18% nickel. Other brazes may be applicable as well. The rhenium to stainless steel joints can be done by this alloy as well. This operation should be done in a vacuum and the heat should be applied either in a conventional vacuum furnace for five minutes at a temperature of 1240° to 1250°K or by the electron beam welder with the beam diffused slightly. In the latter method one can make pass after pass until all braze material has been melted and flown into the joint. This method is applicable primarily to small parts and easily accessible joints.

SUMMARY OF RESULTS

The use of the electrically conductive ceramic, cubic phased stabilized zirconia, for the heating element gives the highest growth potential and specific impulse of all the biowaste designs studied. Concept 1, using this, can achieve about 192 and 270 seconds on carbon dioxide and steam, respectively. It has a high voltage alternating current operating characteristic that promotes low power transmission losses. A special controller is required. Because it requires a starting heater, it has a redundant operating mode, also, using the preheater which also meets the specific impulse criteria of the study of 133 seconds. When operating off a separate power bus, it represents potentially one of the most reliable of the designs.

If limited to metallic heaters, Concept 3 is selected as the next best candidate. Concept 3 has the lowest design temperatures involved. The gas approaches its heater wall temperature very closely before entering the nozzle and has a fast thermal response. A low temperature case is used, made of ordinary stainless steel, which improves its reliability. The bicoil heater has the lowest terminal voltage.

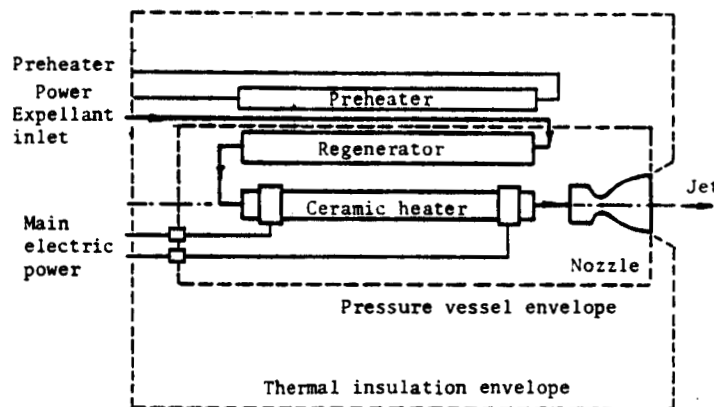
The radiant heater design, Concept 4, requires a rhenium heater or other refractory metal operating at significantly higher temperatures than the study guidelines, but under the circumstances, within the design operating conditions of the study for hydrazine augmenters under similar environment. The radiant power transfer link, however, must be pressurized in order to meet the design specific impulse minimums. An extra gas line is required. Loss of this gas pressure drops the specific impulse below the study goal.

Hydrazine augmenters, the two designs studied were the convective and the radiative type resistojets. The convective, in this case, clearly had a specific impulse advantage and a growth advantage in that gas approaches very closely to the limiting heater temperature. The augments radiative design did not meet the minimum goal specific impulse of 300 seconds. Again the terminal voltage of Concept 5, the convective design, is low. That of Concept 6, the radiative one, is high, 24 volts. By pulsed mode control, both can be readily operated on 28 volts with equal power conditioning requirements. The convective design, again, is recommended.

APPENDIX A

CONCEPT 1 -ELECTRICALLY CONDUCTING CERAMIC HEATER WITH EXPOSED INTERNAL FLOW

Concept 1 is a biowaste resistojet based upon a heat exchanger made with an electrically conducting ceramic. Zirconia, stabilized into the cubic phase, is used. The primary attraction of zirconia is its tolerance to the biowaste gases at higher temperature (mp 2998°K) than its nearest metallic heater counterpart, platinum (mp 2047°K). It is an update and reappraisal of a prior NASA supported technology base (circa 1971-72) reported in reference 14. Improvements in the design made possible since that time are included. It is functionally described below.



The ceramic heater contains multiple heat exchanger passages in a pentagonal pattern for a short, compact final stage. At 1573°K (1300°C), the specific electric resistivity of zirconia is 3 compared to 5×10^{-6} ohm-cm for platinum or 6×10^6 times more. See figure 6. This allows generous structural heater cross sections, less sensitive to erosion, which results in a high voltage - low current design of the order of 100 volts and a few amperes. Because zirconia is effectively an electrical insulator below about 1000°K, a starter heater must be provided.

The preheater is located outside the pressure case and is therefore unexposed to biowaste gases and can be made of grain stabilized rhenium (mp 3453°K). It can be encapsulated in an electrically insulating support. Operation on the preheater alone achieves the goal specific impulse and, hence contributes to reliability. The expellant passes in counter flow through a regenerator, part of the pressure case made of platinum, before passing through the short, compact, essentially constant wall temperature ZrO_2 heater exchanger. The power controller stably operates the ZrO_2 exchanger without need of ballast resistors.

Description

The physical description of the final preliminary design of Concept 1, which is Configuration D2, is shown to scale in figure 9. Table 8 gives identification of its components and materials.

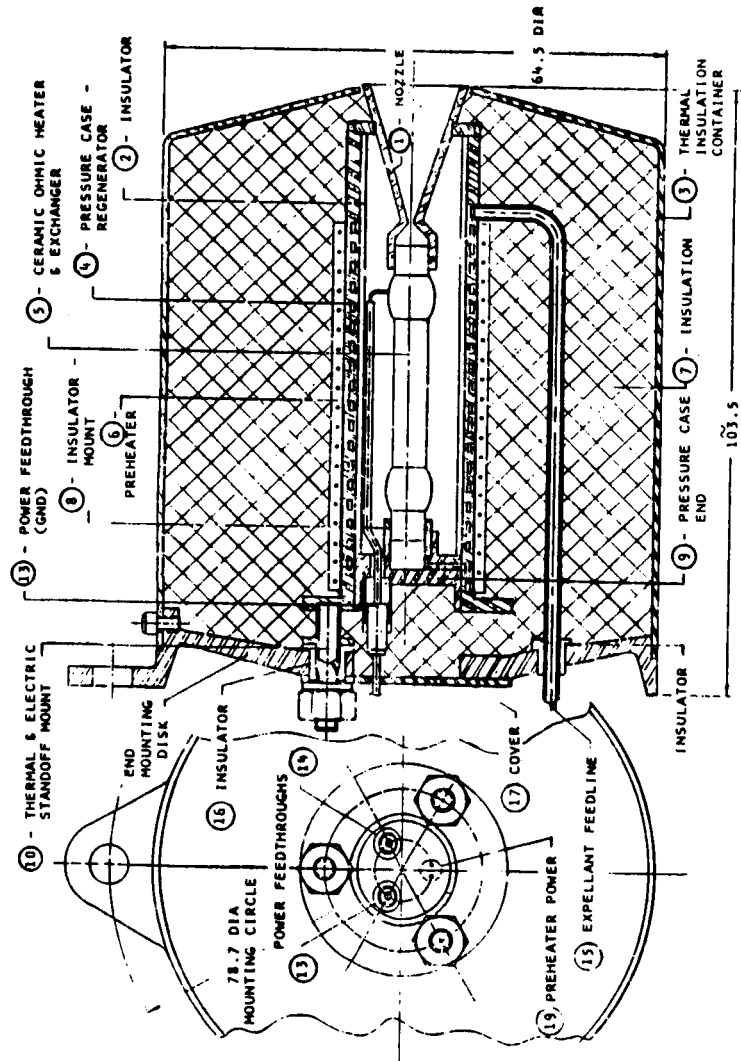
TABLE 8
CONCEPT 1 - COMPONENT PARTS, MATERIALS OF CONSTRUCTION

| <u>Item</u> | <u>Component</u> | <u>Material</u> |
|-------------|---|---|
| 1. | Nozzle | Composite platinum with zirconia gas path surface |
| 2. | Insulator | Alumina 99.5% |
| 3. | Thermal insulation container | AISI 321, stainless steel |
| 4. | Pressure case-regenerator | Grain stabilized platinum |
| 5. | Ceramic ohmic heater & heat exchanger | Stabilized zirconia w/noble metal electrodes |
| 6. | Preheater | Rhenium encapsulated ceramic assembly |
| 7. | Thermal insulation | Min-K 2000 ¹ |
| 8. | Electric insulator & mount | Alumina 99.5% |
| 9. | Pressure case end | Grain stabilized platinum |
| 10. | Thermal standoff & mount | AISI 321 |
| 11. | Container attachment screw | AISI 321 |
| 12. | End mounting disks | AISI 321 |
| 13. | Main power electric feedthrough into case | Metal to ceramic seal materials ² |
| 14. | Same | Same |
| 15. | Expellant feedline | AISI 321 |
| 16. | Insulator | Al ₂ O ₃ |
| 17. | Cover and mounting bracket for connectors | AISI 321 |
| 18. | Case mounting nut | AISI 321 |
| 19. | Preheater power | Rhenium |

1. Data for Min-K 2000, Johns-Mansville Aerospace Products, N.Y., NY.

2. Typical materials: nickel A conductors; glazed high alumina ceramic (85% min. Al₂O₃) insulators; vacuum tube grade brazing alloys and nickel-iron caps. Data from Ceramaseal, Inc., New Lebanon Center, NY.

The pressure envelope is formed by the pressure case regenerator (-4) with its headers, the case end (-9) and the nozzle assembly (-1). The ceramic ohmic heater and exchanger is mounted within this pressurized cavity between these headers. The entrance end of the zirconia heater is held by an electric



Scale: Full Size

Figure 9. - Concept 1, a biowaste resistojet using an electrically conducting ceramic heater with exposed internal flow. (Length not to scale)

insulator and mount (-8). The gas pressure in the cavity is made the same as the exchanger inlet by means of porting. The exchanger thus has a regulated small compressive pressure across its design. The fit between nozzle (-1) and exchanger (-5) is close to minimize gas bypass around the exchanger. The thermal expansion coefficients of zirconia and platinum at this joint are the same. This helps to maintain a close fit.

Figure 9 shows the main power feedthrough (-13) to the exit electrode which is power supply ground. Not shown as being out of the drawing plane is a similar feedthrough (-14) connecting the high side of the power supply to the entrance electrode. The high temperature central assembly is thermally and electrically isolated from the thruster mount (-12), hence spacecraft, by three standoffs (-10). This is for thermal efficiency and separation of power supply ground from spacecraft ground.

The preheater (-6) is located external to the pressure case and not exposed to biowaste gases. It can be constructed of rhenium. This permits a redundant backup operation which meets minimum study performance goals itself off of an independently powered second source which contributes to reliability.

The propellant feed line enters the case to enter the regenerator at the nozzle end as a "shuttle line". The "shuttle line", because of its intentionally poor heat transfer design, enters the nozzle end cool. This entrance was chosen, as opposed to one at the mount end, for reasons of power efficiency and the desire to keep the entrance electrode higher in temperature for electric conduction reasons. The flow then spirals to the ceramic ohmic heater-exchanger entrance through the regenerator-pressure case (-4). There it passes through heater-exchanger (-5) and exits via the nozzle (-1).

Performance

The projected performance on the candidate propellants CO_2 and H_2O for the study heater temperature of 1573°K are shown in table 9.

Because the zirconia heat exchanger is shown operating so much below its temperature capability, an advanced design point comparable in life to the others of the study is also presented in a second column at 2000°K . Operation less than this advanced design then represents a contribution to reliability.

These figures on basis of performance are superior when compared to all the other biowaste concepts of the study.

TABLE 9
CONCEPT 1 - CONFIGURATION D2 - PERFORMANCE SUMMARY

| | Projected Performance | | | |
|-----------------------------------|-----------------------|---------------------|-----------------|---------------------|
| | Design | | Updated Design | |
| | CO ₂ | H ₂ O | CO ₂ | H ₂ O |
| Specific impulse, s | 167.5 | 236 | 192.5 | 269 |
| Maximum heater temp., °K | 1573.2 | 1573.2 | 2000 | 2000 |
| Electric input | | | | |
| Voltage, V | 153.33 | 173.74 | 85.31 | 98.26 |
| Current, A | 1.182 | 1.282 | 2.988 | 3.155 |
| Power, W | 181.30 | 222.67 | 254.90 | 310.04 |
| Power/thrust, W/mlb _r | 3.72 | 4.54 | 5.13 | 6.20 |
| Nozzle chamber | | | | |
| Total pressure, Atm | 3.0 | 3.0 | 3.0 | 3.0 |
| Total temp., °K (J=29) | 1448.0 | 1459.0 | 1839.8 | 1841.9 |
| Expellant inlet | | | | |
| Total temperature, °K | 300 | 441.67 ¹ | 300 | 441.67 ¹ |
| Mass flow, gms/sec | .1319 | .0941 | .117 | .0839 |
| Initial gas power, W | 28.28 | 77.35 | 25.08 | 68.96 |
| Power lost from heater, W | 14.31 | 18.95 | 47.59 | 47.76 |
| Total input power, W | 209.58 | 300.02 | 279.98 | 379.00 |
| Maximum gas temp., °K | 1468.4 | 1472.2 | 1876.7 | 1872.0 |
| Max. case temp., °K | 777.2 | 791.7 | 1257.1 | 1207.3 |
| Electrode temp., °K | | | | |
| Entrance | 1164.1 | 1155.2 | 1516.5 | 1469.4 |
| Exit | 1392.2 | 1403.2 | 1731.3 | 1736.4 |
| Power efficiencies | | | | |
| Overall, η _o | .849 | .840 ¹ | .745 | .770 ¹ |
| Overall electric, η* _o | .981 | 1.130 | .818 | .940 |
| Heater, η _H | .932 | .930 | .830 | .845 |
| Nozzle, η _N | .910 | .903 | .897 | .910 |
| Thrust check, lb _r | .0487 | .0490 | .0497 | .050 |

1. Inlet phase is a vapor. The latent heat of vaporization of steam is not charged to the thruster but to a separate evaporator.

Thermal Analysis

The heat transfer analysis of the ceramic ohmic heater exchanger may be previewed in an approximate way by equations A1 and A2 to guide the designer as to the effects of changes in the design parameters (ref. 14). These equations are based upon a number of simplifications. A constant wall temperature and gas properties are assumed. These do, however, provide a basis for roughing in the starting point configuration, for a more exact study by the mathematical model via a microcomputer.

$$T_w - T_{g_r} = \frac{T_w - T_{g_i}}{e^x} \quad (A1)$$

where

$$x = \frac{\pi n L k Nu}{\dot{m} C_p} \quad (A2)$$

The ceramic heater, because of its logarithmic decrease in resistivity with temperature, tends to approximate the heat transfer boundary condition of a constant temperature wall. The relatively small change in resistivity of the metallic tube heater, by contrast, causes a boundary condition of constant heat input per unit length.

Which of these two conditions for a given maximum temperature of the wall produces a shorter gas passage to heat a given mass flow to the same exit gas temperature? Comparison with the analysis of Concept 5 shows that the constant temperature wall produces a substantially shorter gas passage.

T_w = constant temperature of heater wall, °K

T_{g_r} = final gas temperature, °K

T_{g_i} = initial gas temperature, °K

n = number of gas passages

L = effective heating length, cm

k = thermal conductivity of gas, cal/(sec-cm-°K)

C_p = specific heat, cal/g-°K

\dot{m} = total mass flow, g/sec

Nu_d = Nusselt number (hd/k)

The adjustable variables seen in equation A1 are the number of passages, n , and exchanger length, L . The greater the number of passages, the less the length required for the same temperature of the gas at exit temperature. Sixteen passages represents a practical upper number for a reliable state of the art in multiple passage tube manufacture. It results in a 30 mm long exchanger which is acceptable.

Steady state analysis by generalized computational model.-

The node diagram representing the final preliminary design choice is shown in figure 10. The temperature distributions are shown in figures 11 through 12 at 50 mlb, for both CO_2 and H_2O steam at the study design point of 1573°K (1300°C) and at an advanced condition of 2000°K (1727°C). The latter is shown as perfectly feasible in light of the capabilities of ZrO_2 material.

The alternatives to this final selection are reviewed with reasons for the selections made as baseline.

1) The platinum nozzle wall should be thin, not massive, to avoid axial heat losses. Thick walled nozzles caused the temperature of the gas at the throat to be 246°K below the maximum heater temperature. The thin composite nozzles of Configuration D2 were 125°K by comparison.

2) A ZrO_2 inner surface to the nozzle reduces the loss in gas temperature and to a lesser extent lowers the platinum backup wall structural temperature and erosion loss.

3) With regard to the ceramic heat exchanger length, after the peak gas temperature axial station is reached, the n passages can be reduced to one to minimize the drop in gas temperature by propellant "shuttle" to the nozzle. This also reduces heating the exit electrode unnecessarily.

4) Only one flow pass should be made through the regenerator-pressure case. The gas otherwise tends to retrace its temperature back to its near starting temperature. The expellant can be put into the case either at the nozzle end or the mount end. In the latter case a fast single tubular transfer is desirable as a shuttle pass to the mount end so that the gas entering the ceramic heater-exchanger is at its maximum temperature from the regenerator. The single pass promotes thermal efficiency about 3%. Regenerator entry at the nozzle end in Configuration D2 favorably keeps the rear electrode electrically conductive. The propellant entry to the regenerator at the nozzle end was also the least complex mechanically.

5) The n gas passage diameters were the same and hence not optimized. The walls of the inner gas passages are 40°C hotter than the outer ten. The inner 6 passages can be increased in diameter to increase their flow. This could adjust the heater

walls to the same maximum temperature uniformly. This would increase the net gas temperature about 15°C, but is not included in the results of D2 here.

The net effect of the optimization study to arrive at Configuration D2 was to:

1) Increase the specific impulse from 159 to 168 seconds, a propellant savings of 5.6%.

2) Increase the overall thermal efficiency from 76.7% to 82.7%, a power savings of 7.8%.

3) Give a reduction in maximum case temperature from 746°K to 684°K.

Starting cycle analysis.- Since the starting cycle has been often suggested as a problem for this design, a thorough transient thermal analysis was undertaken. Such an analysis is much more difficult for any device than a steady state one. It was only undertaken in this study for Concept 1 to show that the application of this resistojet potentially to space station is readily accommodated.

The application of resistojets to manned space stations do not require fast thermal response based upon the results of the MORL studies (ref. 6). Their long firing times for drag makeup, for control moment gyro desaturation, etc., represent the bulk of the total impulse requirement. Only small percentages of the total impulse requirement were used for roll control where a fast response might be required. It is for this reason that in the study the unscheduled mode for fast response and specific impulse was included as well as the scheduled one.

These modes were studied to provide current systems trade-off response data. A summary of permissible thruster operating states is defined in table 10 to study how to provide for these modes. Also summarized are the resulting performance figures determined during the analysis.

Table 11 summarizes the transient operation times between the important states with citations to the included results in figures and tables. These transitions between states were studied as a series of solutions of temperature distributions through the resistojet at the intervening time intervals. The special transient analysis, as well as the steady state type analysis, was required to find the asymptotic value. The times cited refer to temperature conditions which are within approximately 3% of the steady state values as a somewhat arbitrary, practical criteria.

TABLE 10
SUMMARY OF CONCEPT 1 OPERATING STATES
DATA SHOWN FOR CARBON DIOXIDE

| State | Powered heater control temperature | | Expellant flow (g/s) | Electric power status | | Specific impulse (s) |
|----------------------|------------------------------------|-----------|----------------------|-----------------------|----------|----------------------|
| | Preheater (°K) | Main (°K) | | Preheater (W) | Main (W) | |
| 1. Rest (cold-300°K) | - | - | 0 | 0 | 0 | - |
| 2. Intermediate hold | 1250 | - | 0 | 80.4 | 0 | - |
| 3. Intermediate hold | - | 1250 | 0 | 0 | 22.6 | - |
| 4. Design | - | 1573 | .1319 | 0 | 181.3 | 167.5 |
| 5. Uprated design | - | 2000 | .0839 | 0 | 254.9 | 192.5 |
| 6. Redundant | 1250 | - | .16 | 166.6 | 0 | 133.0 |
| 7. Redundant | - | - | .31 | 0 | 0 | 63.8 |
| 8. Design hold | - | 1573 | 0 | 0 | 46.9 | - |

TABLE 11
TRANSIENT OPERATING MODES BETWEEN STATES
DATA SHOWN FOR CARBON DIOXIDE

| Initial State | Final State | Figures | Tables | Transient Time (s) |
|---------------|-------------|---------|--------|--------------------|
| 1 | 2 | 14 | 13 | 180 |
| 1 | 4 | 13 | 12 | 195 |
| 2 | 4 | - | 14 | 5 |

The operational algorithms are summarized below for each of the transitions between states. The reasoning behind these are reviewed showing the sequence of power scheduling, flow initiation, etc.

Power initiation from rest (1) to the design state (4): Table 12 describes the programming of the preheater power, expellant flow and main heater power for a full start from the rest state.

TABLE 12
 POWER AND FLOW HISTORY DURING START UP
 FROM REST (1) TO DESIGN (4)
 DATA SHOWN FOR CARBON

| Time (s) | Flow (g/s) | Voltage (V) | Preheater | | | Main Heater | | |
|-----------------|---------------|----------------|----------------|--------------|----------------|----------------|--------------|--|
| | | | Current (A) | Power (W) | Voltage (V) | Current (A) | Power (W) | |
| 1 | 0 | 140 | 7.442 | 1041.9 | 220 | 0 | 0 | |
| 10 | 0 | 140 | 4.886 | 684.0 | 220 | 0 | 0 | |
| 60 | 0 | 140 | 2.902 | 406.2 | 220 | 0 | 0 | |
| 120 | 0 | 140 | 2.389 | 334.5 | 220 | .003 | 0.7 | |
| 180 | 0 | 140 | 2.158 | 302.1 | 220 | .313 | 68.9 | |
| 186.9 | .1319 | 140 | 2.137 | 299.2 | 220 | .716 | 157.5 | |
| 189.1 | .1319 | 0 | 0 | 0 | 220 | 1.092 | 240.3 | |
| 240 | .1319 | 0 | 0 | 0 | 128 | 1.18 | 151.0 | |
| Steady State | .1319 | 0 | 0 | 0 | 153.3 | 1.182 | 181.3 | |

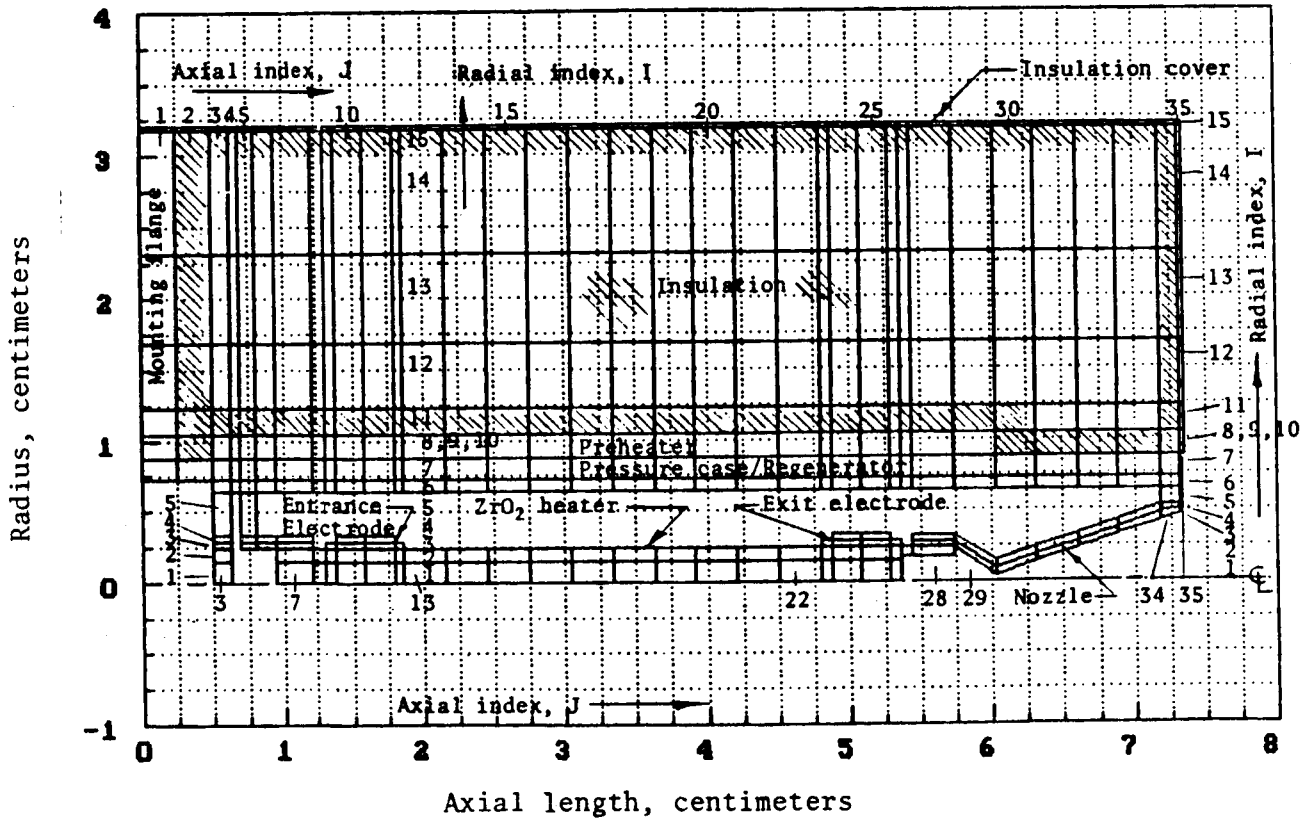
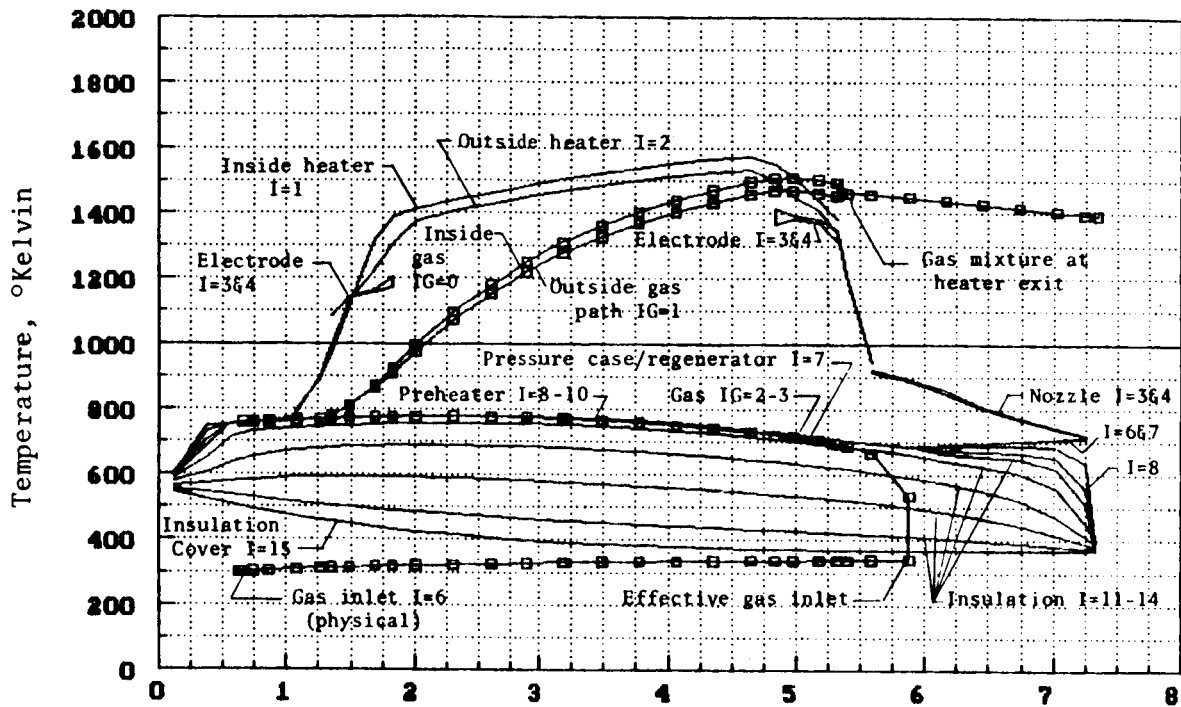
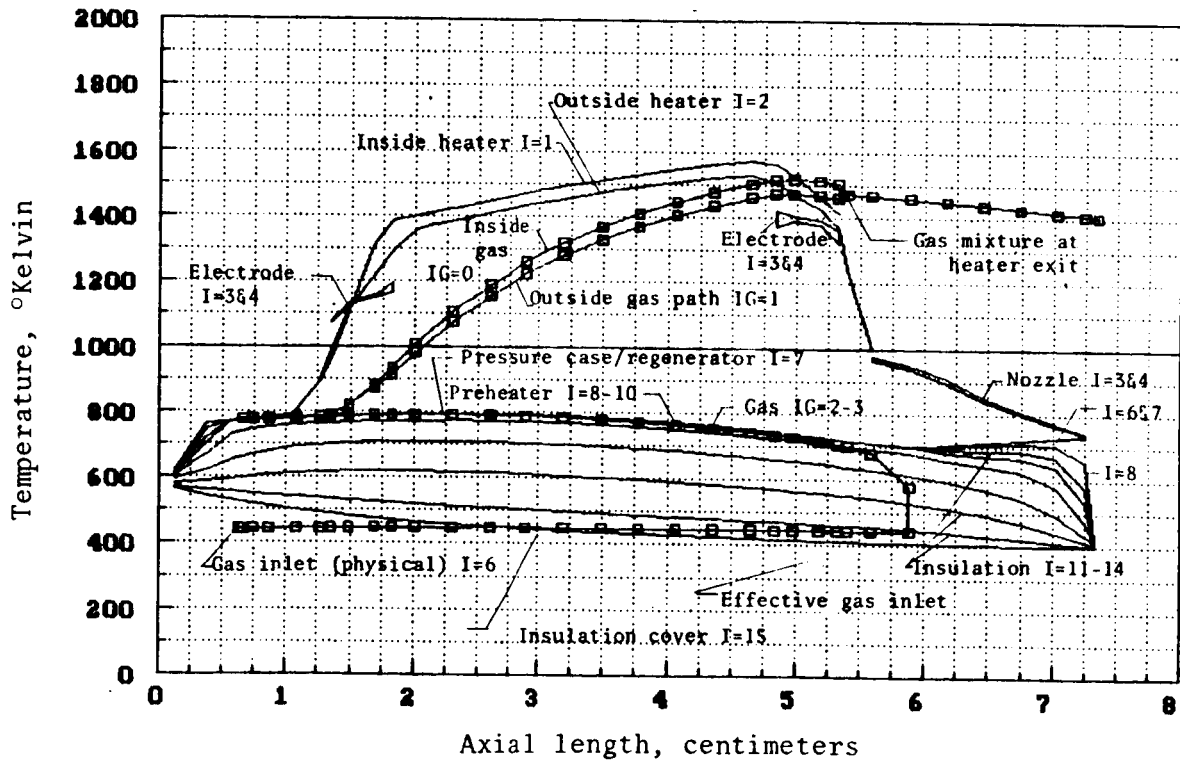


Figure 10. - Thermal node diagram used in the analysis of Concept 1 Configuration D2.



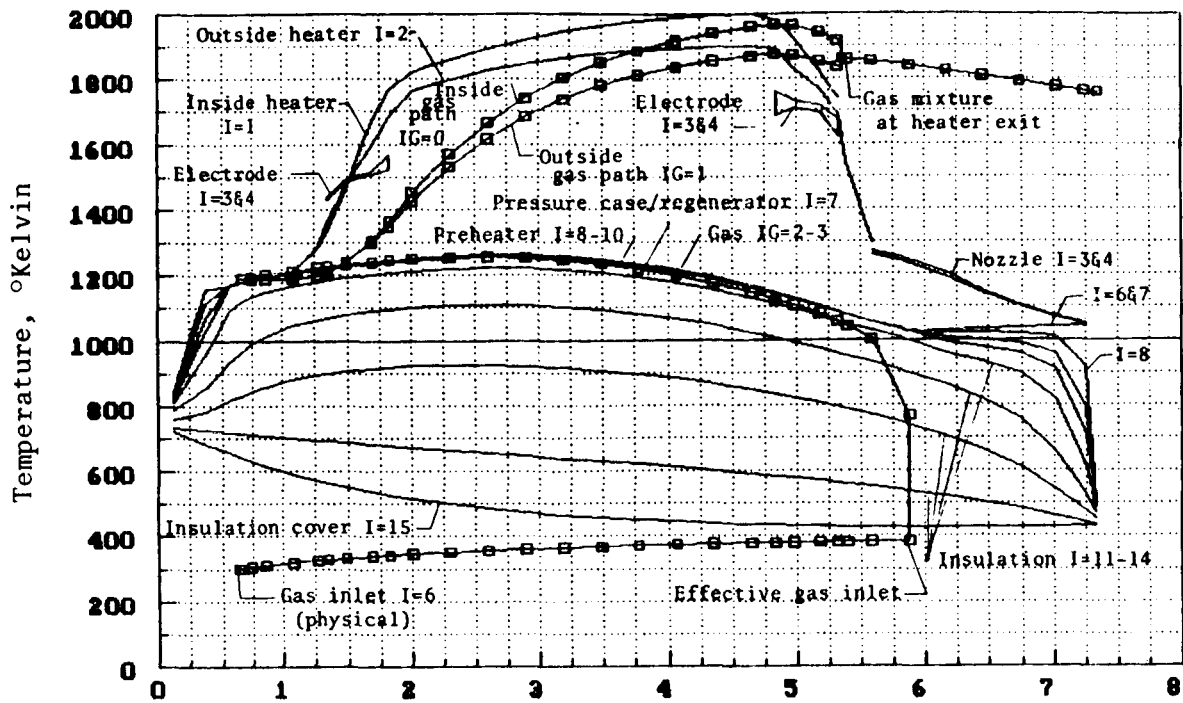
a) Carbon dioxide



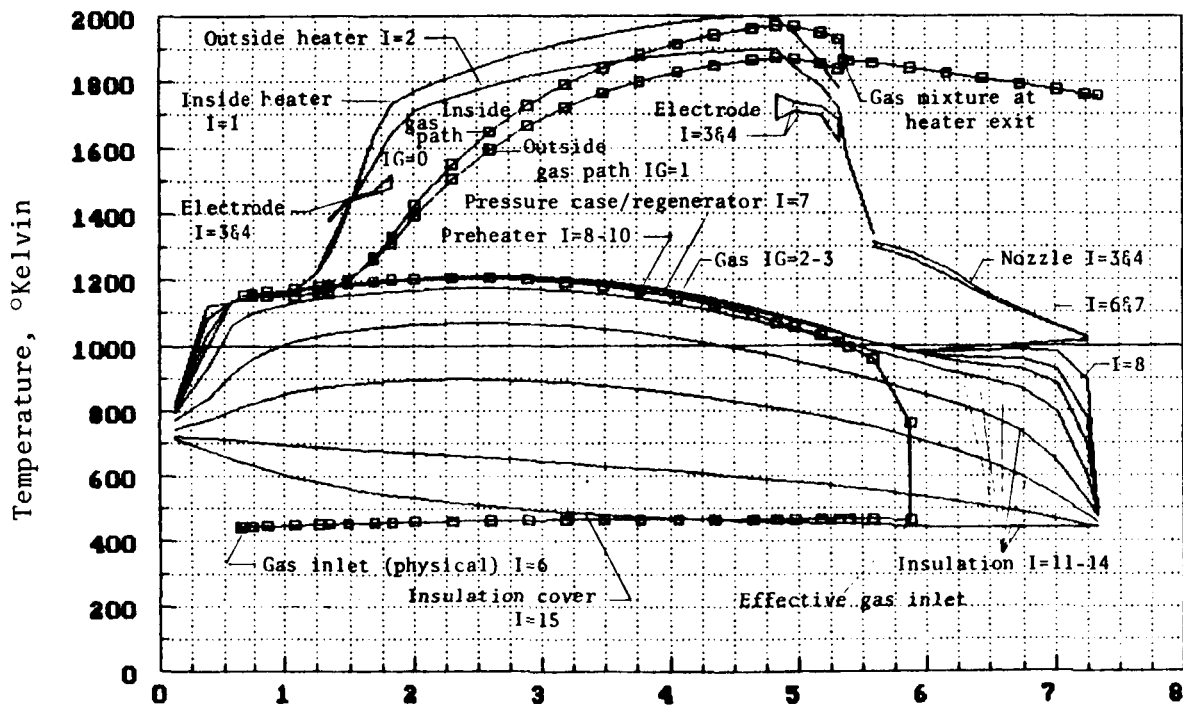
b) Steam

Figure 11. - Resultant temperature distribution of Concept 1 Configuration D2 operating at a design maximum heater temperature of 1573°K (1300°C).

ORIGINAL PAGE IS
OF POOR QUALITY



a) Carbon dioxide



b) Steam

Figure 12. - Resultant temperature distribution of Concept 1 Configuration D2 operating at an advanced performance of maximum heater temperature of 2000°K.

It was found that delaying the start of propellant flow at state 1 substantially reduced the starting time. For the first analysis of this operating starting mode, only judgmental efforts, not rigorous ones, were made to improve the procedure. The initial start required somewhat high power from the preheater system because it was allowed to proceed at constant voltage. The initial resistance of the preheater was low. The power consumption dropped off as the resistivity of the preheater increased with temperature. The maximum preheater temperature limit was 1350°K. The main heater starts to conduct at approximately 75 seconds. Flow was initiated when the main heater current reached approximately 60% of design condition and the preheater shut down. No expellant flows until 186.9 seconds. Up to this time, preheater power is applied at 140 volts. The main heater assumes full responsibility and for all practical purposes, full specific impulse is reached at 189 seconds.

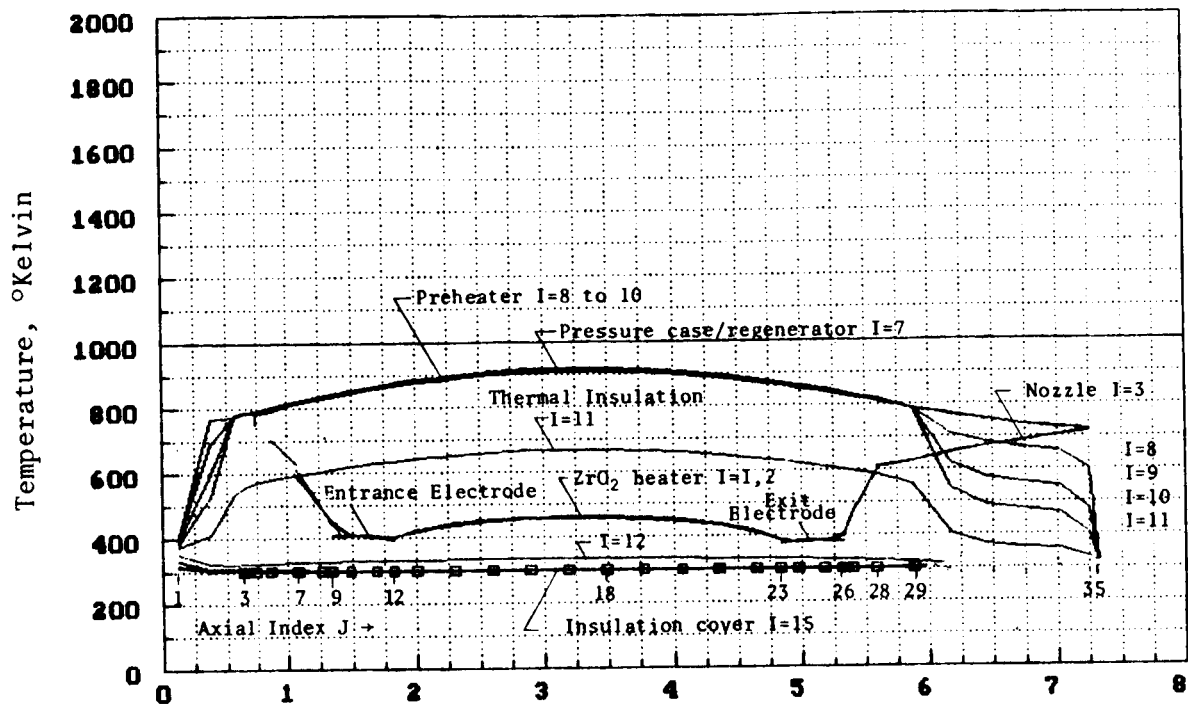
If the initial power level is limited to, say 400 watts above while the preheater itself is cool and thus low resistance, the start is estimated to require 60 seconds longer than that indicated.

The temperature profiles through the thruster are shown in figures 13a through d. Figure 13 also shows the corresponding nodal physical positions in the thruster. The supporting tabular presentation of auxiliary data is found in table 13 for the same corresponding time intervals.

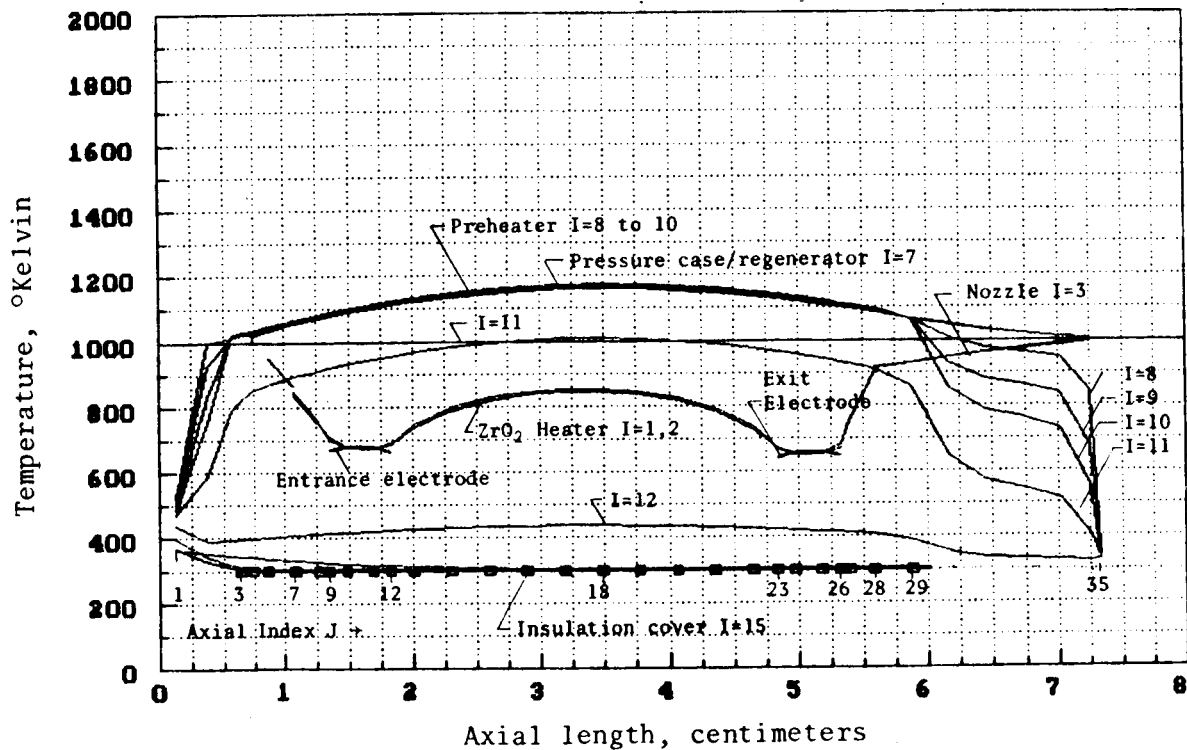
Power initiation from rest state (1) to an intermediate hold state (2): The purpose is to place the thruster in a standby mode by preheater power only from which thrust and specific impulse may be obtained readily by main power initiation. The temperature distribution with time is identical with the case of start from rest (1) to design state (4) for the first 120 seconds because during this period there is no main heater power. Figures 14a and b describe this interval. At 180 seconds the difference between figure 14a of this transition and figure 13c for full start from rest is not too different as is seen. Figure 14b shows the steady state condition of state 2.

Table 13 shows preheater electric variables and power during this transition for the assumed algorithm of full voltage until a preheater limit of 1250°K is reached after which it is temperature controlled. Other algorithms, such as an initially constant power limit, were not explored.

This transition has no pressing time requirement. Its end state is a hold. If full operation is required during this transition, reversion to full start settings are simply made and maximum time is again 189 seconds from rest as in from state 1 to state 4.

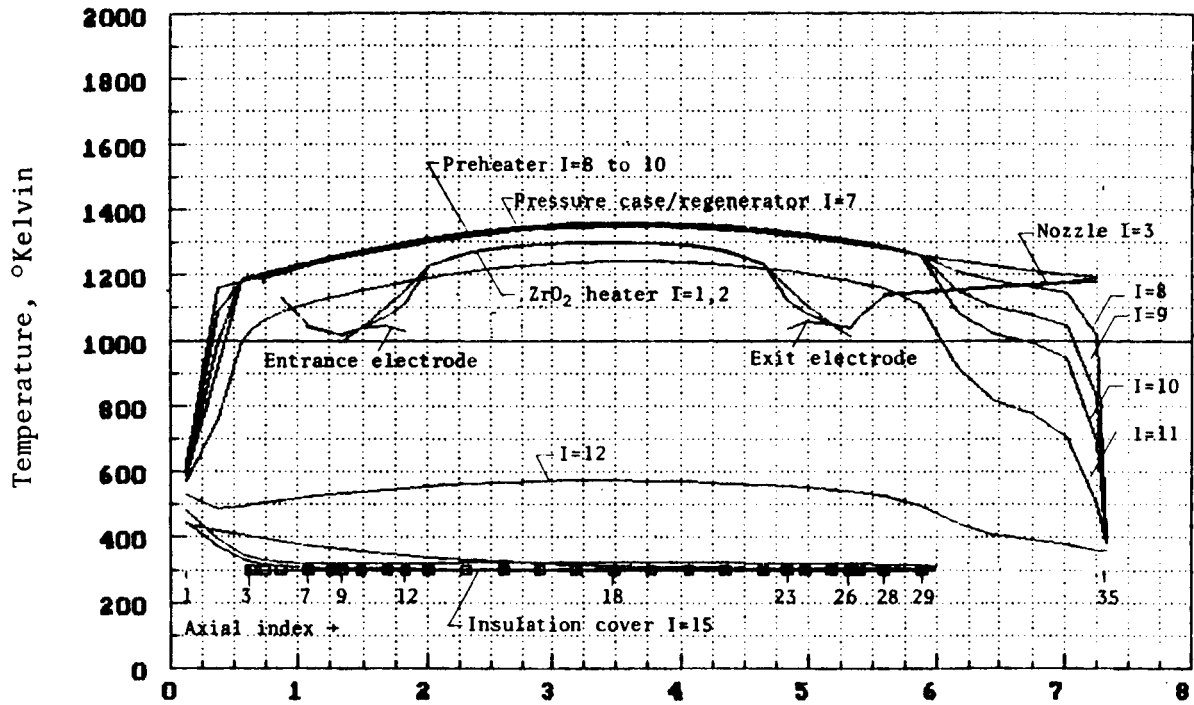


a) 60 seconds

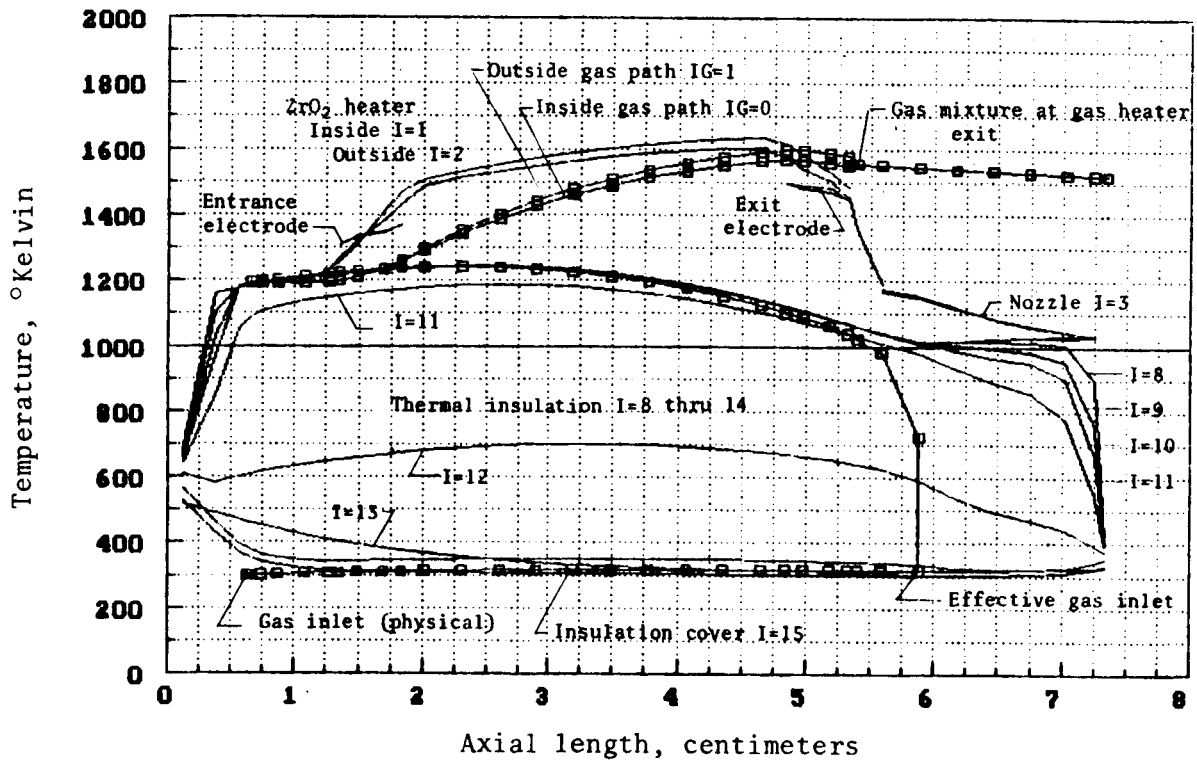


b) 120 seconds

Figure 13.- Transient temperature distribution sequences from power initiation from rest (state 1) to design (state 4). Times shown are from start.

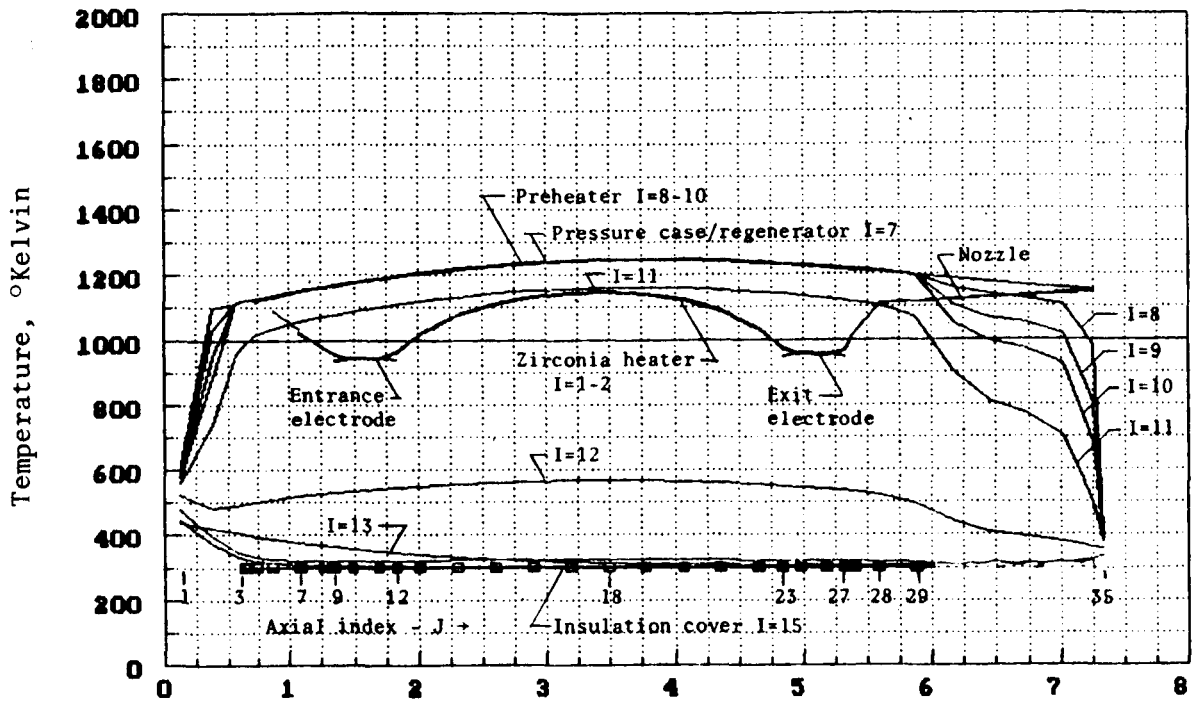


c) 180 seconds

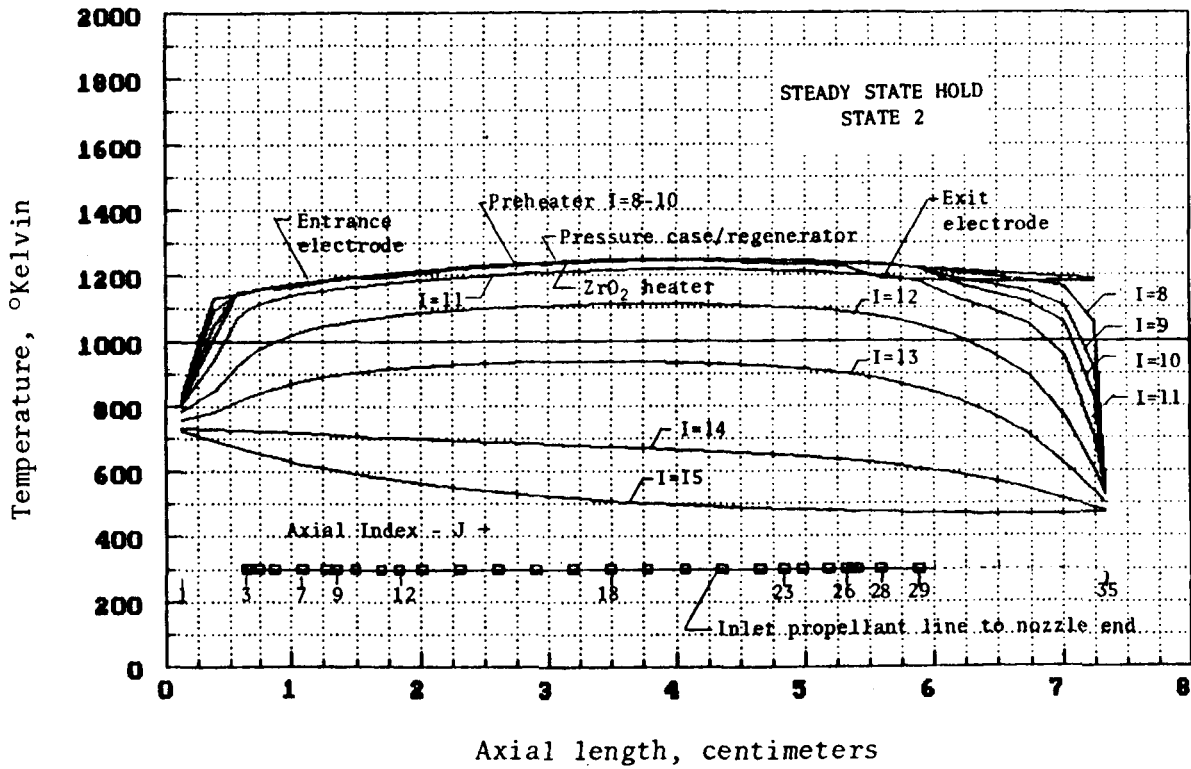


d) 240 seconds

Figure 13. - Concluded.



a) 180 seconds from start



b) Steady state (2), intermediate hold state

Figure 14. - Transient temperature distribution sequence from power initiation from rest (state 1) to intermediate hold (state 2) powered by preheater (1250°K) only.

TABLE 13
 PREHEATER POWER DURING STARTING
 FROM REST (1) TO INTERMEDIATE HOLD (2)

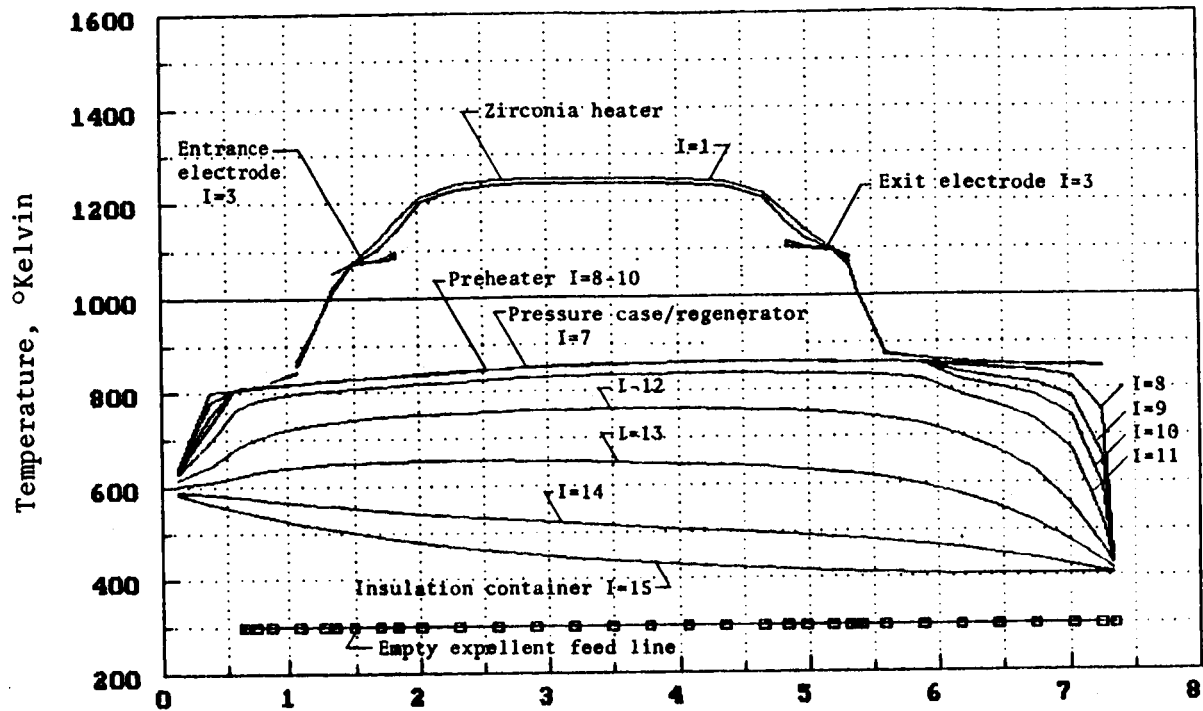
| Time (s) | Voltage (V) | Current (A) | Power (W) |
|-------------|----------------|----------------|--------------|
| 1 | 140 | 7.442 | 1041.9 |
| 10 | 140 | 4.886 | 684.0 |
| 60 | 140 | 2.902 | 406.2 |
| 120 | 140 | 2.390 | 334.5 |
| 180 | 86.21 | 1.400 | 120.7 |
| 240 | 74.84 | 1.214 | 90.9 |
| 300 | 70.44 | 1.142 | 80.5 |

Intermediate hold state (1250°K): There are two means to hold Concept 1 at this steady readiness state of 1250°K. These are by the preheater (state 2) or the main heater (state 3). The temperature distributions within Concept 1 for state 2 and 3 are shown in figures 14b and 15a. The important difference between the two states which serve the same purpose is the power requirement. Low power drain is the selection criteria. Case 2 requires 80.4 watts while case 3 only 22.6 watts!

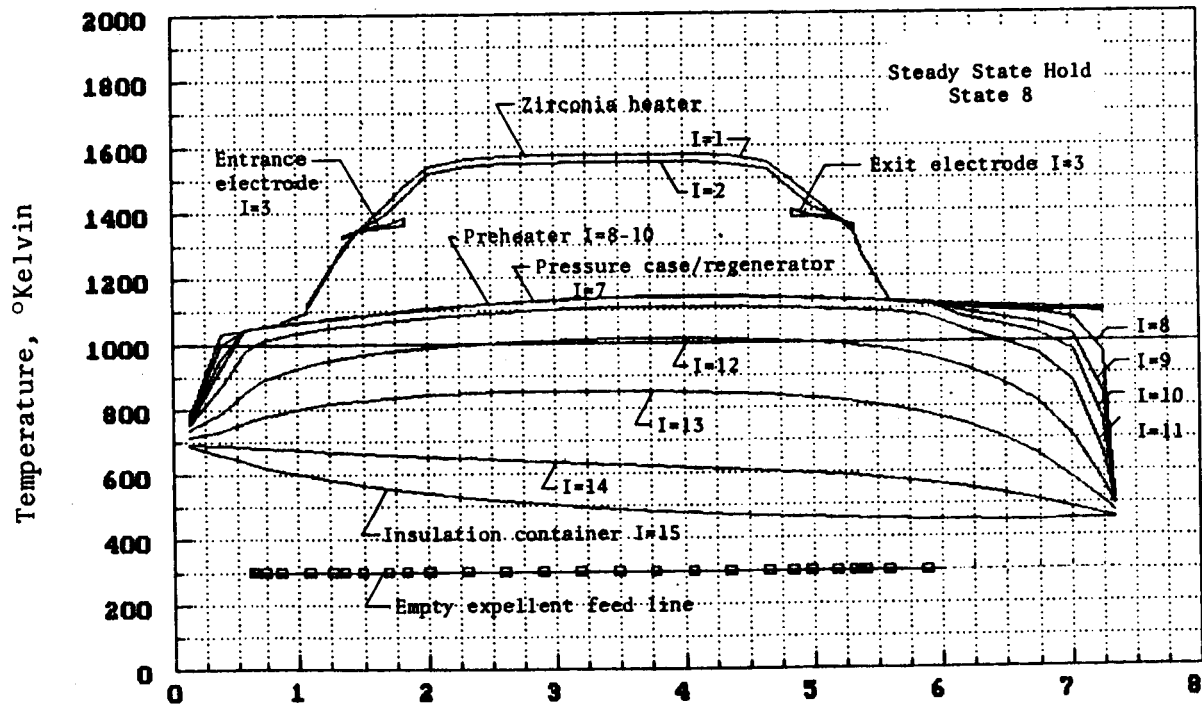
Case 3 is the clear choice not only on lower power but lower temperature of the regenerator-pressure case, a reliability consideration. The case holding temperature is reduced from 1250°K to 1150°K thereby. Case 2 is simply academic as a pass-through state to create state 3.

Transition from intermediate hold state (2) to design state (4): Table 12 shows the power flow history during the transition from the intermediate hold state (2) to the design state (4). In 5 seconds the thruster is at full performance, if 2.5 seconds is anticipated before initiation of propellant flow.

In the algorithm selected it is possible to consider full thrust immediately from this condition but with a slower than 5 second overall response to full specific impulse. This transition is not studied further here because of the importance of state 8 (full temperature, no flow) from which virtually instantaneous thrust and specific impulse can be obtained for a cyclic mode.



a) Intermediate hold at 1250°K (state 3)



Axial length, centimeters

b) Design hold at 1573°K (state 8)

Figure 15.- Temperature holding states by main heater only.
No flow.

TABLE 14
 POWER AND FLOW HISTORY DURING START-UP
 INTERMEDIATE HOLD (2) TO DESIGN (4)
 DATA SHOWN FOR CARBON DIOXIDE

| Time (s) | Flow (g/s) | Preheater | | | Zirconia Main Heater | | |
|-------------|---------------|----------------|----------------|--------------|----------------------|----------------|--------------|
| | | Voltage (V) | Current (A) | Power (W) | Voltage (V) | Current (A) | Power (W) |
| 1 | 0 | 140 | 2.253 | 315.1 | 220 | .519 | 114.2 |
| 4 | .1319 | 140 | 2.234 | 312.7 | 220 | .862 | 189.4 |
| 5 | .1319 | 0 | 0 | 0 | 220 | 1.028 | 226.1 |
| 15 | .1319 | 0 | 0 | 0 | 142.7 | 1.18 | 168.4 |

Design hold state 8: The main heater may hold the thruster at full design temperature of 1573°K (at no flow) for 46.8 watts and be ready for instantaneous thrusting at full specific impulse! Recall that state 3 requires only 22.6 watts but is 5 seconds from full specific impulse. See figures 15a and b.

Conclusions with regard to starting: The systems applications engineer must ultimately make the final selection of best overall operating schedules. Where the duty cycle is heavy and fast response and thrust cannot be readily anticipated as to schedule, the condition of holding at state 8, a design temperature hold state, is recommended. Power losses are low, the thrust and specific impulse response are high. From MORL studies (ref. 6) roll control was a small total impulse requirement and not a driving requirement.

Where firing times are long and separated by long periods of no thrust, the power-up mode from rest to design is recommended. Where firing times are long and only separated by short inactive periods, state 3 is recommended as the hold state. Power-up to design from this condition will take ≈5 seconds. Reliability will be enhanced by avoidance of heavy thermal cycling.

Reliability by means of redundancy.- Note that the inclusion of a preheater permits an additional powered mode at 1250°K heater temperature (state 6) as a redundant liability feature of the design. This powered mode will produce a specific impulse of 133 seconds (CO₂) and meets contractual goals. The power required is 166.6 W and the gas total temperature is 1001°K! See figure 16 for the thermal distribution of this mode, state 6.

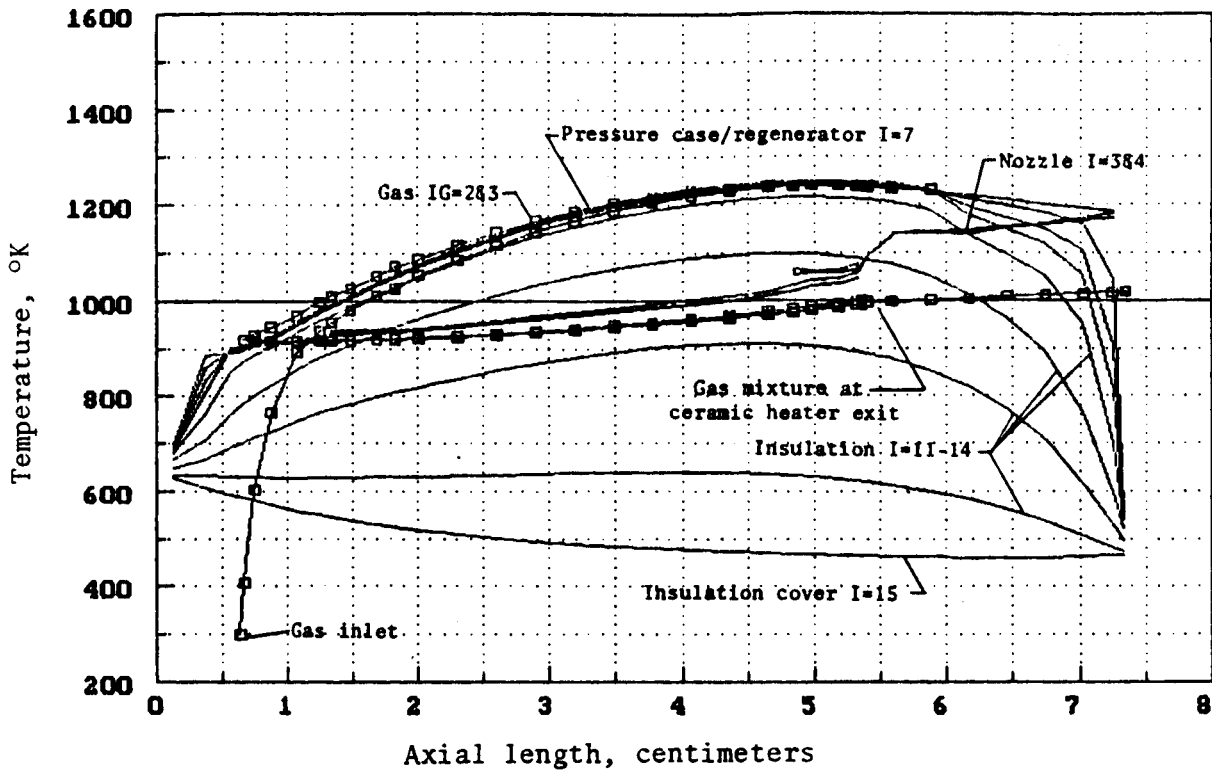


Figure 16. - Preheater powered thrusting mode (state 6).

Gas Dynamic Analysis

The local gas flows through the thruster were taken into account during the thermal analysis in the mathematical computational modeling. A summary of the parameters is shown in table 15 for a design heater temperature of 1573°K and mass flow of 0.131 grams per second.

TABLE 15
SUMMARY OF FLUID FLOW PARAMETERS
DATA SHOWN FOR CARBON DIOXIDE

| Station | Total temp. (°K) | Total pressure (Atm.) | Total pressure (Psi) | Mach no. (Avg) | Flow area, A _r (cm ²) | Reynolds Number |
|----------------|------------------|-----------------------|----------------------|----------------|--|-----------------|
| Inlet line | 300 | 3.18 | 46.68 | .05 | 17.87x10 ⁻³ | 7436 |
| Ceramic heater | | | | | | |
| Inlet | 761.1 | 3.17 | 46.53 | | 21.28x10 ⁻³ | 1083 |
| Outlet | 1492.2 | 3.01 | 44.24 | .099 | 21.18x10 ⁻³ | 573 |
| Nozzle throat | 1442.9 | 3.00 | 44.09 | 1.00 | 3.80x10 ⁻³ | 5898 |

The results on H₂O steam are similar with the pressure drop inconsequential.

Note that the flow is laminar in the ceramic heater and that the flow passages before the nozzle are below a Mach number of 0.10. This results in a rather low pressure drop in the design. This is seen to be beneficial structurally in the next section.

The problem of the stability of the laminar compressible flow with friction and heat addition in parallel passages with equal pressure drops (the so-called nuclear rocket problem) (ref. 28) was investigated in reference 14. It was found to be stable. The type of flow stability problem can be thought of as one arising from the negative flow resistance characteristics of such a system under certain combinations of conditions. The stability criterion depends only on the temperature exponent of viscosity of the propellant gas in question and the temperature ratio across the heater. Analysis of Concept 1 shows it meets this flow stability criterion as well.

Mechanical Design

The structural design in reference 14 was found more than adequate, hence, is not repeated here in keeping with the broad investigative nature of the study.

Chemical Corrosion, Sublimation and Deposition

Since the zirconia heater is an oxide, it resists chemical reactions with the oxygen based biowaste propellants. This allows higher temperatures to be used than would be feasible with any metallic heaters such as stabilized platinum. It is for this reason that this design was presented first. The high performance capability of this design suggests a highly reliable design at the reduced temperature of 1573°K chosen contractually as design.

Compatibility with H₂O (steam), CO₂ and vacuum has been experimentally demonstrated to 1935°K for 500 hours without failure (ref. 13.).

The ceramic heater at 2000°K with a recession rate of 2x10⁻⁴ millimeters per second in a vacuum is expected to operate for 4000 hours and about 10 times longer at a gas pressure of 3 atmospheres for a 10% reduction in cross sectional area. Life tests in air have achieved 7000 hours without ceramic failure. The platinum heater element wire is expected to last 1x10⁴ hours under the same criteria with careful design of the electrodes.

No deposition studies were undertaken within the scope of the investigation.

Rating

Advantages.- (1) The heating element resists oxidation, so is expected to have longer life and to be able to run at higher temperature than would be feasible with a metallic element. Thus, it provides significant growth potential. Although metal electrodes are required, it has been found feasible to design the unit with lower temperature at the electrode contact locations for reliable operation even at advanced design (2000°K).

(2) A zirconia element has high electrical resistivity, so is readily designed to operate with a high voltage and a low current. This permits small light leads and small lead losses.

(3) High resistivity in the heating element also allows a compact lightweight thruster design with low thermal losses to be used. There is no need to lengthen the heater (or otherwise increase its size) to achieve an acceptable operating voltage.

(4) A backup heater is available from the preheater providing a redundant mode for increased reliability that can provide the goal specific impulse.

Disadvantages.- (1) A zirconia heating element is nonconductive at room temperature. It requires a conventional metallic heater for starting. This results in a more complicated system, and a time delay during start-up. The metallic heater can be outside of the gas path, so the advantages listed above are not negated.

(2) An alternating current power supply is required for the zirconia heating element.

APPENDIX B

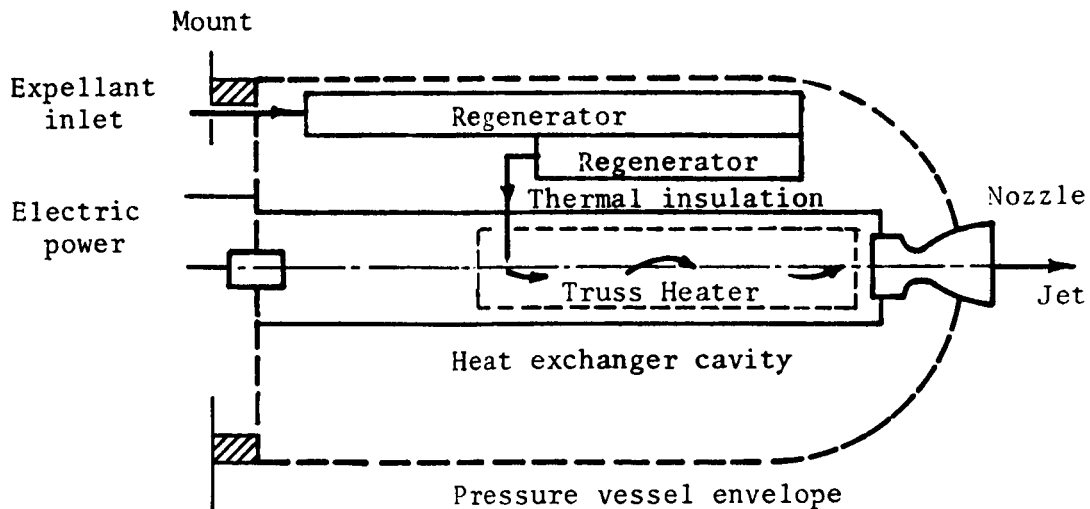
CONCEPT 2 - EXPOSED METALLIC TRUSS HEATER IN EXTERNAL CROSS FLOW

This new design is based upon two novel features. These are the radially inverted functional design and the truss heater. This biowaste resistojet uses the metal-oxide grain stabilized platinum for the highest temperature components as contrasted to Concept 1 where ZrO_2 is used.

The pressure case is its outermost member. The wide passages regenerators are adjacent and interior to the pressure case. All thermal insulation is contained within these. It is radially inverted from all others here except Concept 3. The inverted approach results in a pressure vessel of low temperature and, consequently, one of implied higher structural reliability. No pressure balancing considerations are required within the design to prevent creep of the critical inner elements.

The truss heater here is a wire heater which is structurally designed for transverse strength yet axial compliance and high electric resistance. This design eliminates all electrical insulators from the high temperature zone. The radially broad regenerators, when cool expellant inlet gas of low thermal conductivity are used, provide better thermal insulation and cooler cases than the traditional design order. Flow splitters shown are used to minimize free convection during ground testing. This approximates the freedom from free convective heat transfer experienced in space.

The schematic below illustrates these above functional relationships.



Description

A preliminary layout drawing of Concept 2 is shown in figure 17. Table 16 identifies its components and materials. The heating element area envelope has been outlined. At the end of this section, the details of this truss type heater are best described in the developed sections in figures 18 and 19 and in table 18.

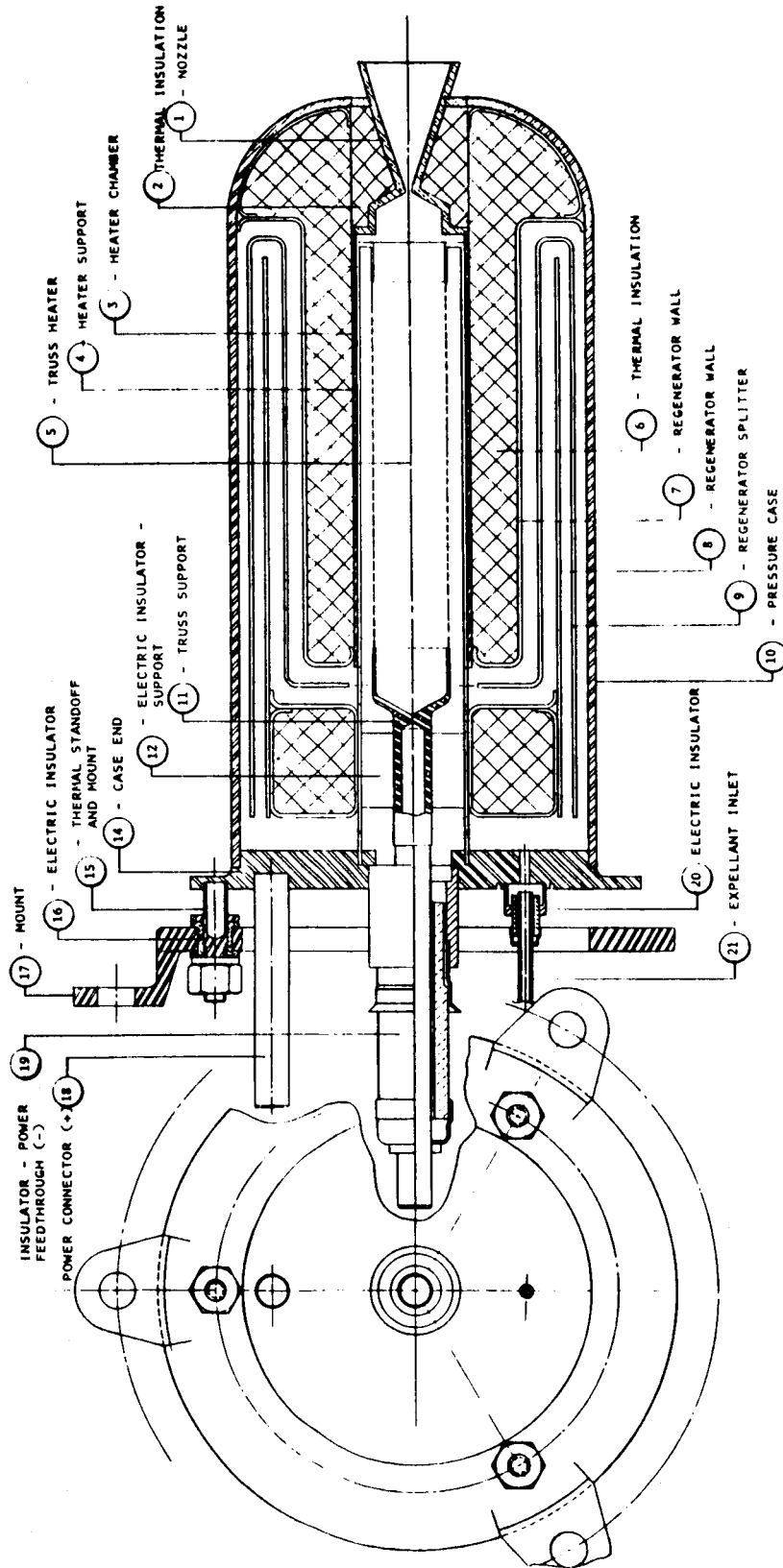
TABLE 16
CONCEPT 2 - COMPONENT PARTS, MATERIALS OF CONSTRUCTION

| <u>Item</u> | <u>Component</u> | <u>Material</u> |
|-------------|-----------------------------------|--|
| 1. | Nozzle | Grain stabilized platinum |
| 2. | Thermal insulation | Min-K 2000 ¹ |
| 3. | Heater chamber | Grain stabilized platinum |
| 4. | Heater outer support and return | Grain stabilized platinum |
| 5. | Truss heater | Grain stabilized platinum |
| 6. | Thermal insulation | Mink-K 2000 ¹ |
| 7. | Inner regenerator wall | AISI 321 |
| 8. | Regenerator wall | AISI 321 |
| 9. | Regenerator splitter | AISI 321 |
| 10. | Pressure case | AISI 321 |
| 11. | Truss support | Nickel 200 |
| 12. | Electric insulator - support | Alumina 99.5% |
| 14. | Case end | AISI 321 |
| 15. | Thermal standoff and mount | AISI 321 |
| 16. | Electric insulator for case mount | Delrin |
| 17. | Mount | AISI 321 |
| 18. | Power connector (+) | Nickel 200 |
| 19. | Insulator - power feedthrough (-) | Metal to ceramic seal materials ² |
| 20. | Electric insulator | (TBD) |
| 21. | Expellant inlet line | AISI 321 |

1. Data for Min-k 2000, Johns-Mansville Aerospace Products, N.Y., NY.

2. Typical materials: nickel A conductors; glazed high alumina ceramic (85% min. Al₂O₃) insulators; vacuum tube grade brazing alloys and nickel-iron caps. Data from Ceramaseal, Inc., New Lebanon Center, NY.

The pressure envelope is now formed, unlike early resistojet designs, by the outermost member (-10). This being the coolest location, this case can be designed out of conventional high grade stainless steels. The case end (-14) insulator power feedthrough and the nozzle (-1) complete the pressure envelope. The regenerator consists of a wide annular passage passing from



Scale: Full Size

Figure 17. - Concept 2, a biowaste resistojet using grain stabilized platinum with truss heater in external cross flow.

the mount toward the nozzle immediately within the pressure case, and hence, returning in a second pass back to the zone of the heat exchanger inlet. All fibrous thermal insulation (-6) is radially contained between the regenerator and the nonpressurized heater chamber (-3). The truss heater (-5) is mounted within the heater chamber supported by its truss support (-11) and at the nozzle end by the heater outer support and return (-4) as shown.

The power feed connection (high) is by means of the feedthrough (-19) which also serves as the rear support to the truss heater. The principal voltage drop occurs across the truss heater (-5). The return to the ground side of the power feed, the terminal, (-18) is primarily through the heater outer support and return (-4) and case end (-14). The resistojet itself is thermally and electrically isolated from the mount (-17) by means of which it is mounted to the spacecraft. Note that the propellant feedline similarly must be electrically isolated to avoid ground loops. Shown is an example of such an isolation (-20). This function could occur at a number of sites.

The dimensions of the outer package are summarized in the table that follows.

TABLE 17
DIMENSIONS OF INSULATION, REGENERATOR AND PRESSURE CASE

| Description | Diameters ¹ | | Length ¹ |
|--|------------------------|---------------|---------------------|
| | Inside mm | Outside mm | |
| Heater chamber | 15.3 | 16.5 | 84.5 |
| Thermal insulation | 16.3 | 29.2 | 61.0 |
| Inner regenerator wall | 29.2 | 30.4 | 61.0 |
| Regenerator (1st and 2nd pass) separator wall | 39.8 | 41.0 | 62.0 |
| Pressure case | 48.1 | 50.4 | 105.4 |

1. Part dimensions are functional ones.

The description of the truss wire heating element is presented next. Its electrothermal design is discussed under thermal analysis.

The heating element area is shown only in outline in figure 17. The truss heater is designed so as to be a nonredundant structure. It is free to expand axially due to temperature expansion along the thrust direction, but because of its lateral stability, resists movement radially within the heater cavity.

In effect, a series of elements in a family of nine electrically parallel systems span the inlet support to the exit. They are joined with each other many times during the course of the span in a nonredundant way such as to satisfy structural stability, join nodes of equal electrical potential, in a cyclic repeating pattern. The design, while complex in appearance, can be simply wound on a sacrificial mandrel which is later dissolved away. Following is the description of one such design.

Geometry of the truss type heating element.- The configuration for the heating element consists of a truss with the links arranged at a shallow angle to the tangential. This is done to provide an acceptable operating voltage. It is much more rigid than the usual simple coil (but not bicoil) type of heater, and some flexibility can be advantageous as a simple means of providing for thermal expansion without the development of excessive thermal stresses.

The truss geometry can be described as a series of junction points arranged on an imaginary cylindrical surface and joined by a repeating pattern of connecting links. Each junction point in the center region joins six links, giving the total number needed to provide a rigid truss with no redundancy. The location of the junction points is described in the table below in cylindrical coordinates. All junction points are at a radius of 0.5 cm. For brevity, only approximately the first and last cycles are shown in the table to illustrate the construction. The others can be simply constructed from these.

There are a total of 307 links connecting the junction points, including ten (five at each end) that connect to a stationary mounting base at one end. The links are made of platinum wire for biowaste applications, and of rhenium wire for high temperature applications where the heater is not subjected to an oxidizing gas (when hydrogen or hydrazine are used as the propellant).

The electrical current follows nine parallel paths through the main body of the truss. The paths are of three types as described below. The truss geometry and the wire diameters are selected in a manner that tends to keep the wire temperature variation the same for the nine paths.

1) There are two right hand helix type paths made up of links that join junction points in the order listed in the above table. Both of these helical paths are made up of 50 links, each of which is 5.56 mm long by .254 mm (0.10 in.) in diameter.

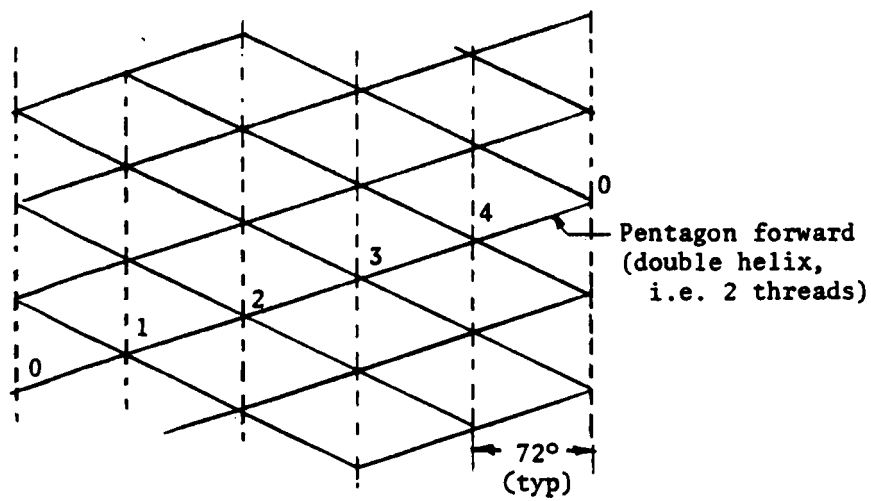
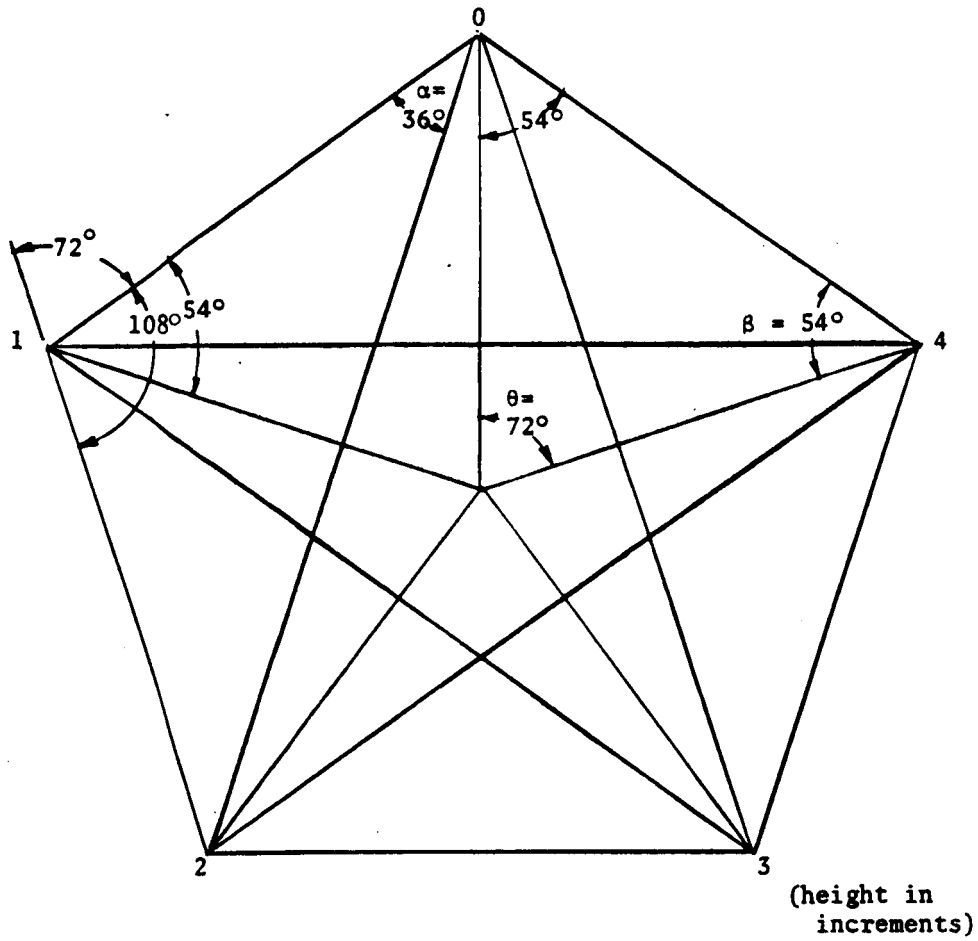
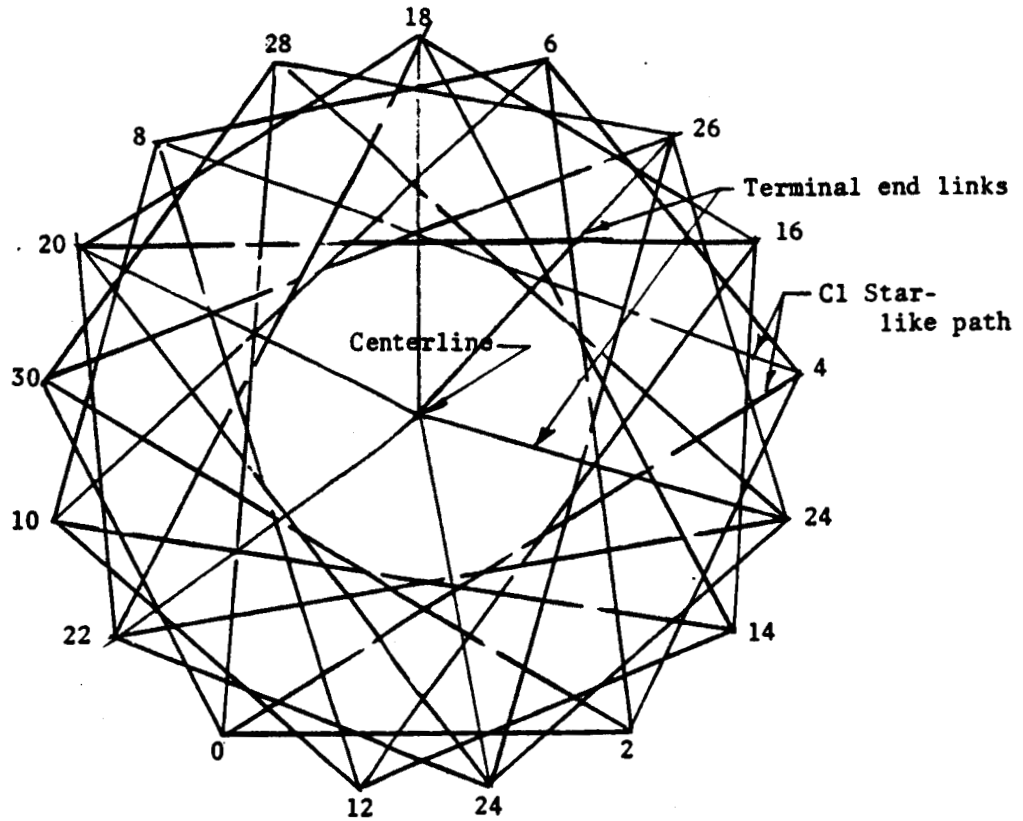
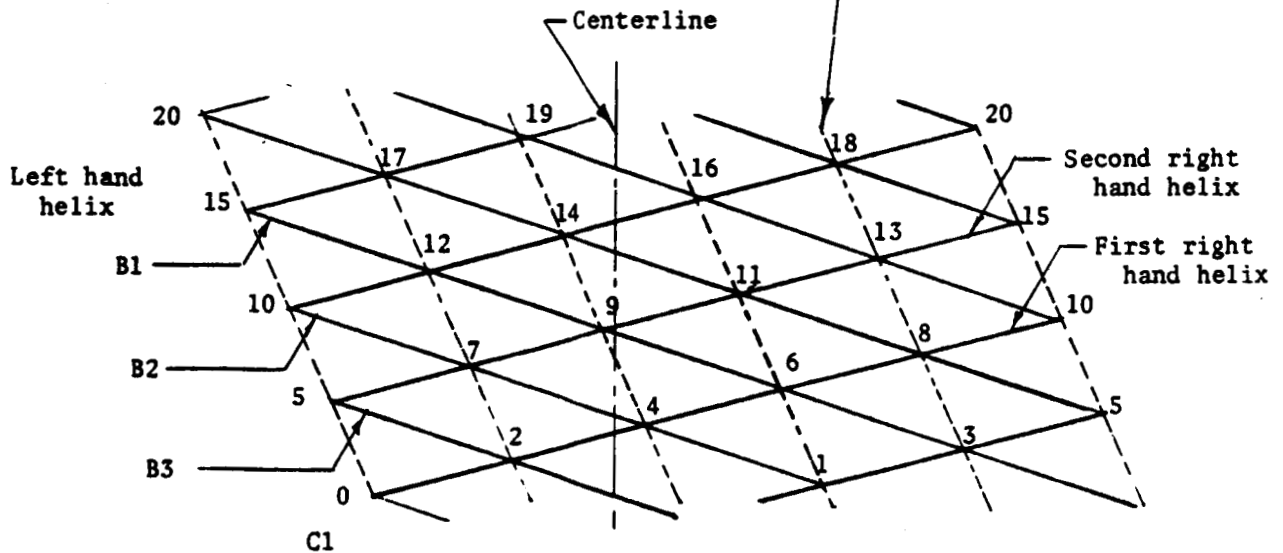


Figure 18. - Pentagon truss with no axial twist.



a) End view of one right hand helix with star-like paths shown as well

Note: Dotted lines show node alignment only.



b) Developed surface of imaginary cylinder of nodes.

Figure 19. - Continuous pentagon truss with twist. (See text).

TABLE 18
TRUSS GEOMETRY

| Junction points on the first right hand helix | | | Junction points on the second right hand helix | | |
|--|-------------------------|----------------------------|---|-------------------------|----------------------------|
| Junct. number | Axial locat. (cm) | Angular locat. (deg) | Junct. number | Axial locat. (cm) | Angular locat. (deg) |
| 0 | 0 | 0 | 1 | 0.05 | 211.76 |
| 2 | 0.10 | 63.53 | 3 | 0.15 | 275.29 |
| 4 | 0.20 | 127.06 | 5 | 0.25 | 338.82 |
| 6 | 0.30 | 190.59 | 7 | 0.35 | 42.35 |
| 8 | 0.40 | 254.12 | 9 | 0.45 | 105.88 |
| 10 | 0.50 | 317.65 | 11 | 0.55 | 169.41 |
| 12 | 0.60 | 21.18 | 13 | 0.65 | 232.94 |
| 14 | 0.70 | 84.71 | 15 | 0.75 | 296.47 |
| 16 | 0.80 | 148.24 | 17 | 0.85 | 0 |
| 18 | 0.90 | 211.76 | 19 | 0.95 | 63.53 |
| .. | | | .. | | |
| .. | | | .. | | |
| 92 | 4.60 | 42.35 | 93 | 4.65 | 254.12 |
| 94 | 4.70 | 105.88 | 95 | 4.75 | 317.65 |
| 96 | 4.80 | 169.41 | 97 | 4.85 | 21.18 |
| 98 | 4.90 | 232.94 | 99 | 4.95 | 84.71 |
| 100 | 5.00 | 296.47 | 101 | 5.05 | 148.24 |

2) There are three left hand helix type paths made up of links that join junction points in the order indicated below.

Path B1: 0-3-6-9-12- - - - -87-90-93-96-99

B2: 1-4-7-10-13 - - - -88-91-94-97-100

B3: 2-5-8-11-14 - - - -89-92-95-98-101

Each of these paths is made up of 33 links, all of which are 6.90 mm long by .203 mm (.008 in.) in diameter.

3) There are four star like paths made up of longer links that skip alternate junction points, joining them in the order indicated below.

Path C1: 0-4-8-12-16- - - - -84-88-92-96-100

C2: 1-5-9-13-17- - - - -85-89-93-97-101

C3: 2-6-10-14-18 - - - -86-90-94-98

C4: 3-7-11-15-19 - - - -87-91-95-99

Each of these paths is made up of 24 or 25 links, all of which are 9.17 mm long by .203 mm (.008 in.) in diameter.

The combination of wire length and diameter for these numbers was selected to provide a uniform voltage gradient through the truss, as well as a uniform temperature variation. This is true of the ten base mounting links as well as the links in the main body of the truss.

Performance

The projected performance is summarized in table 19 for the study propellants at the heater design temperature of 1573°K.

The results of the design study of Concept 2 show an attractive overall efficiency of 81.5% for CO₂ at a specific impulse of 164 seconds. The heat loss per unit length is less than that of Concept 1. However, the length of Concept 2 is 11.5 cm because of heat exchanger design compared to Concept 1 of 7 cm. The result of the overall length effect is that the shorter Concept 1 does have a more attractive overall efficiency of 84.9% and a specific impulse of 167.5 seconds for CO₂.

The principal contribution of Concept 2 is the efficient inverted design notion and the genesis of another truss heater, the bicoil, presented as Concept 3 herein.

TABLE 19
CONCEPT 2 PERFORMANCE SUMMARY

| Propellant | CO ₂ | H ₂ O |
|-----------------------------------|-----------------|------------------|
| Specific impulse, s | 164.0 | 230.4 |
| Maximum heater temp., °K | 1573.3 | 1573.2 |
| Electric input | | |
| Voltage, V | 7.385 | 8.24 |
| Current, A | 24.510 | 27.12 |
| Power, W | 181.0 | 223.45 |
| Power/thrust, W/mlb _r | 3.79 | 4.67 |
| Nozzle chamber | | |
| Total pressure, Atm | 3.0 | 3.0 |
| Total temperature, °K | 1384.1 | 1391.2 |
| Expellants inlet | | |
| Total temperature, °K | 300 | 441.7 |
| Mass flow, gms/sec | .1319 | .0941 |
| Initial gas power, W | 14.31 | 18.95 |
| Power lost from heater, W | 20.69 | 30.25 |
| Total input power, W | 209.28 | 300.80 |
| Maximum gas temp., °K | 1413.8 | 1418.4 |
| Maximum case temp., °K | 553.4 | 588.8 |
| Power efficiencies | | |
| Overall, η _o | .815 | .799 |
| Overall electric, η* _o | .941 | 1.075 |
| Heater, η _H | .901 | .899 |
| Nozzle, η _N | .904 | .889 |
| Thrust check, lb _r | .0477 | .0478 |

Thermal Analysis

The analysis consists of three substudies: 1) a geometric study of simplified regenerative passages; 2) the truss heater configuration; and 3) a mathematical computational model of the overall Concept 2 system.

Regenerators.- The effect of the regenerative passage geometry on thermal losses from the housing of a resistojet are studied by means of a simplified model which is used to represent a 50 millipound resistojet running on CO_2 propellant. The following assumptions are made to simplify the model:

1) Gas properties are assumed to be independent of temperature. The specific heat is taken as $.2681 \text{ cal}/(\text{g}^\circ\text{K})$ while the thermal conductivity is taken as $.0001141 \text{ cal}/(\text{cm}\text{-sec}\text{-}^\circ\text{K})$.

2) Material properties are taken as constants. The emissivity of the passage walls is taken as $.16$, while the emissivity of the outer surface of the housing is taken as $.12$. Two alternative values were used for the thermal conductivity of the insulating material. A low value of $.0001791 \text{ cal}/(\text{cm}\text{-sec}\text{-}^\circ\text{K})$ is used for a layer at moderate temperature in a vacuum. Otherwise, a high value of $.0005927 \text{ cal}/(\text{cm}\text{-sec}\text{-}^\circ\text{K})$ is used.

3) Heat flows due to conduction or radiation in the axial direction are neglected. The only axial heat flows considered are those due to gas flow in the regenerative passages.

4) The primary resistojet heater is represented by a central cylinder 1.4 cm in diameter at a uniform temperature of 1573°K . The ambient temperature (and the inlet gas temperature) is taken as 300°K .

5) The propellant flow rate is taken as $.1316 \text{ g}/\text{sec}$. This corresponds to a specific impulse of 172.3 seconds with 188 watts to heat the gas.

6) The heater length is taken as 5 cm which is believed to be representative for a "truss type" wire heating element, while the housing O.D. is also taken as 5 cm for most of the study. The latter figure appears to be a reasonable choice based on the present study.

The study is conducted in two parts. The first, to gain insight, used a single pass of the gas through an annular passage, while the second utilized a second pass, at a reduced radius, to return the flow to the inlet end of the engine. The geometries of the two cases are depicted in figure 20. A parametric study shows estimated thermal losses with the passage dimensions varied in a systematic manner.

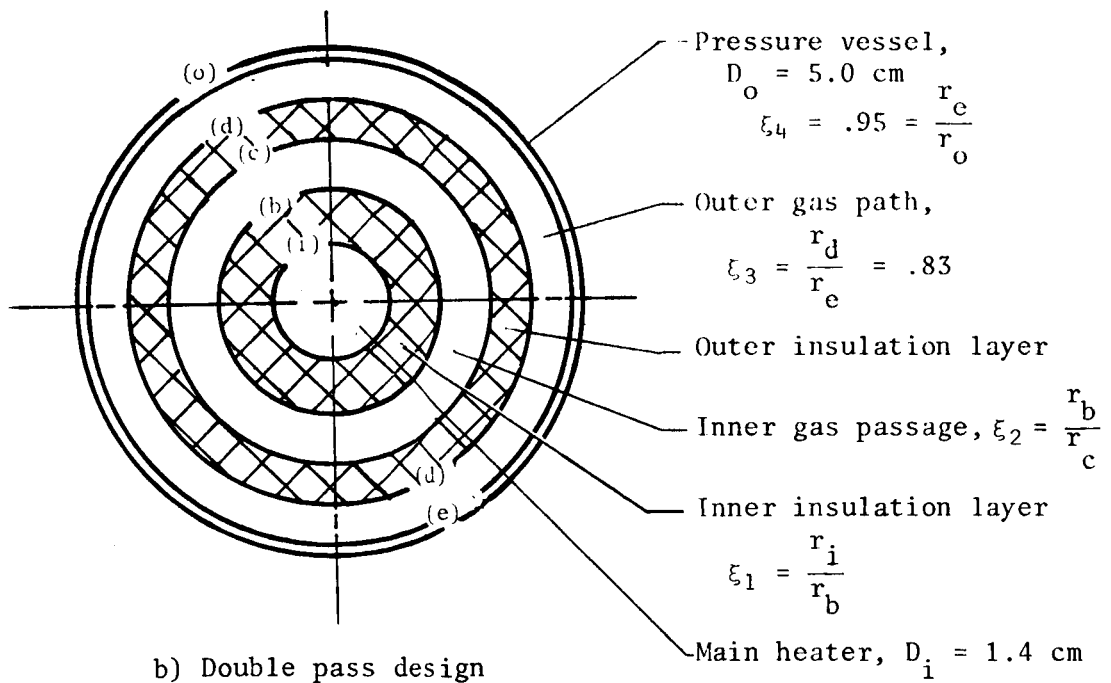
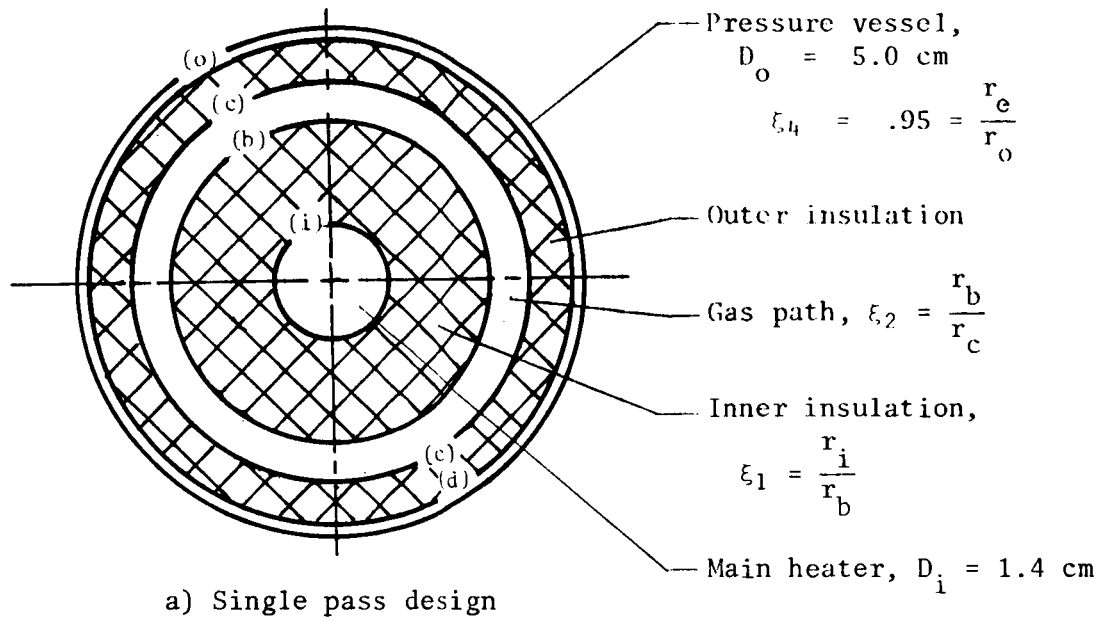
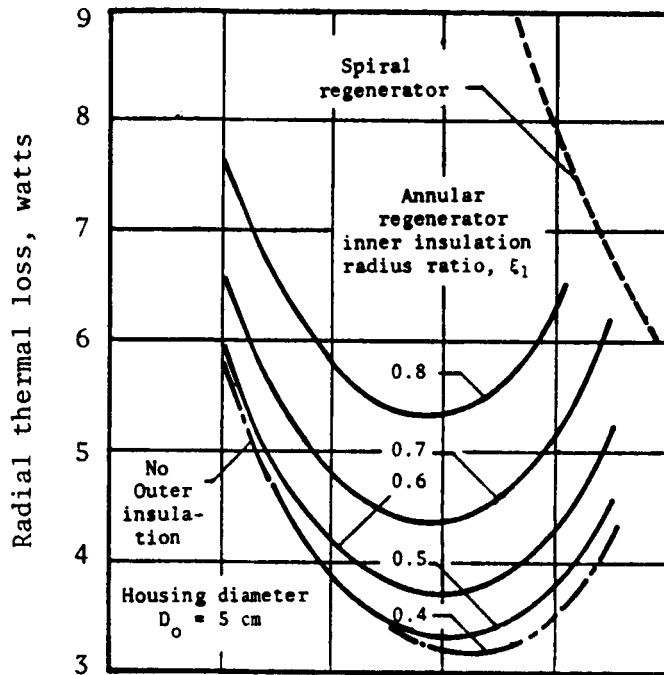


Figure 20. - Regenerative passage study parameters.

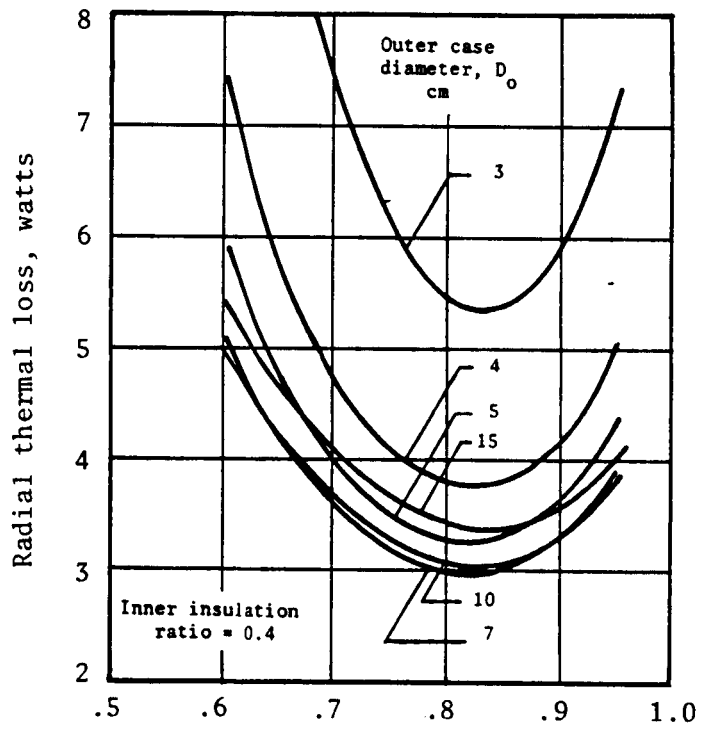
Single pass cases: In the single pass case, the insulation layer inside of the passage is assumed to have the higher value of thermal conductivity while the outer layer is assumed to have the lower value. Estimated losses are shown in figure 21a as a function of the radius ratio of the inner insulation layer and of the radius ratio of the regenerative gas passage. Shown is the case with the passage moved all the way to the outside, completely eliminating the outer layer of insulation. The analysis shows minimum losses with the passage at or near the outer wall. The choice of no outer insulation layer seems attractive due to its simplicity. A relatively thick gas passage appears desirable. Losses seem to be minimum when the passage radius ratio is in the neighborhood of .80 to .85. The flow was found to be laminar in the gas passages, which enhances their effectiveness in blocking the radial conduction of heat and makes increased passage thickness advantageous. Note that reduction of the thickness of the outer layer of insulation improves performance even though that layer was assumed to have a much more favorable value for the thermal conductivity. There is evidently a strong incentive to minimize heating of the gas in the regenerative passage so that the outer wall can be kept cool along its entire length. This is accomplished by providing a thick layer of insulation inside the passage. It is worth noting that when the gas enters the thruster in the cool condition, regenerative passages can be very effective in reducing the heat lost to the housing.

Figure 21a also shows a line near the top of the page labeled "spiral". This line shows estimated losses for a passage modified to enhance convective heat transfer to the gas. Spiral flutes of metal join the inner and outer walls and cause the gas to follow a spiral path. The cases shown for spiral passages are all for the passage at the housing O.D. with no external insulation. The outer wall temperature is increased by conduction through the flutes which helps to increase convection to the gas. Increased heat flow through the insulation to the gas increases the temperature drop in the insulation, which, it was hoped, would also reduce the outer wall temperature and external radiation losses. This is not the case.

The calculations show that a flow of cool inlet gas is the most effective in keeping the outer wall temperature at a low value. Best advantage is taken of this effect by using a thick annular passage rather than the spiral type of passage. Rather large temperature differences between the inner and outer passage walls are obtainable when thick annular passages are used. It seem to be preferable to minimize convection heat transfer to the gas so that it will remain relatively cool along the entire length of the housing.



a) Effect of passage and insulation diameter ratios.



b) Gas passage radius ratio, ξ_2

Figure 21. - Simplified parametric study of regenerative passage geometry study for the single pass showing effect of diameter.

Figure 21b shows losses for a number of housing diameters. In all of these cases, there is no external insulation. Although minimum loss seems to occur with a housing diameter between 7.0 and 10.0 cm. there is only a small penalty in performance if the diameter is reduced to 4.0 or 5.0 cm. Use of a 5.0 cm housing diameter with a passage radius ratio of 0.83 is suggested for a preliminary design which is analyzed in more rigorous detail.

As the gas progresses down stream through a passage, its temperature increases, and it loses its ability to keep the outer wall cool and minimize external radiation losses. The longer the thruster, the more difficult the problem becomes. As length increases, losses increase at a rate that is more than proportional. The effect is illustrated in figure 22 for thrusters with no external insulation. It is important to minimize the heater length so that the housing can be kept relatively cool over its entire length.

Two pass cases: Results for the study with two regenerative passes are shown in figure 23. To reduce the number of variables, the first pass geometry was fixed with a configuration that looked attractive in the single pass study. A passage radius ratio of 0.83 is used with no insulation layer outside of the first pass. The radial location of the second pass and its radius ratio were then varied parametrically. It shows estimated losses as a function of the radius ratio of the inner insulation layer, and the radius ratio of the second gas passage. In addition, two dotted lines appear on the figure. The upper one is for the case with no inner insulation layer, while the lower one has no insulation layer between the two gas passages. Results for the second pass are similar to those obtained for the single pass study. The penalty associated with eliminating the outer of the two insulating layers is not large. In the interest of simplifying the design, we tentatively select a design with a single insulating layer on the inside of the gas passages. A radius ratio of 0.83 is suggested for the outer pass, while a lower value (say 0.73) appears attractive for the second pass.

The truss heater.- In principle, it should be possible to design a wire heating element with an intricate array of fine wires in cross flow which would provide excellent heat transfer characteristics and would operate at an attractively high voltage. Although simple coil type heaters are subject to vibration problems, it was felt that a truss type configuration could be used to stiffen the heater and raise its natural frequencies above the expected excitation frequency range. Accordingly, a gas heater having a fairly complex truss type wire heating element was designed and an analysis made to estimate its performance.

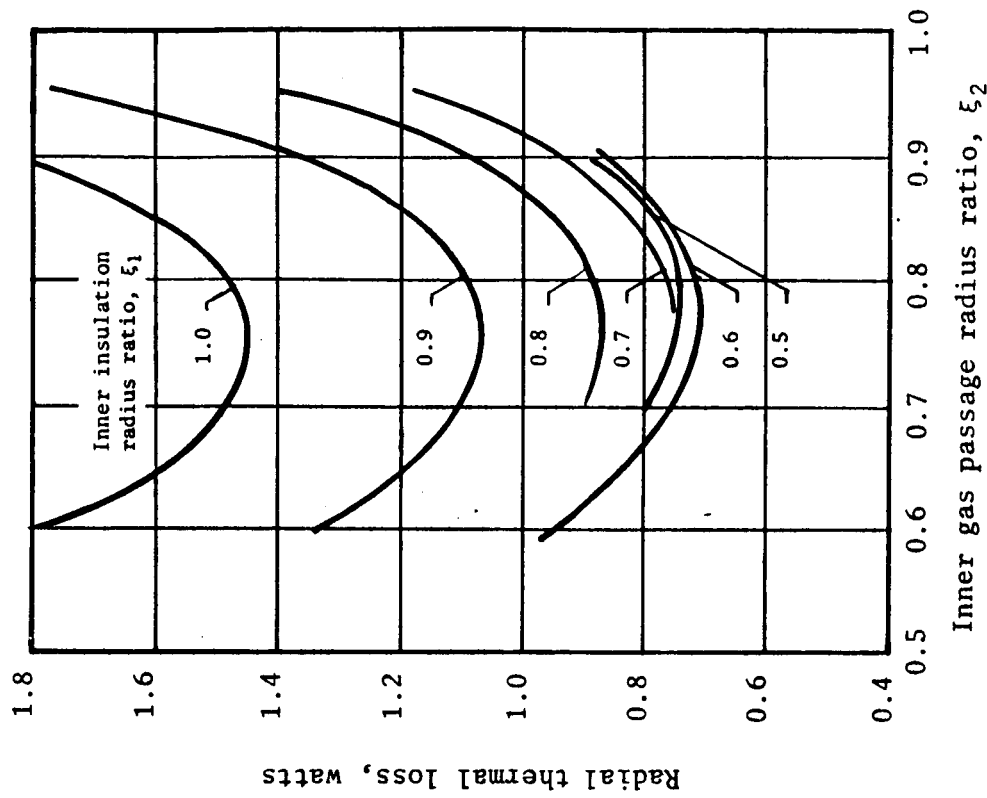


Figure 22. - Simplified parametric regenerator passage geometry study for the single pass case showing the effect of heater length on thermal loss. Heater housing diameter is 5, inner insulation ratio $\xi_1 = 0.4$ and no external insulation.

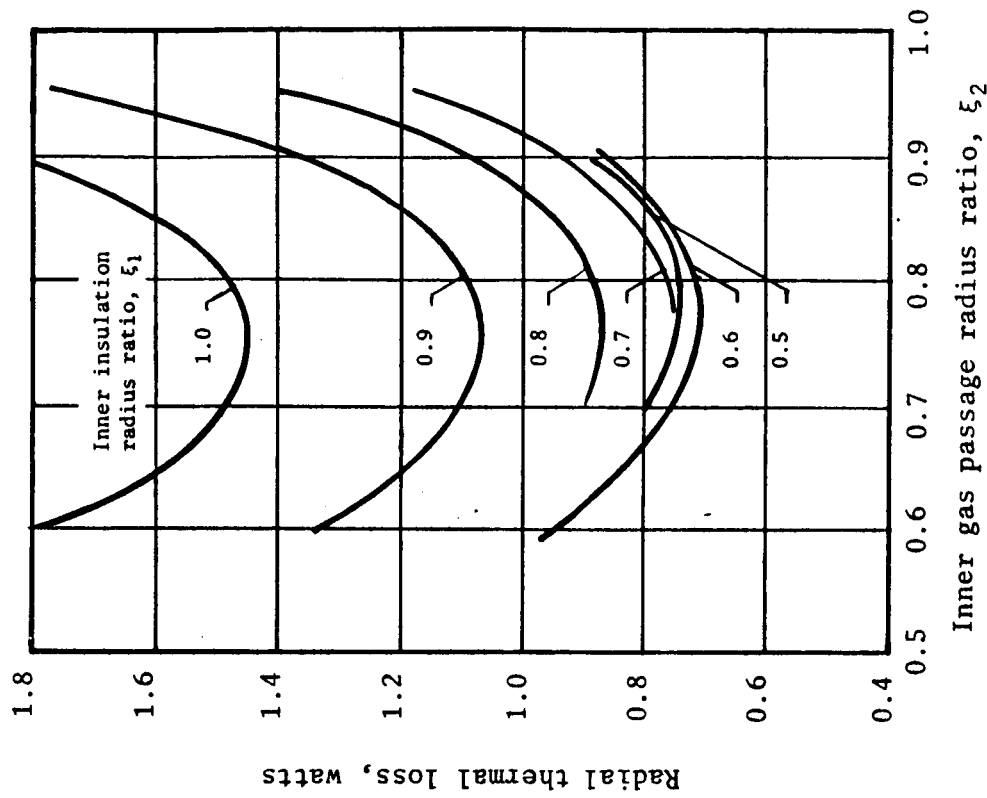


Figure 23. - Simplified parametric regenerative passage geometry study for the two pass cases showing effect of inner passage ratio, ξ_2 . Heater housing is 5 cm, with first pass $\xi_3 = 0.83$ and no external insulation.

Although it was found possible to keep the heating element no larger in size than most of the other designs studied, the thermal analysis shows the gas temperature obtained for a given 1573°K heater temperature is 96°C less than Concept 3, a bicoiled tube type of heater.

To minimize thermal distortion of the heating element, a truss configuration should be symmetrical, and the wires should be sized so that they all operate at about the same temperature. It seems to be generally true that a heater designed as a truss with six wires connecting to each node will not have the same voltage gradient (E/L) in all of the wires. As a result, the electrical power heating some wires will differ from the others and the wire temperature will be different even if the gas temperature and velocity are the same at all of the wires. A method is needed for choosing wire diameters that will tend to equalize the wire temperatures. For illustration, consider a case with convection the dominant heat transfer mechanism, and with radiation negligible. The heat transfer performance is estimated from reference 29. At the low Reynolds numbers here the Nusselt number for flow across a cylinder is proportional to the square root of the Reynolds number, so:

convective cooling = electrical heating

$$\frac{N_u k A_{\text{surface}} (T_{\text{wire}} - T_{\text{gas}})}{D_{\text{wire}}} = \frac{E^2}{R}$$

$$\text{Const} \sqrt{\frac{\rho V D_{\text{wire}}}{\mu}} \frac{(k \pi L D_{\text{wire}})}{D_{\text{wire}}} (T_{\text{wire}} - T_{\text{gas}}) = \frac{4E^2 \sigma}{\pi D_{\text{wire}}^2 L}$$

If the gas flow conditions are the same at all of the wires, this becomes:

$$(D_{\text{wire}})^{3/2} = \frac{\text{Const}_1}{(E/L)^2} \quad \text{or} \quad D_{\text{wire}} = \frac{\text{Const}_2}{(E/L)^{4/3}} \quad (\text{B1})$$

An alternate case is one in which radiation from the wires dominates, and convective heat transfer is neglected. Overlooking variations in the shape factors and assuming constant wire temperatures, radiative heat transfer is taken proportional to the wire surface area:

radiative cooling = electrical heating

$$\text{Const } A_{\text{surface}} (T_{\text{wire}}^4 - T_{\text{wall}}^4) = \frac{E^2}{R}$$

$$\text{Const } \pi L D_{\text{wire}} (T_{\text{wire}}^4 - T_{\text{wall}}^4) = \frac{4E^2 \sigma}{\pi D_{\text{wire}}^2 L}$$

$$D_{\text{wire}} = \frac{\text{Const}_3}{(E/L)^2} \quad (\text{B2})$$

Since equation (B2) differs from equation (B1), there isn't a simple relation expressing the desired adjustment in wire diameter. With Concept 2 work carried to a more detailed study phase, it is anticipated that wire diameters ultimately would be selected utilizing the computer heat balance program with its estimates of gas temperature and wall temperature variation. For this initial study, the minimum wire diameter was taken as .02 mm (.008 inches), with the diameter increased for other current paths to a weighted average of values given by equations (B1) and (B2). The convective heat transfer expression was weighted twice as heavily as the other.

Steady state modeling of the thermal system.- Steady state thermal analysis was undertaken by generalized computational model. The specific node diagram representing the Concept 2 configuration of figure 17 is shown in figure 24. The temperature distributions resulting from the case of the study design goal of 50 mlb thrust at 1300°C (1573°K) heater element temperature are shown for both CO₂ and H₂O (steam) in figures 25a and b, respectively.

The CO₂ gas temperature at nozzle entrance is 1384°K or 189°K below maximum heater wall temperature of 1573°K. The pressure case temperature is only 633°K at the nozzle exit joint. The metal to ceramic (-19) seal joint is at 471°K, well below its rating of 623°K. The thermal profile shows the favorable design characteristic of an increasing temperature towards the nozzle. This keeps the thruster mount cool. This feature deters deposition of metallic vapors on insulators at the feedthrough (-19).

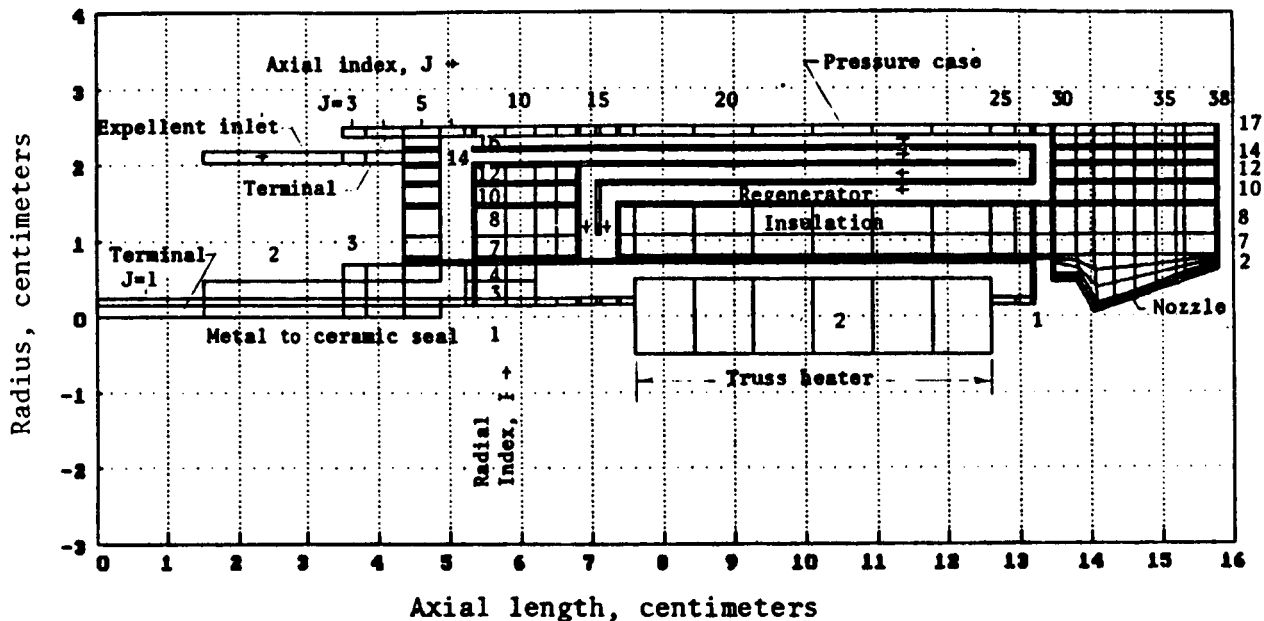


Figure 24. - Thermal node diagram used in the analysis of Concept 2.

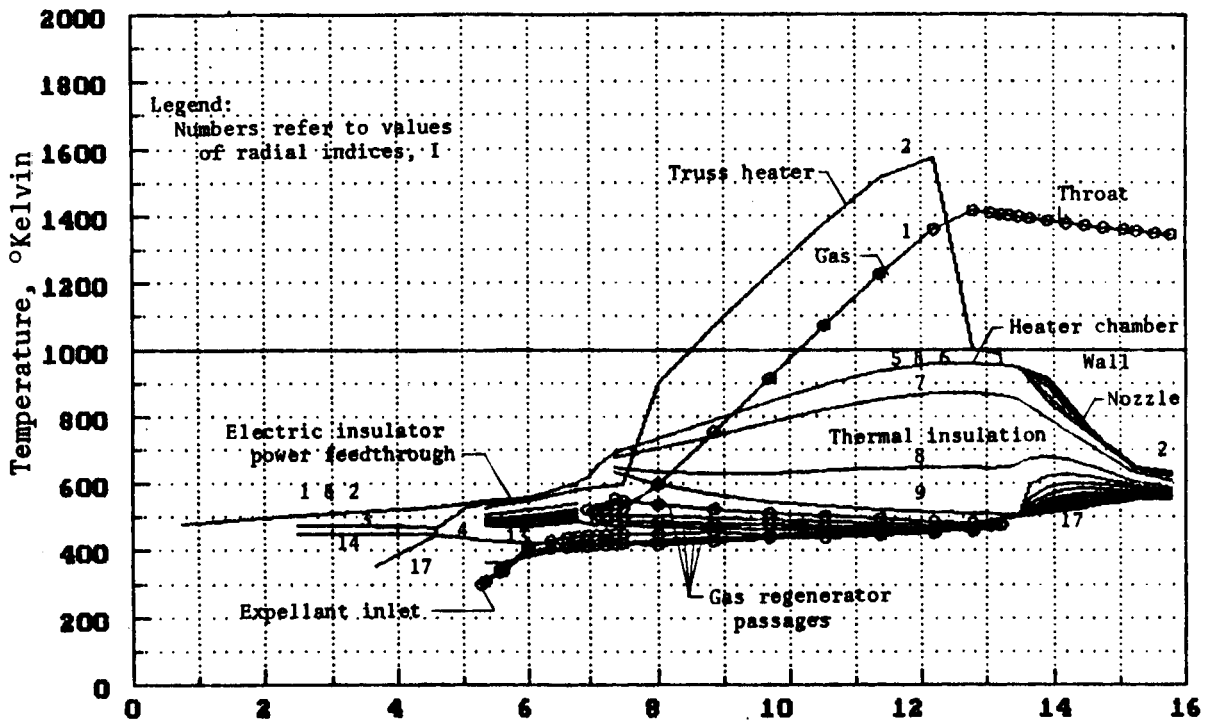
As a result of the favorable thermal design, the thermal efficiency is 90%, second only to Concept 1, an extremely short design because of its ceramic heater.

No further improvement of Concept 2 was attempted because Concept 3, using the same basic inverted structure, continued that development.

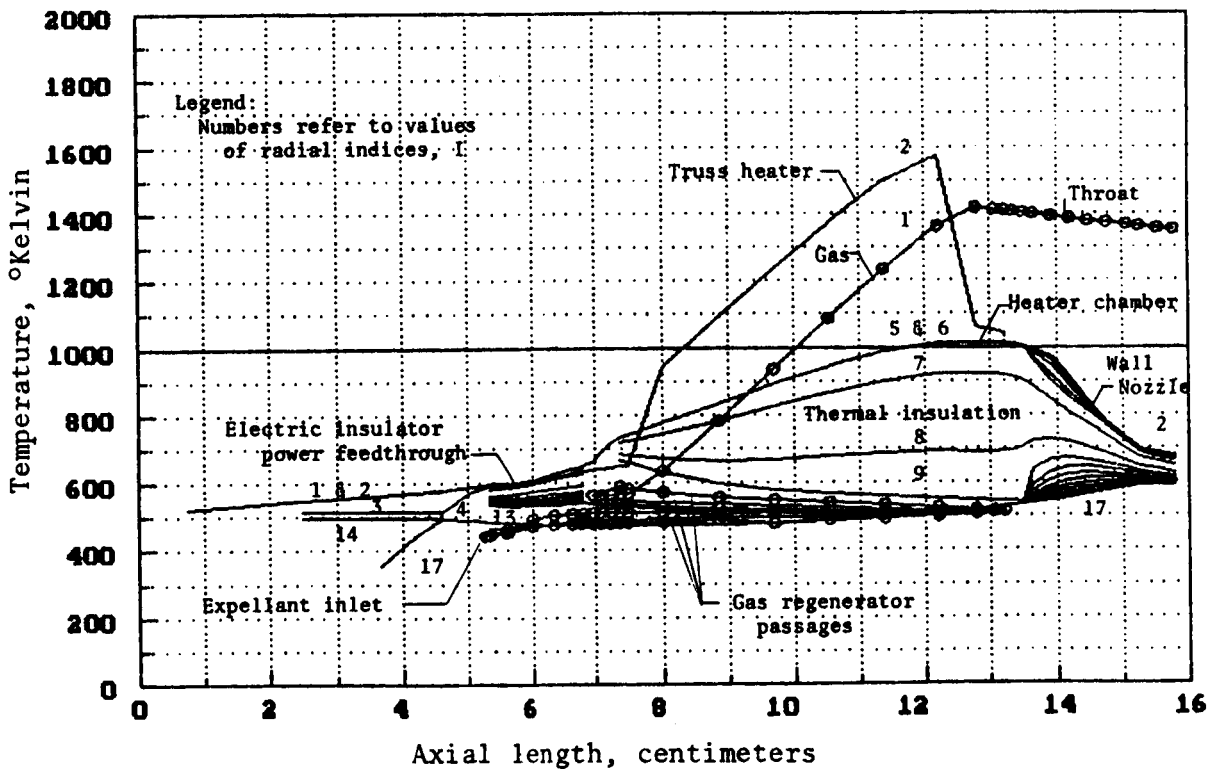
Gas Dynamic Analysis

The heating element is enclosed in a circular passage sized to produce a low gas velocity which is .3 to 3 meters/sec depending on the propellant and the gas temperature. The corresponding Reynolds numbers based on a wire diameter of .2 mm (.008 inches) vary from 2.6 to 15.6. Referring to Hoerner (ref.30), figure 1 page 3-2, we see that this is well below the range of Reynolds numbers in which vortex streets form in the wake of a cylinder. Although this feature of the design reduces the convective heat transfer to the gas by reducing the Nusselt number, this can be offset by increasing the length of wire in the heater. An increase in the wire length has the added advantage of an increase in the operating voltage but increases the overall losses. Because of the low gas velocities, there is no pressure drop of consequence.

ORIGINAL PAGE IS
OF POOR QUALITY



a) Carbon dioxide



b) Steam

Figure 25. - Temperature distribution of Concept 2 at a maximum heater temperature of 1573°K.

Structural and Other Mechanical Effects

A truss type of structure rather than a simple coil is used for the heating element. This increases the rigidity and the natural frequency of the heater. Structural problems are relieved because it is easier to provide mounts that will isolate the unit from resonant frequencies if those frequencies are high. It is planned to use a "complete" truss for the heater (a configuration that would be rigid if all the joints between links were pivots).

Redundant members are avoided in the structure. This is to avoid high thermal stresses and permanent distortion if one member heats up at a different rate than the others. The number of links (n) required for a truss with (j) joints is given by the relation:

$$n = 3j - 6$$

For example, a tetrahedron with four joints requires six linking members. A cube with 8 joints requires 18 linking members (including a brace in each of the six faces). An additional brace across the internal space between opposite corners would be redundant and could generate locked in stresses. The tension or compression forces in the links can be found by solving a set of simultaneous equations consisting of three force balance equations (one for each coordinate) at each joint. There are, therefore, $3j$ unknowns requiring $3j$ linking members if the base mounts are counted. With more links there would not be a unique solution. Links required for mounting the structure to a base are not included in the above expression which explains the subtraction of six links.

For the center part of the heating element, it is planned to use a repeating pattern with all of the joints using the same configuration. Since each link connects two joints, there are a total of six links connected to each joint. Departures from this rule occur at the two ends where the deduction of six links are made without disturbing the repeating pattern used elsewhere.

A twist in the truss geometry is used to stagger the wires in the gas flow path and to help equalize wire diameters.

Truss geometries considered are described as right and left hand helical patterns wound on a mandrel having a polygon shaped cross section. The wires intersect at the polygon corners where they are welded together to form the joints. Internal welded joints are avoided. Slots of saw cuts in the mandrel are needed for winding the deep star-like patterns. The mandrel may be either a straight or a twisted polygon cylinder. It must be destructible so that it can be removed when the part is finished.

Since the heating element is axially compliant, no special flexibility is required in its mounting to allow for thermal expansion in the axial direction.

Examples.- Two figures are attached to illustrate the type of truss geometries that can be developed based on a polygon shaped mandrel. Both examples use a mandrel with a pentagon cross section shape. The first sketch depicts a case with no twist in the mandrel. The top view shows the pentagon shaped outer windings and the star shaped inner windings in an end view, while the lower sketch shows a developed view of the pentagon surface. It is not to scale.

The star shaped pattern is wound first. There are four of these windings in a form that advances like a right-hand helix, but each link advances only one unit axially; while the second is a triple left-hand helix advancing one and a half units for each link. The difference between the right and left hand polygon helix patterns is necessary in order to get all of the wires to intersect at the same points when there are an odd number of sides on the polygon. There are a total of nine paths for electrical current in parallel. The vertical lines in the lower view represent the corners of the polygon, and are not part of the truss. Wires in the axial direction would be too low in resistance.

The second sketch shows the same basic geometry with a twist introduced in the mandrel to stagger the wire pattern. A second effect is that the left-hand helix is lengthened which helps to increase its resistance. This is advantageous because it has a steeper advance angle and is therefore exposed to a higher voltage gradient than the right-hand elements. In the configuration selected, a balance was achieved between the star windings and the left-hand windings. Both of these can use a wire diameter of .2 mm. However, the other pentagon shaped windings still have a lower voltage gradient and need a somewhat larger wire diameter (about .010 inches) to provide their share of the heating.

Chemical

There are no chemical problems in the design in the choice of materials used. Concept 3 gives a quantified level of anticipated oxidation and sublimation recession losses which are very low and typical for the inverted biowaste thrusters.

Rating

Advantages.- (1) The heater is structurally rigid transversely yet axially accommodating for expansion compensation.

(2) Closely spaced staggered wires provide a relatively effective heat transfer to the gas compared to radiative designs.

(3) No electric insulators are required in the hot zone.

(4) The single heater required can run with either AC or a DC power supply.

Disadvantages.- (1) With biowaste propellants, the temperature is limited to the level that can be tolerated by platinum wire. This is expected to be about 1300°C as opposed to values of at least 2000°C that appear to be attainable with a zirconia heater.

(2) If subjected to a high velocity gas flow, wire elements can shed a vortex street accompanied by an oscillating force acting on the wire. A structural problem results if a resonant condition occurs.

(3) Usually heater wire coil designs have low natural frequencies leading to the possibility of resonant vibrations induced by launch conditions or by the operation of other equipment while in orbit.

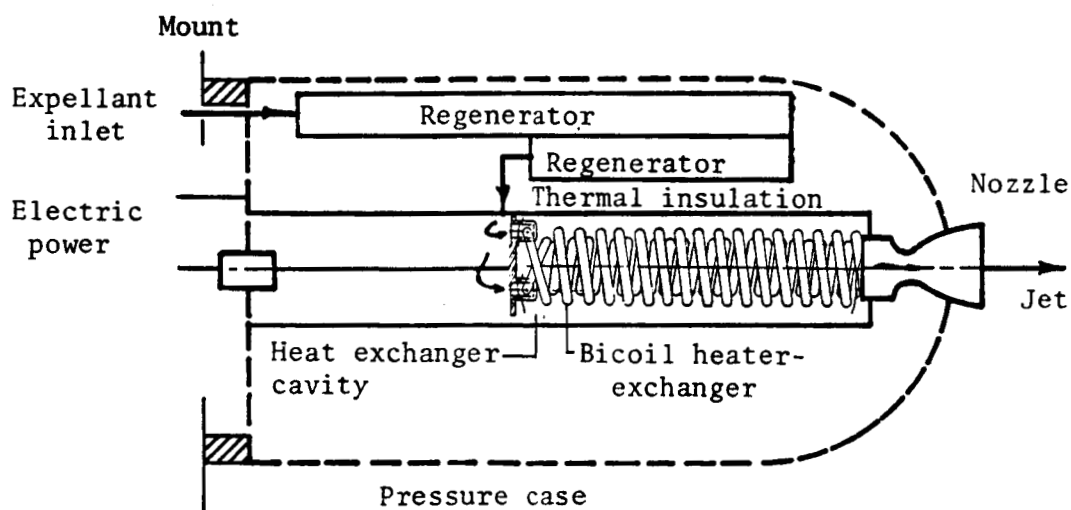
APPENDIX C

CONCEPT 3 - EXPOSED METALLIC BICOIL TUBULAR HEATER IN INTERNAL FLOW

This new design is based upon two novel features. The radially inverted design of Concept 2, described previously in detail, is used identically. The bicoil, an integrated tubular ohmic heater and gas heat exchanger, is introduced. It is made of metal-oxide grain stabilized platinum.

The figure below summarizes the conceptual relationship of elements. The favorable features of a low temperature outer pressure case with its radially broad regenerator is retained from Concept 2. No electric insulation is used in the high temperature zones. Propellant flow deters backstreaming of any sublimed metallic vapors onto electric insulators.

The bicoil consists of two coils of precisely the same tubular heating length and cross-sectional diameter coiled in opposite rotation, one closely fitting within the other. The pressure drop and flow of each passage and the resistance heating length are the same. The cross-over points are at the same voltage potential and the two coils are physically bonded to one another there. As a result, the bicoil design is found by stress analysis to be stable and transversely rigid yet accommodating for axial thermal expansion compensation. The operating voltage of the bicoil can be designed relatively high. The temperature of the gas flowing through the tubes of the bicoil approaches here to within 63°C of that of the wall at exit.



Description

The final preliminary design of Concept 3 is shown in figure 26. Table 20 identifies the components and materials. The construction of Concept 3 is identical to 2 except for the geometry of the heater. The bicoil heater is made of grain stabilized platinum.

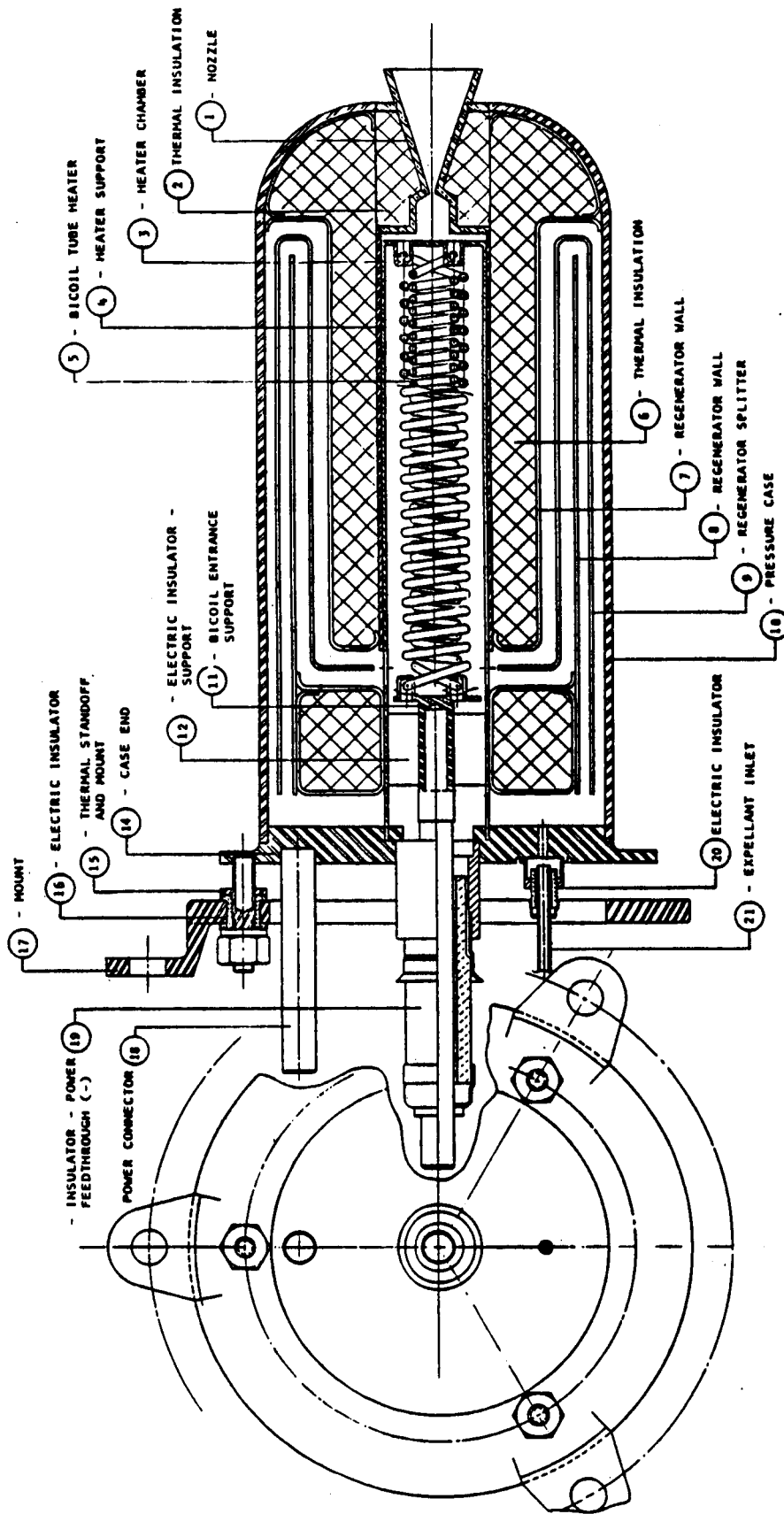
TABLE 20
CONCEPT 3 - COMPONENT PARTS, MATERIALS OF CONSTRUCTION

| <u>Item</u> | <u>Component</u> | <u>Material</u> |
|-------------|-----------------------------------|--|
| 1. | Nozzle | Grain stabilized platinum |
| 2. | Thermal insulation | Min-K 2000 ¹ |
| 3. | Heater chamber | Grain stabilized platinum |
| 4. | Heater outer support and return | Grain stabilized platinum |
| 5. | Bicoil heater | Grain stabilized platinum |
| 6. | Thermal insulation | Min-K 2000 ¹ |
| 7. | Inner regenerator wall | AISI 321 |
| 8. | Regenerator wall | AISI 321 |
| 9. | Regenerator splitter | AISI 321 |
| 10. | Pressure case | AISI 321 |
| 11. | Bicoil support, entrance | Nickel 200 |
| 12. | Electric insulator - support | Alumina 99.5% |
| 14. | Case end | AISI 321 |
| 15. | Thermal standoff and mount | AISI 321 |
| 16. | Electric insulator for case mount | Delrin |
| 17. | Mount | AISI 321 |
| 18. | Power connector (+) | Nickel 200 |
| 19. | Insulator - power feedthrough (-) | Metal to ceramic seal materials ² |
| 20. | Electric insulator | (TBD) |
| 21. | Expellant inlet line | AISI 321 |

1. Data for Min-K 2000, Johns-Mansville Aerospace Products, N.Y., NY.

2. Typical materials: nickel A conductors; glazed high alumina ceramic (85% min. Al₂O₃) insulators; vacuum tube grade brazing alloys and nickel-iron caps. Data from Ceramaseal, Inc., New Lebanon Center, NY.

One of the novel features of this concept is the bicoil, an integral tubular ohmic heater and gas exchanger (-5). The bicoil is mounted within the heater chamber (-3). Its exit is supported by member (-4) which also serves as an electric terminal and gas plenum feeding the nozzle. The bicoil at the entrance end is supported by its terminal and support (-11).



Scale: Full size

Figure 26. - Concept 3, a biowaste resistojet using grain stabilized platinum with a bicoil heater - exchanger in internal parallel flow.

Figure 26 describes the bicoil geometry of Concept 3 and the following table gives key dimensions.

TABLE 21
DOUBLE COILED TUBE HEATER DIMENSIONS
Millimeters (Inches)

| | Inner Coil | Outer Coil |
|----------------------|---------------|---------------|
| Tube outer diameter | 1.24 (.049) | 1.24 (.049) |
| Tube inner diameter | .99 (.039) | .99 (.039) |
| Coil pitch line diam | 6.22 (.245) | 8.76 (.345) |
| Lead per turn | 1.768 (.0696) | 2.489 (.0980) |
| Number of turns | 33.94 | 24.10 |
| Tube length | 666.2 (26.23) | 666.2 (26.23) |
| Axial length | 60.0 (2.362) | 60.0 (2.362) |

The ground side of the power line is connected to the terminal (-18) which connects to the case end (-14). Current passes through the gas exit terminal support (-4) to the bicoil ohmic heater and gas exchanger to the entrance terminal and support (-11). The circuit is completed through the power feed through (-19) to the high side of the power line.

The expellant feed line enters the thruster through an insulated fitting (-21) at the case end (-14) and into the parallel pass annular regenerators. Exiting from the regenerator it enters the heater cavity (-3) at the station of the bicoil entrance. The gas can only exit the thruster nozzle through the twin passages of the bicoil, and hence the nozzle. Since the heater is immersed in the expellant gases, low pressure differentials, hence low stresses across the wall, are involved with careful optimal heater design.

The features of the bicoil are described in detail in Concept 5 where it is used in a hydrazine augments.

Performance

The projected performance is summarized in table 22 for the study propellants at the heater design temperature of 1573°K.

TABLE 22
CONCEPT 3 PERFORMANCE SUMMARY

| Expellant | Projected performance | |
|----------------------------------|-----------------------|------------------|
| | CO ₂ | H ₂ O |
| Specific impulse, s | 170.2 | 240 |
| Maximum heater temp., °K | 1573.2 | 1573.2 |
| Electric input | | |
| Voltage, V | 6.83 | 7.76 |
| Current, A | 29.71 | 32.83 |
| Power, W | 203.0 | 255.26 |
| Power/thrust, W/mlb _r | 4.11 | 5.13 |
| Nozzle chamber | | |
| Total pressure, Atm | 3.0 | 3.0 |
| Total temperature, °K | 1486.2 | 1501.9 |
| Expellants inlet | | |
| Total temperature, °K | 300 | 441.7 |
| Mass flow, gms/sec | .1319 | .0941 |
| Initial gas power, W | 14.31 | 18.95 |
| Power lost from heater, W | 27.38 | 38.71 |
| Total input power, W | 231.28 | 332.61 |
| Maximum gas temp., °K | 1510.3 | 1518.9 |
| Maximum case temp., °K | 592.0 | 628.1 |
| Power efficiencies | | |
| Overall, η_o | .793 | .784 |
| Overall electric, η_o^* | .903 | 1.025 |
| Heater, η_h | .882 | .884 |
| Nozzle, η_n | .899 | .887 |
| Thrust check, lb _r | .0494 | .0498 |

Concept 3, the bicoil, the notion for which comes as a result of the studies of Concept 2, has the highest specific impulse of the biowaste concepts at the 1573.2°K heater condition. For CO₂, this is 170.2 seconds, but a slightly lower overall efficiency than Concept 1 of 79.3%. The reason for the latter is the higher gas temperatures generated of 1510.3°K as compared to 1468.4°K for Concept 1. The key point for Concept 3 is the closeness to which the bicoil heater can raise the gas temperature at its exit to its own design heater temperature, a difference of only 63°C. The Concept 2 difference is 159°C and Concept 1 is 104.6°C.

Thermal analysis

The heat transfer analysis of an ohmically heated tube as a heat exchanger can be approximated by means of the following equations to see the general effect of the design parameters. These equations are highly simplified. A constant wall heat

flux, q_w , boundary condition, entrance conditions ignored, and constant physical properties of the gas and wall are assumed. The wall of the simple model was considered adiabatic.

The more exact study by means of the mathematical model is presented in the section that follows this which includes variable gas and wall properties with temperature and local heat transfer conditions taken into account.

The cases considered were laminar. The exchanger exit or maximum temperature point was fully developed thermally, hence the Nusselt's number, Nu^∞

$$Nu^\infty = \frac{hd}{k} = \text{constant} = 4.364 \quad (C1)$$

where Nu^∞ is the so called asymptotic or infinity solution. Values of thermal conductivity, k , and viscosity, μ , used in the study are presented under Propellants. The diameter is d .

From the local convective heating equation

$$(q_w)_{x=x_1} = h(T_w - T_g)\pi d \quad (C2)$$

at any location, x , along L , and

$$(q_w)_{\text{ave}} = \frac{Q}{L} \quad (C3)$$

where Q is the total heat input and L the tube length.

From equations (C1), (C2), and (C3) and the approximate analysis assumptions of constant physical properties, any point along L including the exit

$$Q = q_w L = Nu^\infty k \pi ((T_w)_r - (T_g)_r) L \quad (C4)$$

The total heat to the gas, Q , is also given by

$$Q = \dot{m} C_p ((T_g)_r - (T_g)_i) \quad (C5)$$

The $((T_w)_r - (T_g)_r)$ of equation C4 is the excess temperature of the wall over that required of the gas. For a given required total heat input to the gas, Q , a shorter tube length, L , requires higher wall excess temperature penalty or conversely lowers the gas temperature attained because of maximum wall temperature limits.

Equations C4 and C5 show the basis for the assertion that two tubes in parallel, each with one half \dot{m} , sharing the heating requirement, reduces the temperature difference between wall and gas to one half compared to a single tube of the same length. This is one additional reason for the bicoil design presented here. Another is the lateral structural integrity introduced by the two integrated counter rotation coils. Note that the tube diameter in laminar flow drops out of the equation. The only size restriction is one of minimizing pressure drop and preventing choking.

Setting an acceptable design temperature difference defines a gas path length. This is the starting point for the more refined analysis to follow.

Mathematical computational analysis.- The node diagram for Concept 3 is shown in figure 27. The resultant temperature distribution for CO_2 and H_2O are shown in figures 28a and b, taking into account variable properties.

The expellant gas temperature increases in almost a linear manner with length as does the coil wall temperature as expected by the previous simple analysis. The gas more closely approaches at exchanger exit the wall temperature than any of the other designs studied or 63°C and 54°C for CO_2 and H_2O , respectively. The gas temperature drops 24°C and 17°C , respectively, to the

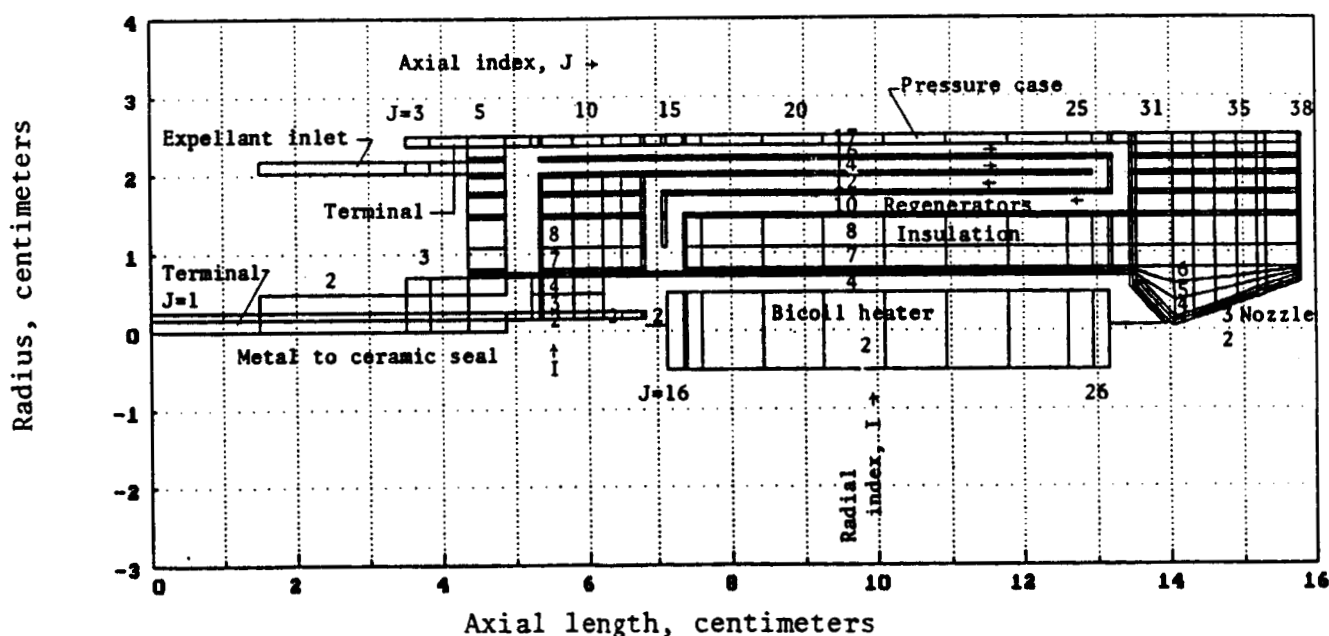


Figure 27. - Thermal node diagram used in the analysis of Concept 3.

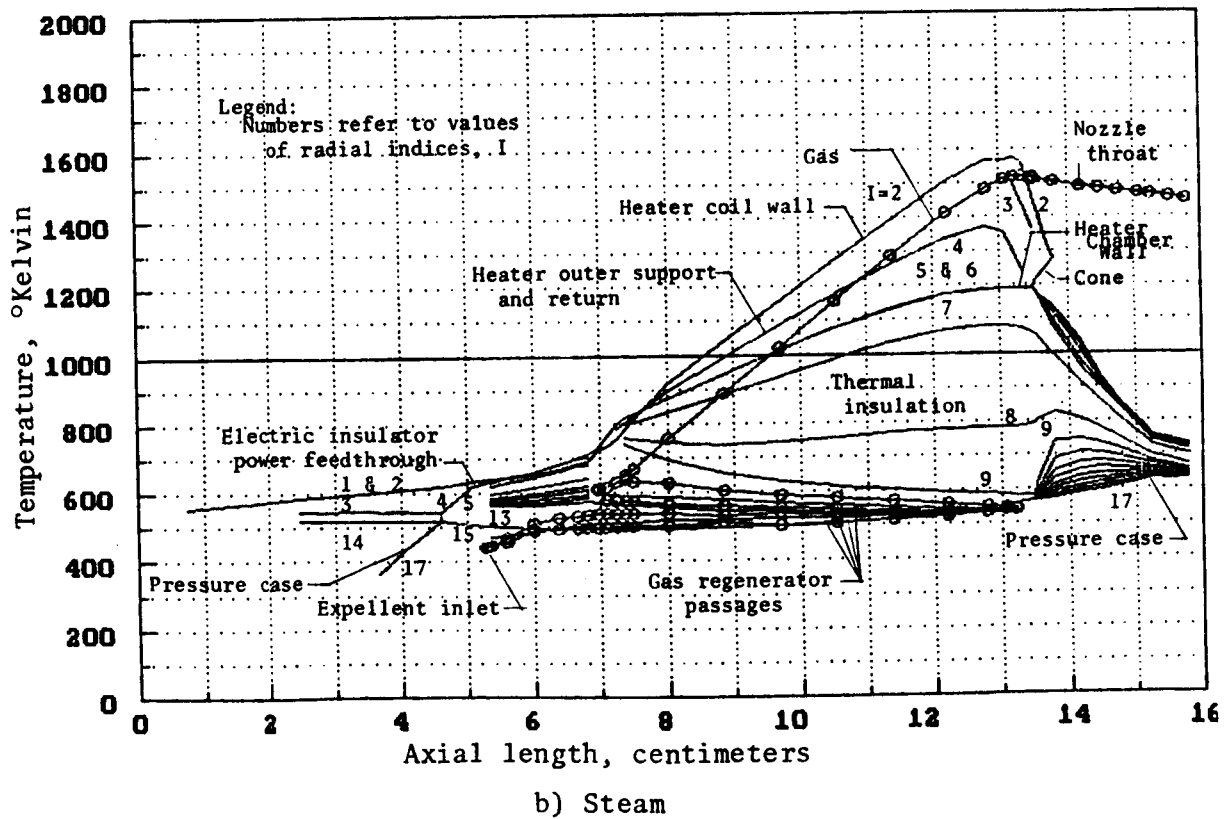
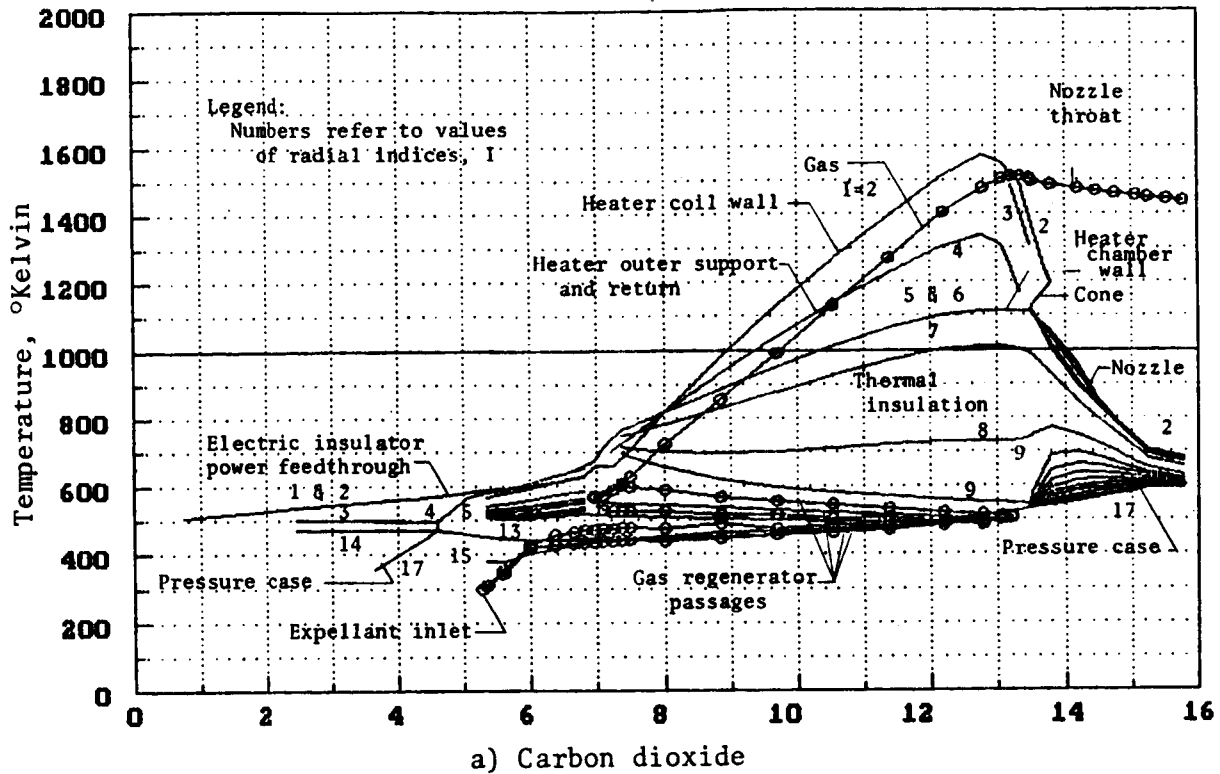


Figure 28. - Temperature distribution of Concept 3 at a maximum heater element temperature = 1573°K.

plenum in being shuttled to the nozzle plenum. The maximum wall temperature of the heater occurs over a very limited region near the exit. This allows some ameliorating design considerations in this region only if required, such as wall thickening, to promote a longer life design without serious compromise of performance. It was not required here in this design.

The attraction of the bicoil is that the tubes heat the exiting gas to near maximum heater structure temperature and in a rapidly responsive way during starting. This is important if short firing cycles are required.

The temperatures of the metal to ceramic seal at the power feedthrough are 560°K versus a 623°K steady state permitted by the the manufacturers. The analysis is made under the conservative assumption of no temperature sinking by the power connector cable, hence a slightly longer design than required.

The pressure case is 600°K maximum at the nozzle exit joint permitting contemporary metalurgical joints by brazing using contemporary structural case materials. This latter fact is felt to be the major contribution of the inverted design rather than any major efficiency advantage.

Gas Dynamic Analysis

A summary of the parameters is shown in table 23 for a design heater temperature of 1573°K and a mass flow of .1319 grams per second of CO₂ as representative. The results for H₂O steam are similar.

TABLE 23
SUMMARY OF FLUID FLOW PARAMETERS

| Parameter | Propellant inlet | Bicoil entrance | Bicoil exit | Nozzle throat |
|---|------------------|-----------------|-------------|---------------|
| Flow area, (cm ²)x10 ³ | 28.5 | 7.71 | 7.71 | 3.97 |
| Total pressure, atm | 3.59 | 3.523 | 3.0 | 3.0 |
| Total pressure, psia | 52.7 | 51.77 | 44.09 | 44.09 |
| Static pressure, atm | 3.59 | 3.52 | 2.96 | 1.71 |
| Static pressure, psia | 52.7 | 51.58 | 43.43 | 25.19 |
| Total gas temp., °K | 300 | 590.4 | 1503.4 | 1486.2 |
| Wall temp., °K | - | 660.4 | 1573.2 | 1004.2 |
| Mach number | .01 | .078 | .157 | 1.00 |
| Reynolds number | - | 2904 | 1627 | 4816 |

The static pressure within pressure case cavity is 51.8 psia. The critical flows within the bicoil are treated everywhere as laminar. The favorably low mach number of the

design in the heat exchanger promotes a relatively low pressure drop. Further, the static pressure at the bicoil exit is only slightly suppressed below the total pressure. This reduces the wall delta pressure to 8.4 psia, and hence, hoop stress at this critical section.

Mechanical Design

Pressure envelope.- The pressure envelope is now the outermost member because of the inverted design. Its temperature ranges from 592°K maximum at its outer radius to 682°K at nozzle junction. The thickness chosen for this pressure shell is not consequential to the thermal design. Ordinary nickel chrome steel is adequate. Its structural design is not critical.

For instance, wall thickness of 1.25 mm (.050 in.) for an outside diameter of 5 cm would develop a stress of 11.6 MPa (1680 psi). The 10,000 hour life data for just 3% chromium steel at 810°K (1000°F) taken for margin is 48.3 MPa (7000 psi). The exact low cost material has yet to be selected.

The balance of the design is static pressure balanced within the pressure envelope. The bicoil is the only member to be considered for stress review here. The applicability of the metal to ceramic seal is treated in the corresponding section of Concept 5. It is not further discussed here. It is not a problem.

Heating element.- The bicoil heater is critical near its exit where the temperature is the maximum value for the thruster of 1573°K. The pressure across the tube wall from the gas dynamic study is the difference between the cavity of 51.8 psia less the internal static pressure of 43.3 psia at the maximum wall temperature point of 8.5 psia difference in pressure. The hoop stress, σ , is $pD/2t$ giving a value of 255 KPa (37 psi) where the mean diameter is .044 inches and the thickness, t , is .005 inches. The stress rupture endurance from the 10,000 hour grain stabilized design line is 5.8 MPa (842 psi).

The structural integrity of the bicoil heater under the maximum expected operating conditions warranted more detailed explanation since the concept is new. It was studied under Concept 5, herein, by means of a finite structural analysis program.

Based upon the results of these analyses, it is concluded that the bicoil design provides a very stable, strong, yet flexible, component which is capable of withstanding the loads produced by the operating environment. The results of the analysis indicated that the load factor is safe against buckling. The resistance of the bicoil to side deflections is very impressive in light of its axial flexibility.

The bicoil was found to exert negligible reaction loads on the components to which it is attached, particularly the hermetic seal.

Chemical Corrosion, Sublimation and Deposition

If there would be a most critical surface, it would be at the exit of the bicoil tubes because:

- 1) Its temperature is the highest, 1573°K.
- 2) The sweeping velocity is the maximum, 90 m/s.
- 3) The wall is the thinnest, 1.25 mm.

From figure 6 a sublimation loss in a vacuum is computed to be .007 mm in 10,000 hours, a trivial amount, and the 3 atmospheres suppressing pressure effect makes it even more so or by about a reducing factor of 10^{-3} .

Oxidation effects on the high temperature zone above may be estimated from figure 7 for air. A static loss of .014 mm in a year is of no serious concern from the surface. This is .02% total thickness loss in a year. Confirming tubular experimental measurements in CO_2 are also in order since in this case it is only two orders of magnitude from being a factor. This is particularly true for CO_2 effects below.

The results of an earlier study with biowaste resistojets (ref. 15) discovered experimentally that carbonyls which form from CO_2 gas are a factor with the rhodium used early as an otherwise favorable alloying metal for platinum. As a practical matter platinum was recommended for such applications in such forms either as pure platinum, thoriated platinum or platinum palladium. Experimental verification of these for the operating time requirement was not undertaken.

Based upon these recommendations, the choice of grain stabilized platinum is made as qualified for this application from a chemical resistance viewpoint.

Rating

Advantages.- 1) The gas approaches the wall temperature very closely, therefore, the highest specific impulse for given wall temperature limit of those concepts studied.

2) Because the pressure surrounding the tube can be made by design only slightly greater than within it, the failure mode due to heater wall stress rupture is reduced.

3) The design is pressure balanced internally with no appreciable creep load for all operating conditions.

4) Thermal expansion compensation is inherent in the bicoil principle.

5) The heater is structurally sturdy transversely because the coils are metallurgically bonded along the transverse length about every half turn at equipotential points.

6) Any coil leak is not catastrophic. There is not any propellant lost. Any specific impulse degradation is minimal.

7) The pressure case is cool and can be made of cheaper materials.

Disadvantages.- 1) High current, low voltage, or 29.71 amperes and 6.83 volts (CO_2). This voltage value can be increased perhaps 2 to 3 times with refined bicoil design.

2) The unit is longer than Concept 1, and hence, has a slightly lower heater efficiency η_h of .88 than the .93 for Concept 1 at the 1573°K wall temperature design point.

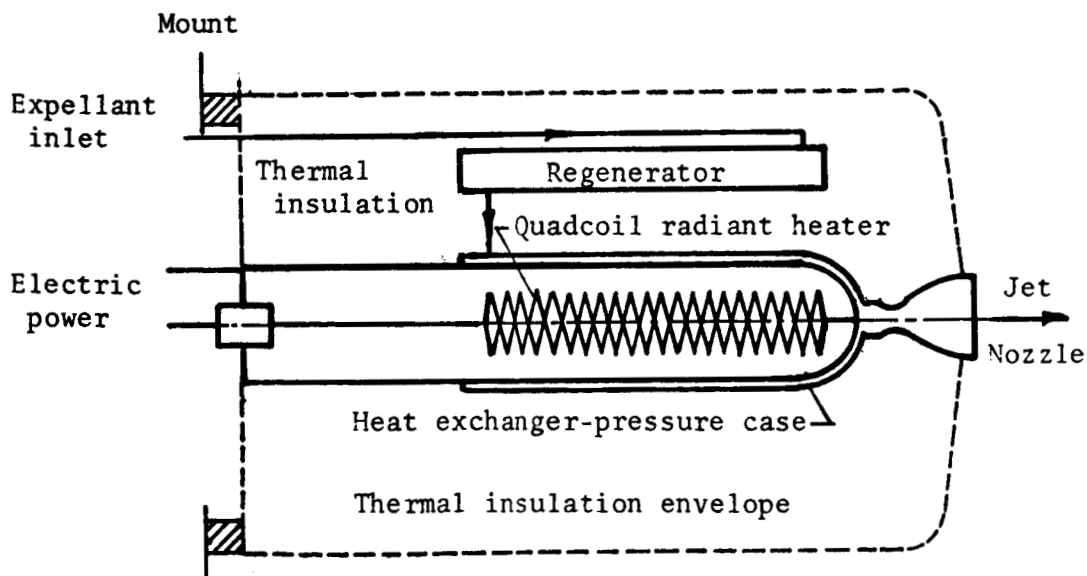
APPENDIX D

CONCEPT 4 - NONEXPOSED RADIANT HEATER WITH FLOW IN THE SURROUNDING CASE PASSAGE - (BIOWASTE)

Concept 4, the last design studied, utilized Concept 6 with a simple transmutation of the high temperature materials to ones which could be exposed to the oxidizing biowaste gas. This is done by substituting grain stabilized platinum for rhenium. The separate heater itself remains grain stabilized rhenium with its same temperature capability as used in Concept 6. This section treats only those things of Concept 6 which must be changed to accommodate biowaste and the different resultant performance. The figure below illustrates the concept schematically.

The design physically separates the heat exchanger function from that of the ohmic heater. Used as a biowaste resistojet, the heat exchanger may be made of grain stabilized platinum of thickness to insure its structural integrity. It is a favorable application of the concept in that a rhenium heater operates at significantly higher temperatures than grain stabilized platinum.

Several variations are presented. These are the unpressurized and pressurized heater designs. The detailed heat transfer results of each are shown. The performance of the pressurized cavity is shown as a significant improvement with a second variation of high emissivity surface incorporation in the radiation heat transfer link as making a notable further improvement.



Description

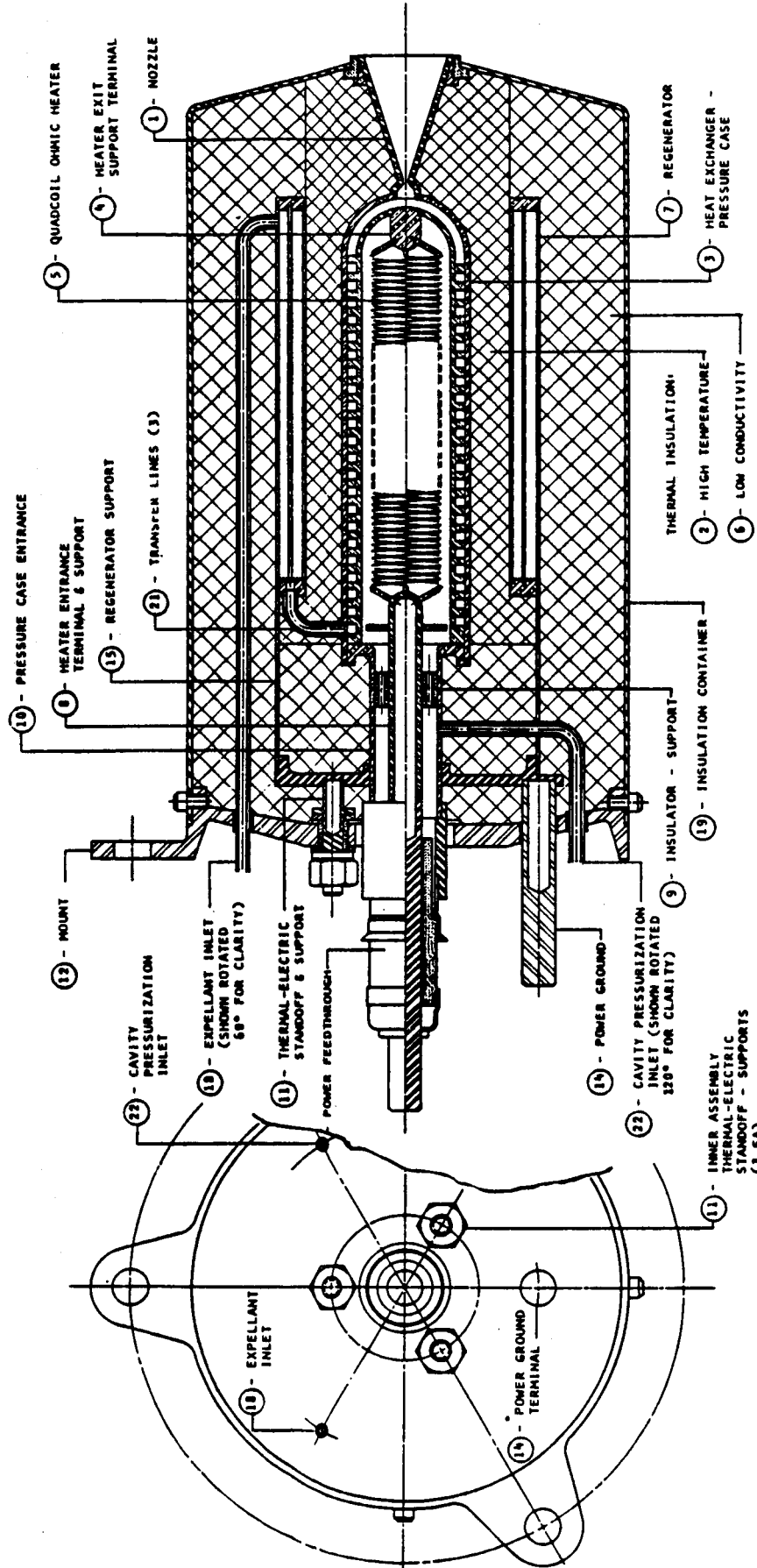
Description.- The final preliminary design of Concept 4 is identical to that of Concept 6, as shown in figure 29. Table 24 gives the identification of the components with new choices for materials. The reader is referred to this section of Concept 6 which is identical to 4 for functional descriptions.

TABLE 24
CONCEPT 4 - COMPONENT PARTS, MATERIALS OF CONSTRUCTION

| <u>Item</u> | <u>Component</u> | <u>Material</u> |
|-------------|-------------------------------------|--|
| 1. | Nozzle | Grain stabilized platinum |
| 2. | High temperature thermal insulation | Fibrous zirconia ¹ |
| 3. | Heat exchanger pressure case | Grain stabilized rhenium |
| 4. | Heater exit support terminal | Bonded grain stabilized platinum to platinum/rhodium |
| 5. | Quadcoil ohmic heater | Grain stabilized rhenium |
| 6. | Low k thermal insulation | Fibrous Aluminosilicates ² |
| 7. | Regenerator | Grain stabilized platinum |
| 8. | Heater entrance, terminal support | Grain stabilized rhenium |
| 9. | Heater electric insulator, support | Alumina 99.5% |
| 10. | Pressure case entrance | Grain stabilized rhenium |
| 11. | Thermal-electric, standoff, support | AISI 304L |
| 12. | Mount | AISI 304L |
| 13. | Power feedthrough | Metal to ceramic seal materials ³ |
| 14. | Power ground | AISI 304L |
| 15. | Regenerator support | AISI 304L |
| 16. | Electric insulator | Alumina 99.5% |
| 17. | Electric insulator | Alumina 99.5% |
| 18. | Expellant inlet | AISI 304L |
| 19. | Insulation container | AISI 304L |
| 20. | Electric insulator | Alumina 99.5% |
| 21. | Transfer lines (3) | Grain stabilized platinum |

1. Data for Mink 2000, Johns-Mansville Aerospace Products, N.Y., NY.

2. Typical materials: nickel A conductors; glazed high alumina ceramic (85% min. Al₂O₃) insulators; vacuum tube grade brazing alloys and nickel-iron caps. Data from Ceramaseal, Inc., New Lebanon Center, NY.



Scale: Full size

Figure 29. - Concept 4, a biowaste resistojet with non-exposed radiant rhenium heater with flow in the surrounding case passage of grain stabilized platinum.

Note that the heater assembly forward connector and mount (-4) penetrates to the gas passage. This terminal is to be made of two pieces. That interfacing the gas surface, the nozzle plenum will be grain stabilized platinum. That at the heater side will be made of platinum/rhodium as it is not exposed to the gas, as the latter enjoys a significant advantage over that of grain stabilized platinum for use in the cavity at the interface.

Performance

The projected performance is summarized for a number of configurational variations and operating temperatures for the study propellants in the following tables. This was necessary as the unpressurized cavity case did not meet projected performance at 1573°K.

Table 25 shows the projected performance on CO₂ and separately H₂O (steam) at the goal heater element temperature of 1573°K specified for the biowaste resistojets. Since the heater element was divorced from the biowaste exposure, the case of the heater element temperature for the augmenters such as in Concept 6 of 2073°K was also studied and is presented in table 25. This increase in heater element temperature will bring the basic design within the goal performance.

Pressurizing the heater cavity separately with nitrogen enhances the heat transfer by the addition of the convective heat transfer mode for the same heater element temperature. Table 26 shows that the specific impulse is increased from 92.6 seconds to 117 seconds projected with pressurization. This is still less than the contractual goal of 130 and 200 seconds, respectively for CO₂ and H₂O. Increasing the heater element in conjunction with pressurization provides a further specific impulse enhancement.

Table 27 shows the effect of adding a high emissivity surface to the inside of the pressure case to promote heat transfer reception radiantly from the heater as well as from nitrogen pressurization. It is seen that this will permit operation above the contractual goal for CO₂ of 130 seconds for the 1573°K heater case, the only case studied, to 138 seconds. By enhancing the performance further with a heater temperature increase above the goal temperature to 2073°K, a specific impulse of 179 seconds can be achieved.

The performances projected here are under space vacuum conditions. In the similar discussion under Concept 6, it is cautioned that test cell pressures to simulate this operational performance should be less than 10 microns in order to simulate free molecule heat transfer in the cavity (like a Dewar or vacuum bottle) for the case of the unpressurized cavity. Otherwise

performance measured under continuum conditions would be measured. This would be like those of Configuration 4D, a pressurized cavity. This would introduce serious over-estimation of the propulsive performance to be expected in space.

TABLE 25
 CONCEPT 4C PROJECTED PERFORMANCE
 EFFECT OF HEATER TEMPERATURE
 WITH HEATER CAVITY IN SPACE VACUUM

| Propellant | CO ₂ | H ₂ O | CO ₂ | H ₂ O |
|----------------------------------|-----------------|------------------|-----------------|------------------|
| Maximum heater temp. °K | 1573 | 1573 | 2073 | 2073 |
| Specific impulse, s | 92.6 | 148 | 160 | 214.5 |
| Heater cavity | | | | |
| Gas atmosphere | Vacuum | Vacuum | Vacuum | Vacuum |
| Pressure, atm | ≈0 | ≈0 | ≈0 | ≈0 |
| Surface material | GSPT | GSPT | GSPT | GSPT |
| Electric input | | | | |
| Voltage, V | 11.19 | 11.30 | 22.61 | 23.08 |
| Current, A | 4.92 | 4.96 | 8.62 | 8.78 |
| Power, W | 55.01 | 56.08 | 194.87 | 202.74 |
| Power/thrust, W/mlb. | 1.27 | 1.18 | 3.89 | 4.03 |
| Nozzle chamber | | | | |
| Total pressure, Atm | 3.0 | 3.0 | 3.0 | 3.0 |
| Total temp., °K | 555.8 | 616.2 | 1332 | 1221.6 |
| Expellant inlet | | | | |
| Total temperature, °K | 300 | 441.7 | 300 | 441.7 |
| Mass flow, gms/sec | .212 | .146 | .1420 | .1058 |
| Initial gas power, W | 45.45 | 120.00 | 30.44 | 86.96 |
| Power lost from heater, W | 2.89 | 5.35 | 29.54 | 25.93 |
| Total input power, W | 100.46 | 176.08 | 225.31 | 289.70 |
| Maximum gas temp., °K | 557.4 | 617.4 | 1341.4 | 1225.5 |
| Max. case temp., °K | 560.1 | 620.3 | 1357.6 | 1251.3 |
| Power efficiencies | | | | |
| Overall, η _o | .870 | .873 | .776 | .808 |
| Overall electric, η _e | 1.589 | 2.742 | .897 | 1.155 |
| Heater, η _h | .971 | .970 | .869 | .910 |
| Nozzle, η _n | .896 | .900 | .893 | .888 |
| Thrust check, lb. | .0433 | .0476 | .0509 | .0503 |

TABLE 26
 CONCEPT 4D PROJECTED PERFORMANCE
 WITH PRESSURIZED HEATER CAVITY AT 3 ATMOSPHERES

| Propellant | CO ₂ | H ₂ O | CO ₂ | H ₂ O |
|----------------------------|-----------------|------------------|-----------------|------------------|
| Maximum heater temp. °K | 1573 | 1573 | 2073 | 2073 |
| Specific impulse, s | 117 | 171 | 171 | 232 |
| Heater cavity | | | | |
| Gas atmosphere | N ₂ | N ₂ | N ₂ | N ₂ |
| Pressure, Atm. | 3.0 | 3.0 | 3.0 | 3.0 |
| Surface Material | GSPT | GSPT | GSPT | GSPT |
| Electric input | | | | |
| Voltage, V | 15.60 | 15.64 | 24.04 | 25.24 |
| Current, A | 6.90 | 6.91 | 9.25 | 9.68 |
| Power, W | 107.63 | 108.12 | 222.39 | 244.40 |
| Power/thrust, W/mlb. | 2.25 | 2.21 | 4.45 | 4.88 |
| Nozzle chamber | | | | |
| Total pressure, Atm | 3.0 | 3.0 | 3.0 | 3.0 |
| Total temp., °K | 817.3 | 812.7 | 1495.5 | 1405.8 |
| Expellant inlet | | | | |
| Total temperature, °K | 300 | 441.7 | 300 | 441.7 |
| Mass flow, gms/sec | .186 | .130 | .1327 | .0980 |
| Initial gas power, W | 39.87 | 106.85 | 28.45 | 80.55 |
| Power lost from heater, W | 8.15 | 9.51 | 40.28 | 36.72 |
| Total input power, W | 147.50 | 214.97 | 240.84 | 324.95 |
| Maximum gas temp., °K | 821.1 | 815.5 | 1507.3 | 1413.5 |
| Max. case temp., °K | 825.9 | 820.4 | 1530.6 | 1435.9 |
| Power efficiencies | | | | |
| Overall, η_o | .830 | .850 | .744 | .780 |
| Overall electric, η^* | 1.138 | 1.690 | .839 | 1.037 |
| Heater, η_h | .945 | .956 | .882 | .887 |
| Nozzle, η_n | .878 | .889 | .844 | .879 |
| Thrust check, lb. | .0479 | .0490 | .0500 | .0501 |

C-2

TABLE 27
 CONCEPT 4F PROJECTED PERFORMANCE
 WITH PRESSURIZED HEATER CAVITY AT 3 ATMOSPHERES
 AND EMISSIVE COATING ENHANCEMENT OF CAVITY WALL

| Propellant | CO ₂ | CO ₂ |
|----------------------------------|--------------------------------|--------------------------------|
| Maximum heater temp., °K | 1573 | 2073 |
| Specific impulse, s | 138 | 179 |
| Heater cavity | | |
| Gas atmosphere | N ₂ | N ₂ |
| Pressure, Atm | 3.0 | 3.0 |
| Surface material | Al ₂ O ₃ | Al ₂ O ₃ |
| Electric input | | |
| Voltage, V | 18.07 | 25.15 |
| Current, A | 8.09 | 9.77 |
| Power, W | 146.23 | 245.78 |
| Power/thrust, W/mlb _r | 2.98 | 4.93 |
| Nozzle chamber | | |
| Total pressure, Atm | 3.0 | 3.0 |
| Total temp., °K(node 29) | 1045.1 | 1627.7 |
| Expellant inlet | | |
| Total temperature, °K | 300 | 300 |
| Mass flow, gms/sec | .161 | .1263 |
| Initial gas power, W | 34.52 | 27.08 |
| Power lost from heater, W | 16.41 | 50.09 |
| Total input power, W | 180.75 | 272.86 |
| Maximum gas temp., °K | 1052.5 | 1643.4 |
| Max. case temp., °K | 1060.2 | 1666.6 |
| Power efficiencies | | |
| Overall, η _o | .816 | .713 |
| Overall electric, η* | 1.008 | .791 |
| Heater, η _h | .909 | .816 |
| Nozzle, η _n | .898 | .874 |
| Thrust check, lb _r | .0490 | .0498 |

1. Exceeds goal temperature for platinum of 1573°K.

Thermal Analysis

The thermal analysis using the mathematical computational method uses the same node diagram as for Concept 6. The methods are the same. Only the methods and materials are different.

The results of the parametric study are best presented in figures 30 through 34.

Configuration 4C which employs a vacuum cavity with radiation directly to the grain stabilized rhenium surface, shown in figure 30 for the case of CO_2 at the maximum heater temperature of 1573°K . The striking feature is the extremely large temperature difference between the wire heater and the resultant gas temperature. Radiant heat transfer is poorer at low temperatures; the effect being T^4 related. Figures 32a and b show the effect of increasing this temperature to the allowable temperature allowed in the hydrazine augments such as Concept 6. The enhancement of gas temperature is significant even though the temperature between wire heater and gas is still very large. The goal specific impulses are met in this way at the price of heater temperature. Note that no grain stabilized platinum materials exceed the 1573°K specification.

Concept 4D employs a nitrogen immersant gas in the cavity with a metal to ceramic seal and a separate pressurization system to the cavity. The temperature distributions shown in figures 32a and b where both 1573°K and 2073°K heater element temperature improve the temperature of the gas over that of the vacuum case in each instance. However, a temperature of 2073°K is still required to achieve goal performance of the study.

Concept 4F is a pressurized cavity with an inner surface of the grain stabilized platinum being enhanced as to emissivity by a metal oxide coating of alumina. Figure 34 shows the gas temperatures much more closely approach the heater wire temperature of all the cases studied for both the 1573°K heater element case where specified goal performance of the contract were met.

Note in all cases that the hermetically insulated feedthrough is at or above critical temperatures specified by the manufacturer. However, the thermal model conservatively assumed there would be no thermal sinking of the terminal by the power feed cable. When this factor is introduced, these values fall within the 623°K specification or below as shown in later studies but not shown here.

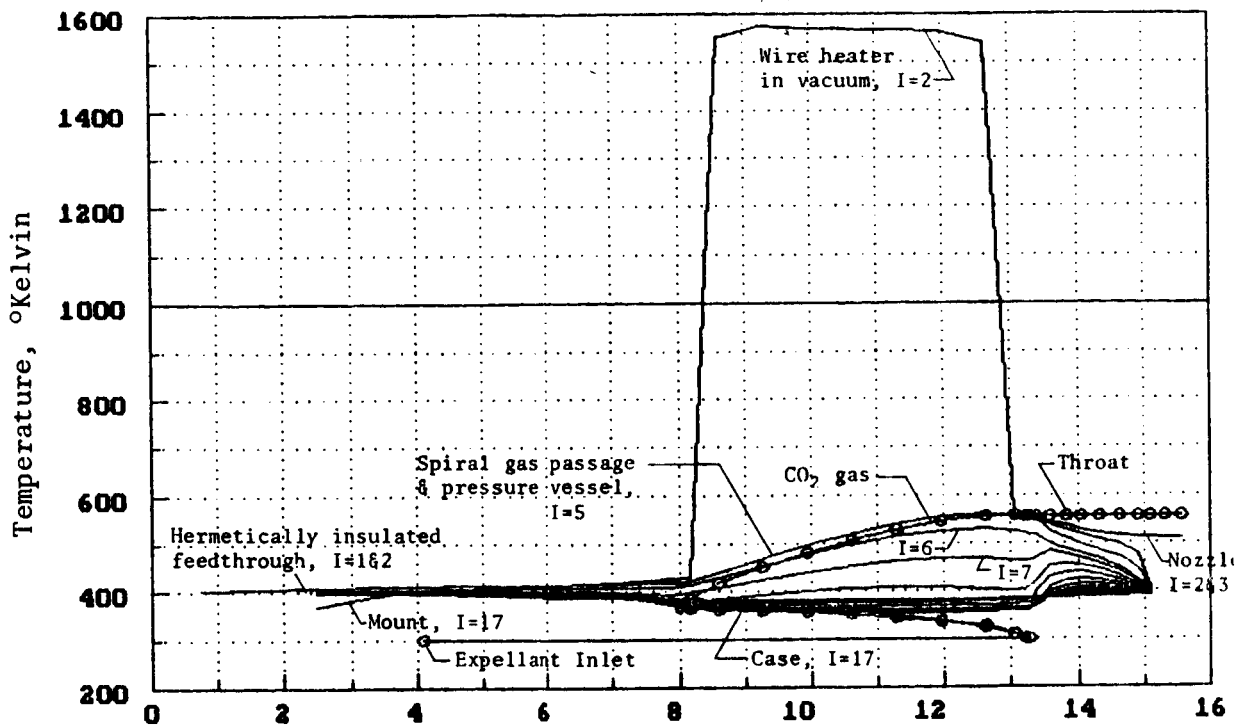


Figure 30. - Temperature distribution of Concept 4C on carbon dioxide at a maximum heater temperature of 1573°K. Shows the large temperature difference between heater and gas when the cavity is exposed directly to hard space vacuum.

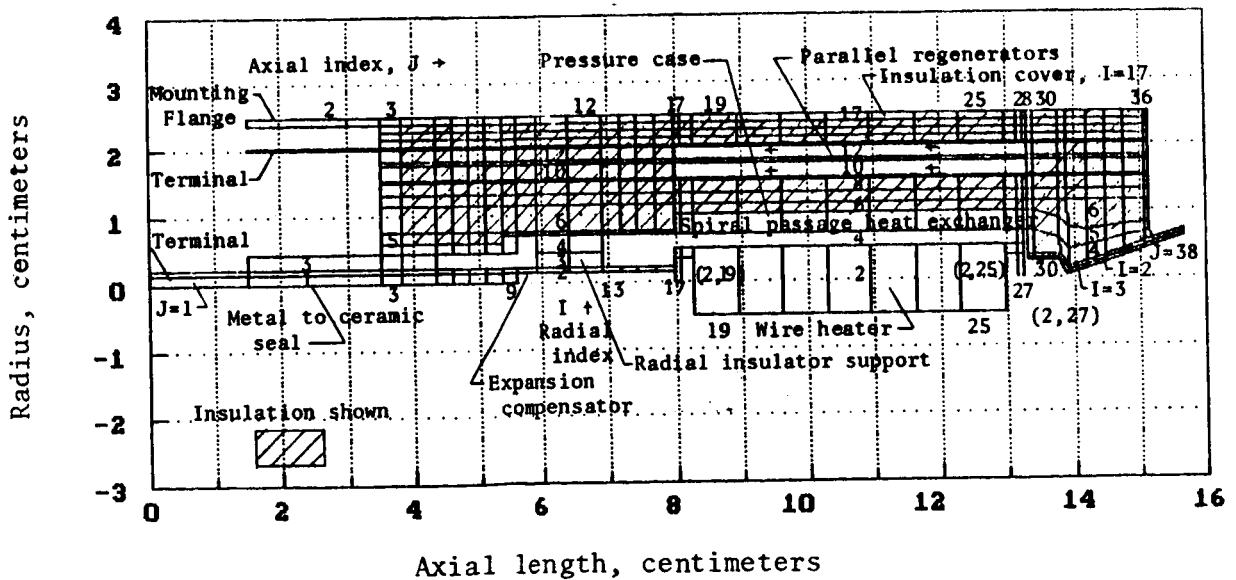


Figure 31. - Thermal node diagram used in the analysis of Concept 4.

ORIGINAL PAGE IS
OF POOR QUALITY

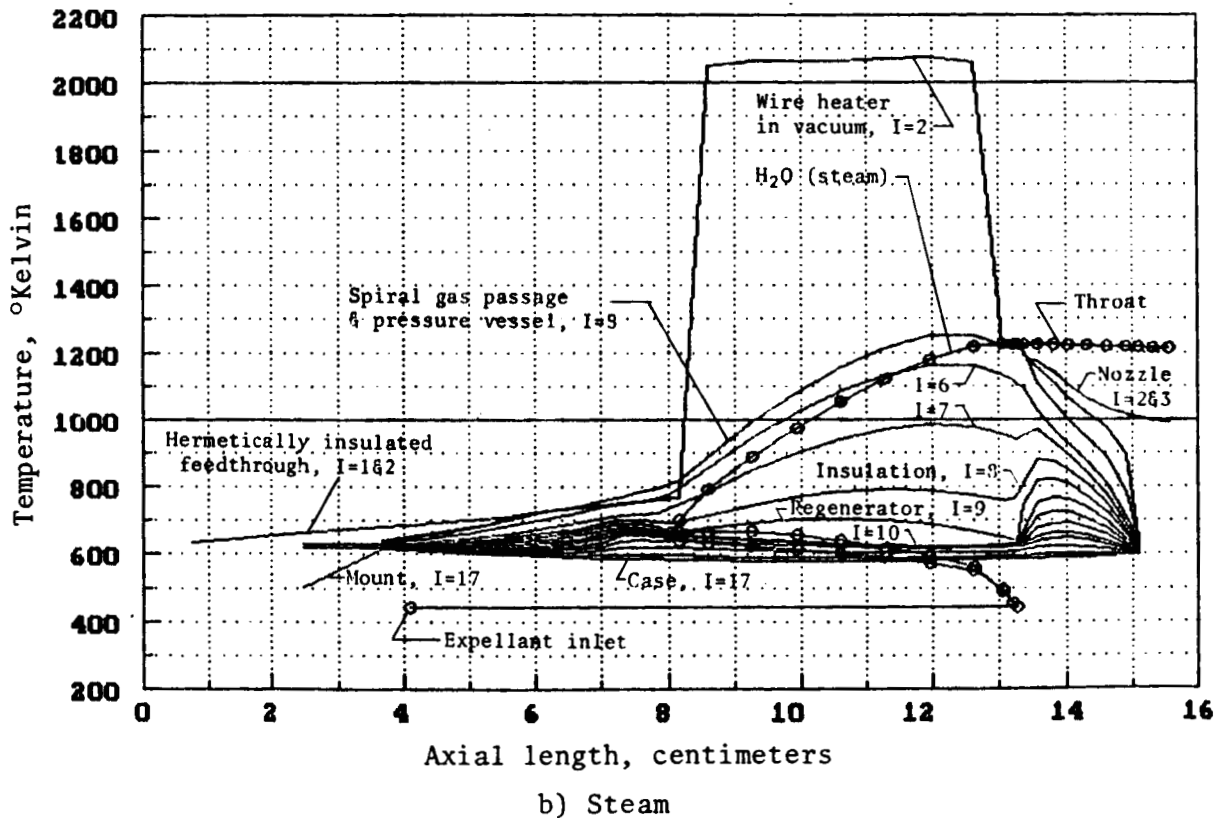
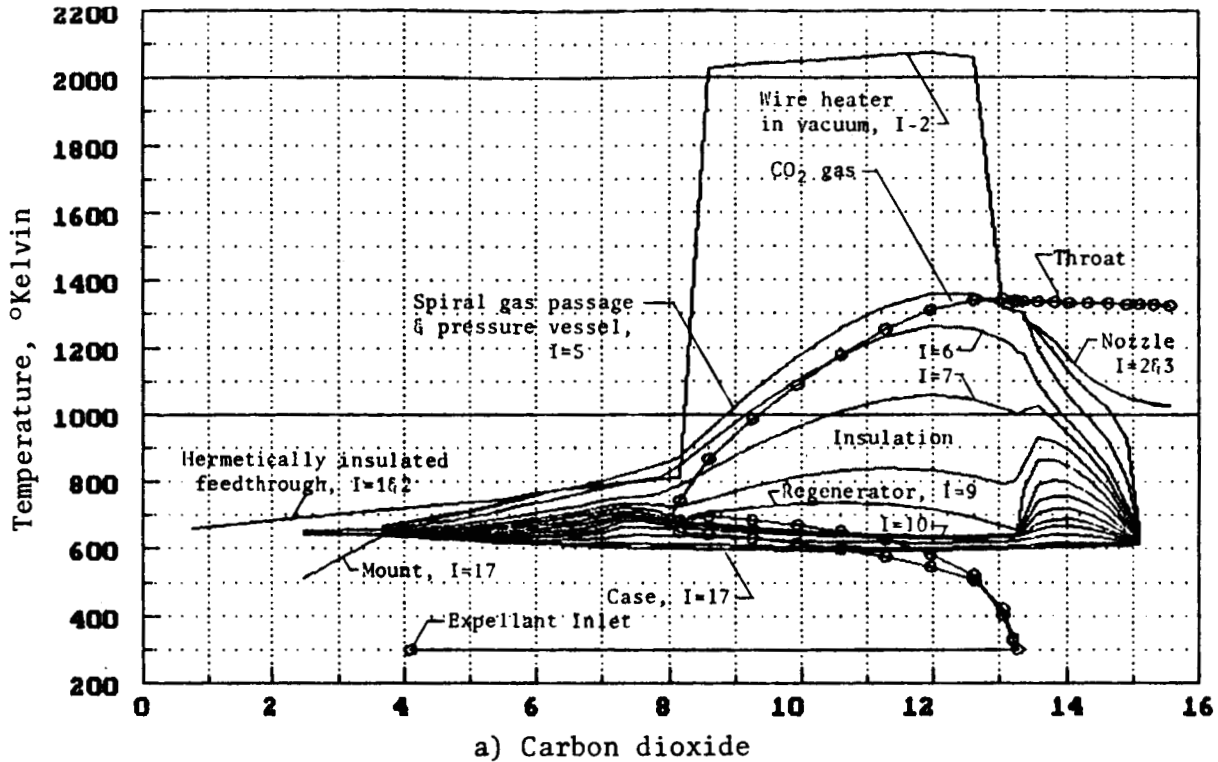
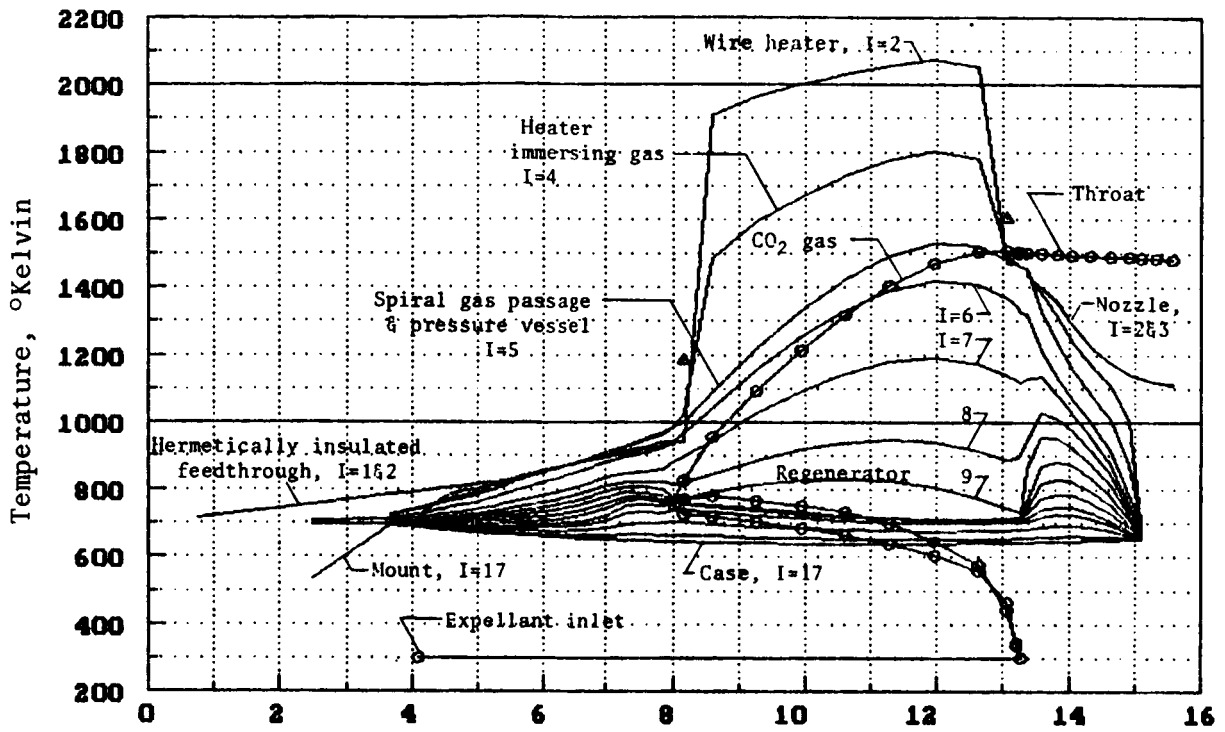
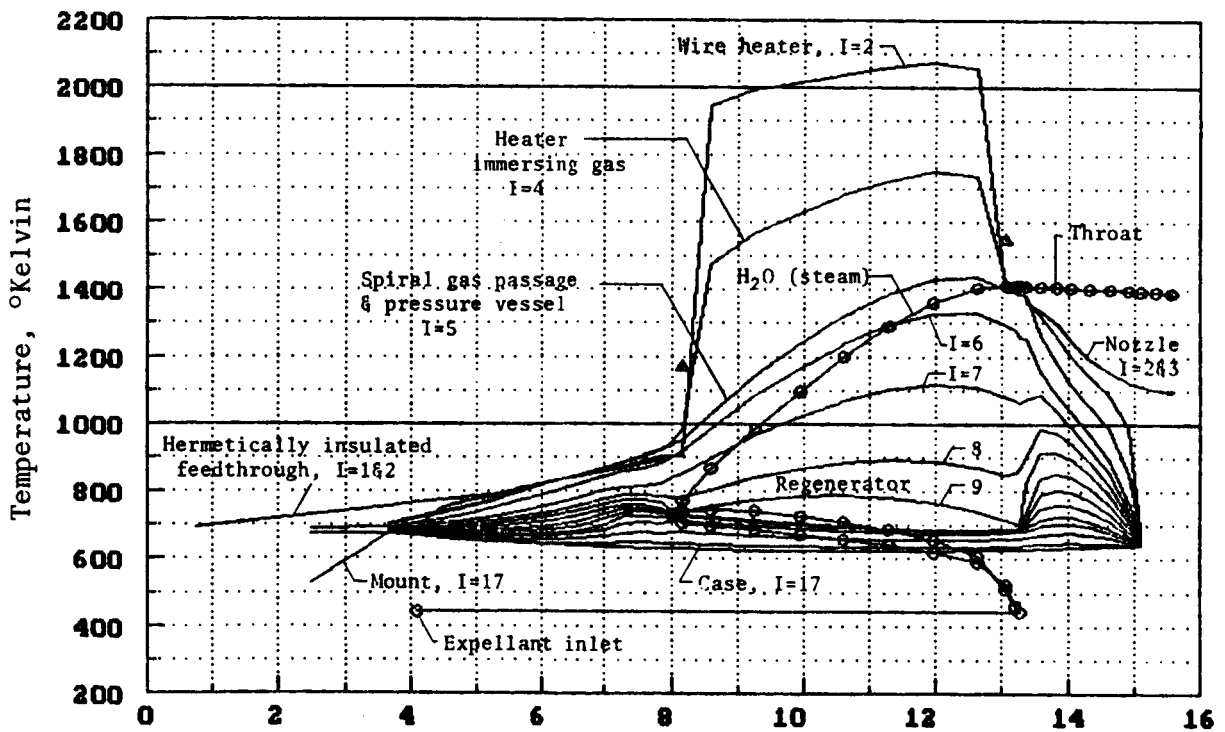


Figure 32. - Temperature distribution of Concept 4C at a maximum heater temperature of 2073°K. Heater wire cavity exposed directly to a vacuum.

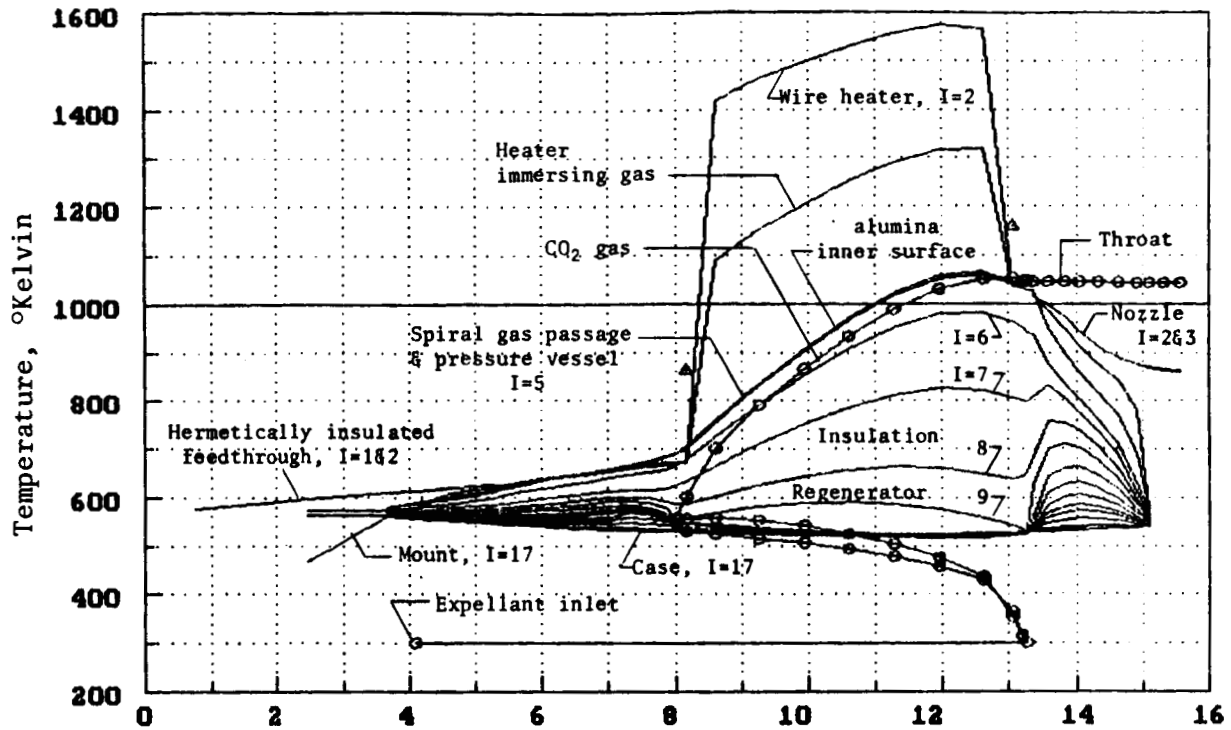


a) Carbon dioxide

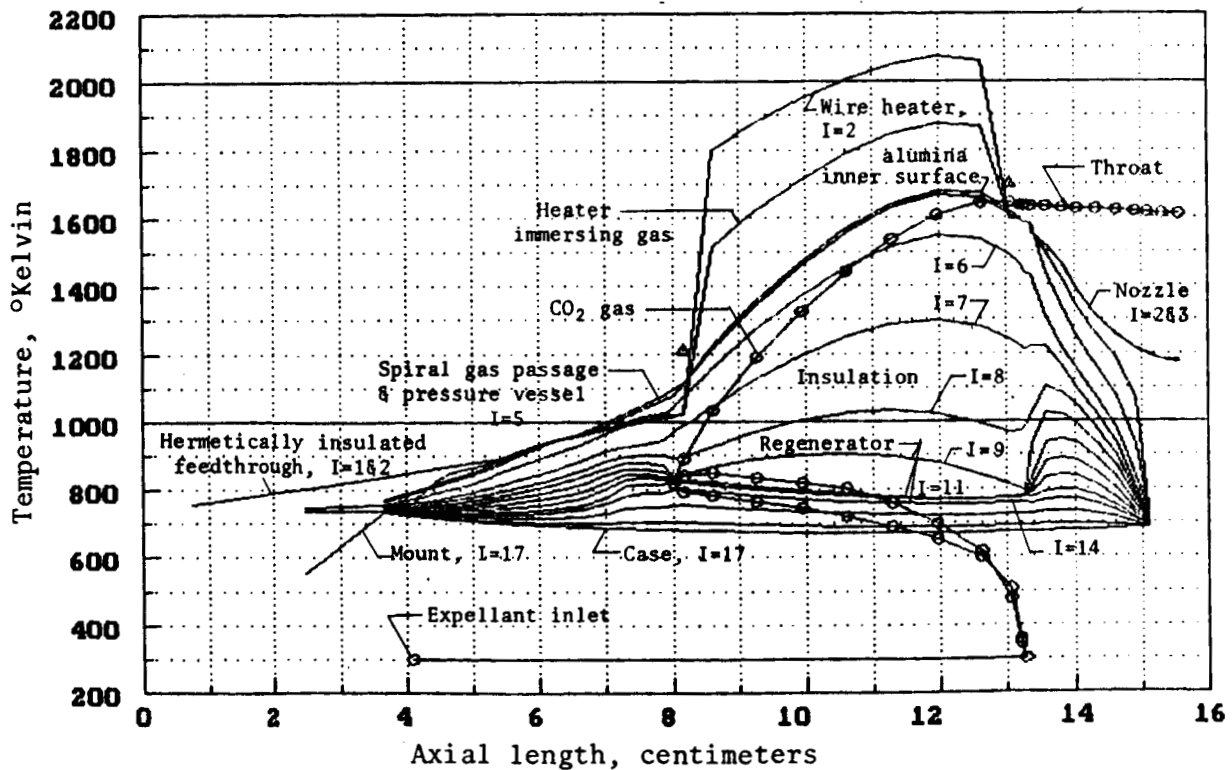


b) Steam

Figure 33. - Temperature distribution of Concept 4D at a maximum heater temperature of 2073°K. Heater wire immersed in nitrogen gas for heat transfer augmentation and sublimation suppression.



a) Maximum heater temperature 1573°K



b) Maximum heater temperature 2073°K

Figure 34. - Temperature distribution of Concept 4F on carbon dioxide. Heater immersed in nitrogen gas. Cavity surface of alumina for high absorptivity.

Gas Dynamic Analysis

The summary of parameters shown in Concept 6 are generally representative of the fluid flow parameters here. The Mach numbers are low. The pressure drops are low. The flow is laminar. For brevity, they are omitted.

Mechanical Design

Pressure envelope.- As in Concept 6, the critical stress region and maximum temperature of the pressure case is at the hemispherical end where the nozzle joins it. Its stress is about 2.1 MPa (300 psi) also. The temperature is now 960°K. The stress rupture endurance for 10,000 hours for the grain stabilized platinum design line projected is 5.8 MPa (842 psi), certainly an adequate factor of safety. The design choice here, of course, is Configuration 4F. The other remarks relative to mechanical design of Concept 6 are applicable here.

Chemical Corrosion, Sublimation and Deposition

Because of the robust character of the Concept 4 design, and the maximum temperatures of the gas passages for 4F at a heater element temperature of 1573°K, no serious problems due to sublimation or oxidation, erosion are anticipated.

Rating

The pros and cons of the radiation type resistojet are similar to Concept 6, differing only in the numerical magnitude. An additional advantage listed for Concept 4 over that shown in Concept 6 is that the performances projected here which can be equally applicable to a type 6 design is that emissive surfaces can lower the heater element temperature required to meet goal performance. It was the only case where goal performance was met at 1573°K for this type design.

Advantages.- 1) Higher voltages than the integral convective designs or 18 volts for Concept 4F as compared to 6.83 for Concept 3. While higher voltages can be incorporated in the convective design, it is with more struggle. The reason is that the radiant electrical heater and gas heater exchanger designs are more independent in these functions than an integral heater - convective heat exchanger.

2) The heater exchanger of Concept 4 is more massive than that of the direct convective Concept 3. Hence, it is less sensitive to erosion.

Disadvantages.- 1) Radiant designs produce lower specific impulse for the same maximum heater temperature. The maximum specific impulse for Concept 3 is 170.2 and 138 seconds for Concept 4F, both on CO₂ for the same heater element temperature.

2) The thermal mass of Concept 4 gas exchanger is 10 times more than that of the Concept 3 convective exchanger and therefore less specific impulse responsive on short firings.

3) The radiant heater type design must be specifically sized with regard to power required for a specific propellant. It is more closely a fixed power thruster. Higher specific heat propellants operate at lower gas temperatures and specific impulse than possible with a convective design under the same temperature maximum heater limits. The latter convective designs operate closely at the same gas temperature, the combined heater element exchanger more closely matching the power requirement needs to do this.

APPENDIX E

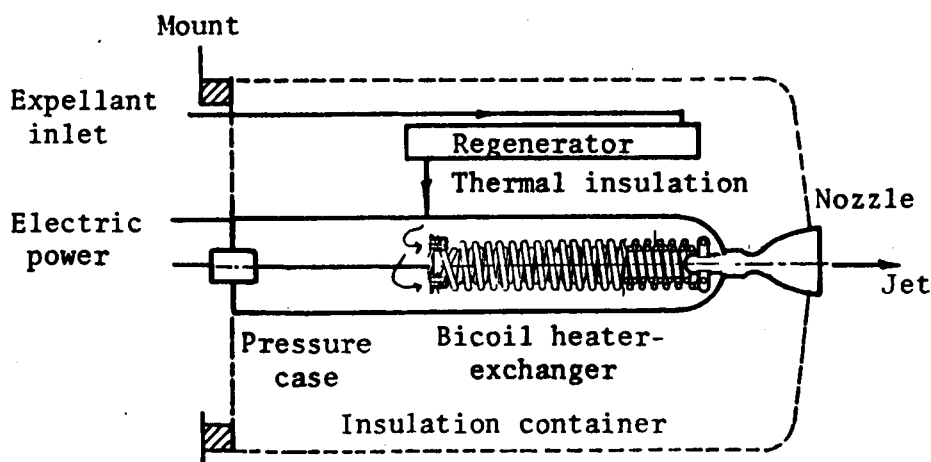
CONCEPT 5 - EXPOSED METALLIC BICOIL HEATER WITH INTERNAL FLOW

Concept 5, like Concept 3 presented earlier as a biowaste resistojet, uses the bicoil configuration as an integrated tubular ohmic heater and gas heat exchanger for a hydrazine augments. The philosophy of the design is to achieve the lowest material temperature operation for the goal specific impulse, that is the required gas temperature at the nozzle. This promotes reliability and longer life.

Primarily because of the high temperature inlet gases from the decomposition chamber of at least 866°K if the ammonia were fully dissociated, and higher if not, a high temperature central pressure case design is used. This is unlike Concept 3 which has a cool inlet gas. The reason for this choice was that a higher heater thermal efficiency was found compared to that with use of the external type pressure case of Concept 3.

All high temperature parts are fabricated of grain stabilized rhenium. No electric insulation is used in the high temperature zones. Propellant flow deters backstreaming of any sublimed metallic vapors onto the metal to ceramic seal.

The bicoil consists of two coils of precisely the same tubular heating length and cross-sectional diameter coiled in opposite rotation, one closely fitting within the other. The pressure drop and flow of each passage and the resistance heating length are the same. The cross-over points are at the same voltage potential and the two coils are physically bonded to one another there. As a result the bicoil design is found by stress analysis to be stable and transversely rigid yet accommodating to axial thermal expansion compensation.



Description

The final preliminary design of Concept 5, Configuration E is shown in figure 35. Table 28 identifies its components and materials.

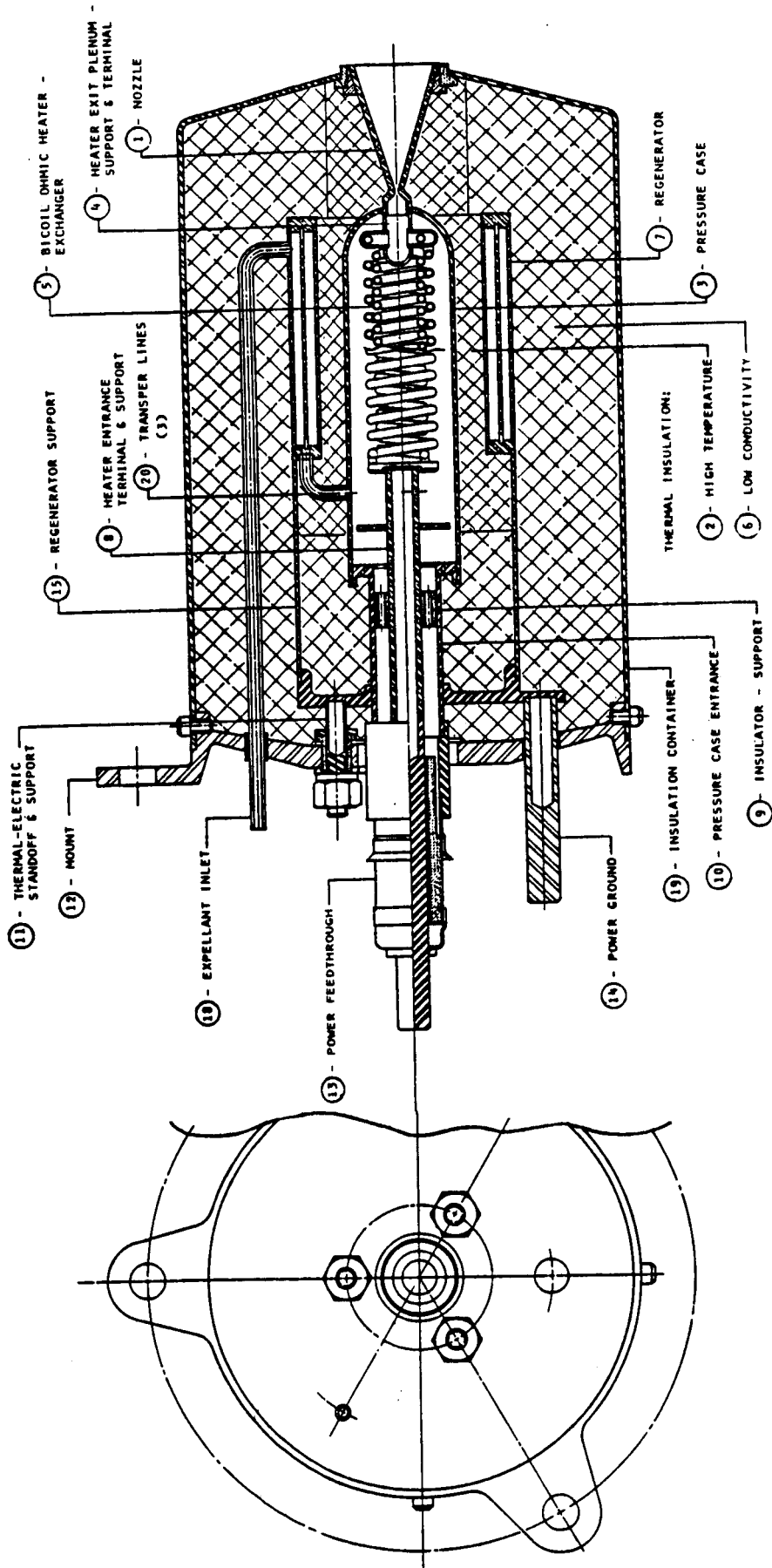
TABLE 28
CONCEPT 5 COMPONENT PARTS, MATERIALS OF CONSTRUCTION

| <u>Item</u> | <u>Component</u> | <u>Material</u> |
|-------------|--|--|
| 1. | Nozzle | Grain stabilized rhenium |
| 2. | High temperature thermal insulation | Fibrous zirconia ¹ |
| 3. | Heater chamber pressure case | Grain stabilized rhenium |
| 4. | Heater exit plenum-support-terminal assembly | Grain stabilized rhenium |
| 5. | Bicoil ohmic heater-exchanger assembly | Grain stabilized rhenium |
| 6. | Low K thermal insulation | Min-K 2000 ² |
| 7. | Regenerator | Grain stabilized rhenium |
| 8. | Heater entrance, terminal support | Grain stabilized rhenium |
| 9. | Heater electric insulator, support | Alumina 99.5% |
| 10. | Pressure case entrance | Grain stabilized rhenium |
| 11. | Thermal-electric, standoff, support | AISI 304L |
| 12. | Mount | AISI 304L |
| 13. | Power feedthrough | Metal to ceramic seal materials ³ |
| 14. | Power ground | AISI 304L |
| 15. | Regenerator support | AISI 304L |
| 16. | Electric insulator | Alumina 99.5% |
| 17. | Electric insulator | Alumina 99.5% |
| 18. | Expellant inlet | Grain stabilized rhenium |
| 19. | Insulation container | AISI 304L |
| 20. | Transfer lines (3) | Grain stabilized rhenium |

1. Data from Zircar, Florida, NY

2. Data for Min-K 2000, Johns-Mansville Aerospace Products, N.Y., NY.

3. Typical materials: nickel conductors; glazed high alumina ceramic (85% min. Al₂O₃) insulators; vacuum tube grade brazing alloys and nickel-iron caps. Data from Ceramaseal, Inc., New Lebanon Center, NY.



Scale: Full size

Figure 35. - Concept 5, a hydrazine augmeter with exposed metallic bicoil heater with internal flow.

The key feature of this concept is the bicoil, an integral tubular ohmic heater and gas exchanger (-5). The bicoil is mounted within the pressure case (-3). Its exit is supported by member (-4) which also serves as an electric terminal and gas plenum feeding the nozzle. The bicoil at the entrance end is supported by its terminal and support (-8).

The bicoil heater geometry is tabulated below. This bicoil uses two rhenium tubes each of 26.91 inches of running, active length. The tube outside diameter is 1.24 mm (0.049 in.) and the inner is 0.99 mm (0.039 in.).

TABLE 29
BICOIL HEATER GEOMETRY

| | Inner Coil | Outer Coil |
|------------------------------|---------------|---------------|
| Coil pitchline diam mm (in.) | 6.223 (.245) | 8.763 (.345) |
| Lead per turn, mm (in.)/turn | 1.765 (.0695) | 2.489 (.0980) |
| Number of turns (heating) | 16.382 | 11.618 |
| Axial length, mm (in.) | 32.13 (1.265) | 32.13 (1.265) |

The hermetic envelope of the pressure case (-3) is completed by the power feedthrough and hermetic seal (-13) and the nozzle (-1). A parallel concentric pass regenerator (-7) in counterflow, located at the radial position shown, reduces the radial heat loss. It is supported by the regenerator support (-15) and by the three transfer lines to the case.

The inner thruster assembly is thermally and electrically stood off from the mount by means of the three (-11) assemblies. The power terminals (-13) and (-4) accept the spacecraft cable connectors. The thruster is designed to be mounted to the spacecraft at three points by the equally spaced attachment holes on the mount.

Two level fibrous thermal insulation systems are shown. The inner, higher temperature material is zirconia and the outer is Min-K 2000. The containing canister (-19) completes the system.

The ground side of the power line is connected to the terminal (14) which connects to the pressure case (-3) via its connector (-15) and entrance section (-10). Current passes through the gas exit terminal support (-4) to the bicoil ohmic heater and gas exchanger to the entrance terminal and support (-8). The circuit is completed through the power feedthrough (-13) to the high side of the power line. A variation of the bicoil is capable of being made a 28 volt design, but is not presented here.

The expellant feed line enters the thruster at the nozzle end of the parallel pass regenerator (-7). Three lines exiting from the regenerator enter the pressure case (-3) at the station of the bicoil entrance. The gas can only exit the thruster nozzle through the twin passages of the bicoil.

Performance

The projected performance of the bicoil convective type hydrazine augmenters in the successive iterative design are shown in table 30 for a heater temperature of 2073°K. The thermal performance is based upon the analysis discussed in the next section. The nozzle is the optimal model as discussed earlier. The geometry of the nozzle shown, while believed close to optimal, is only a generalized one so as to indicate position in the configuration.

TABLE 30
CONCEPT 5 PERFORMANCE SUMMARY
FOR AUGMENTED HYDRAZINE

| Configuration | Projected Performance | | | |
|----------------------------------|-----------------------|--------|--------|--------|
| | 5A | 5B | 5D | 5E |
| Specific impulse, s | 317.5 | 317 | 317.8 | 317 |
| Maximum heater temp., °K | 2073 | 2073 | 2073 | 2073 |
| Electric input | | | | |
| Voltage, V | 13.46 | 13.55 | 8.88 | 8.94 |
| Current, A | 25.69 | 24.88 | 33.11 | 33.04 |
| Power, W | 345.79 | 337.14 | 294.19 | 295.32 |
| Power/thrust. W/mlb _r | 7.03 | 6.89 | 6.00 | 6.02 |
| Nozzle chamber | | | | |
| Total pressure, Atm | 3.00 | 3.00 | 3.00 | 3.00 |
| Total temperature, °K | 2005.4 | 1995.5 | 2007.5 | 1994.2 |
| Expellants inlet | | | | |
| Total temperature, °K | 866.5 | 866.5 | 866.5 | 866.5 |
| Mass flow, gms/sec | .070 | .070 | .070 | .070 |
| Initial gas power, W | 166.84 | 166.84 | 166.84 | 166.84 |
| Power lost from heater, W | 118.72 | 107.98 | 55.21 | 51.12 |
| Total input power, W | 512.63 | 503.98 | 461.03 | 472.16 |
| Maximum gas temp., °K | 2063.5 | 2061.0 | 2062 | 2058.7 |
| Max. case temp., °K | 1859.9 | 1837.0 | 1772 | 1758 |
| Power efficiencies | | | | |
| Overall, η_o | .662 | .671 | .737 | .732 |
| Overall electric, η^* | .981 | 1.003 | 1.156 | 1.145 |
| Heater, η_h | .768 | .786 | .888 | .889 |
| Nozzle, η_n | .862 | .854 | .838 | .823 |
| Thrust check, lb _r | .0492 | .0489 | .0490 | .049 |

Configuration 5E is the overall choice for this type design for the cases studied. Its principal difference from 5D is that it is simpler to build than 5D because of the propellant entry into the nozzle end of the regenerator. It has a lower pressure case temperature and is expected to be of higher reliability and of longer life.

The evolutionary steps in reaching 5E from the initial 5 are discussed in the thermal analysis.

Its attraction is that the tubes heat the exiting gas to within 50°C of its maximum structure temperature and in a rapidly responsive way during starting. Since the heater is immersed in the expellant gases, low pressure differentials, hence low stresses across the wall, are involved.

Thermal Analysis

In the analysis of Concept 3, which introduced the bicoil ohmic heater and exchanger, a simplified heat transfer equation was presented for the boundary condition of constant heat flux at the wall. This was based upon constant physical properties of the gas and wall. The heat transferred to the gas, Q , in laminar flow in a single heated tube of length, L , was shown as

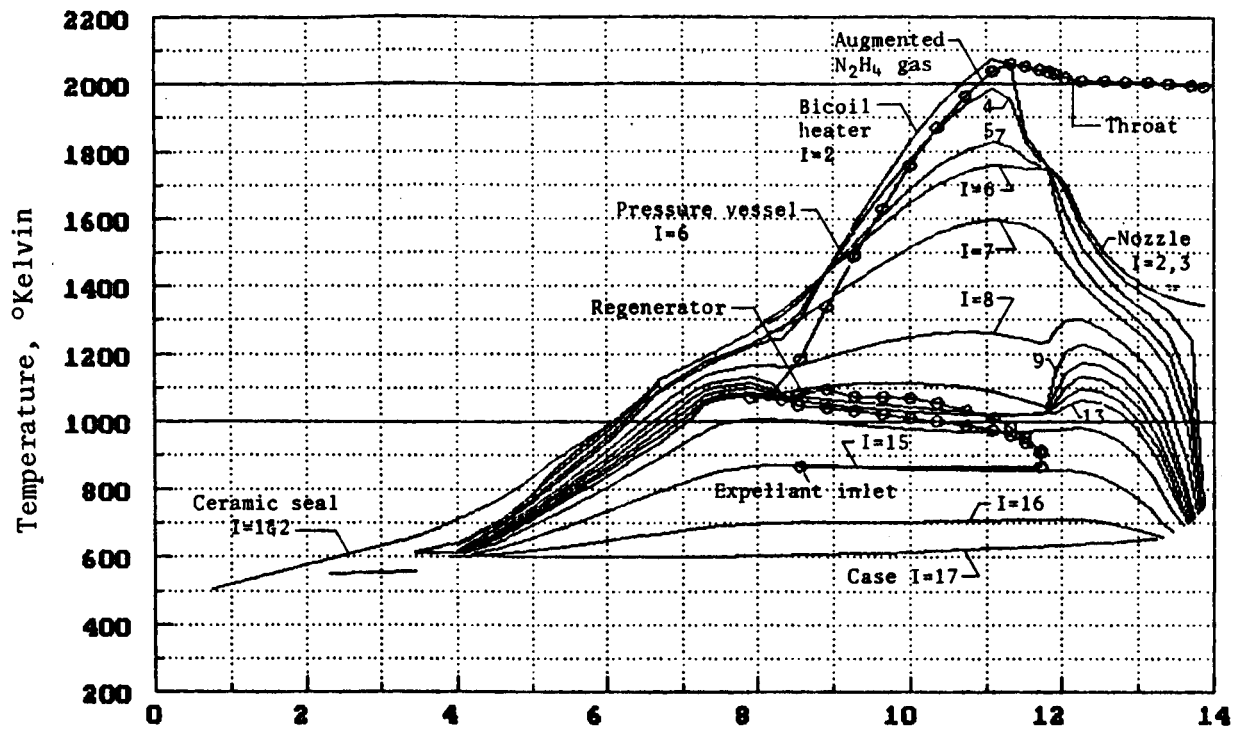
$$Q = Nu \cdot k \pi [(T_w)_r - (T_g)_r] L \quad (C4)$$

Since the asymptotic Nusselt number is a constant, for laminar flow in a tube, the temperature difference is inversely proportional to the length of the tubular heater and independent of its flow diameter, d .

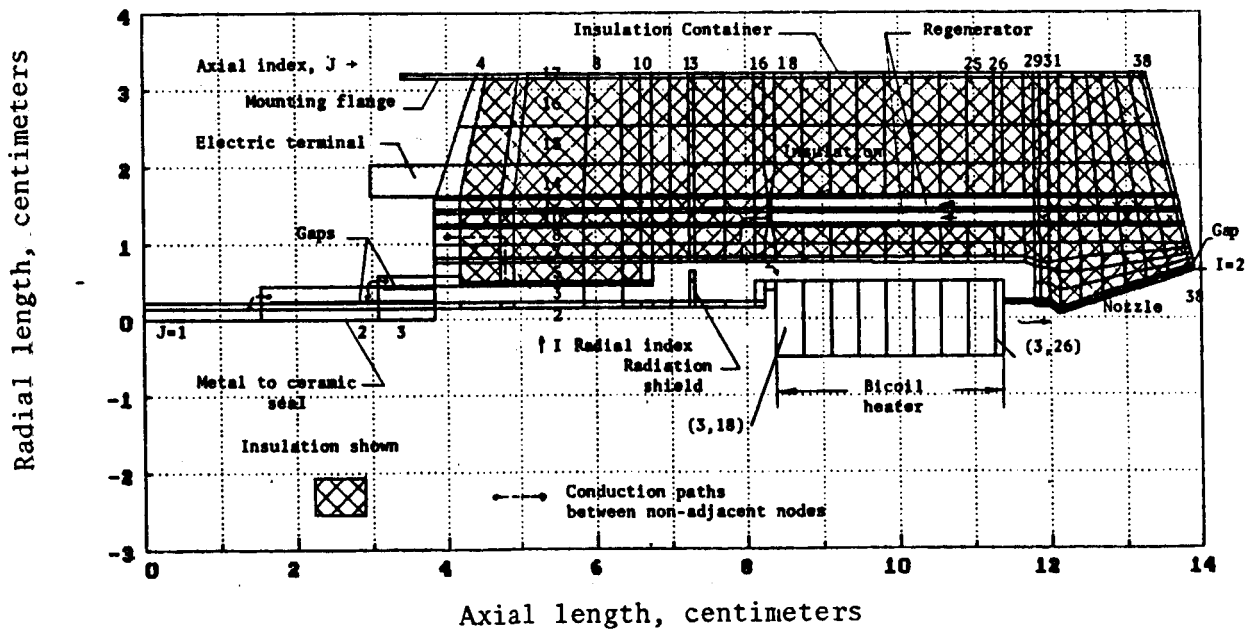
The length of the heat exchanger tube is made axially short by dividing the flow and heat transfer into two tubes, coiling them in opposite rotation coaxially to make a rugged, short compact structure as described.

Analysis by the generalized mathematical computational model: The node diagram for the final design choice of Concept 5 which is Configuration E, is shown in figure 36b. The temperature distribution is shown for the design condition of a heater temperature of 2073°K for hydrazine at 50 millipounds thrust.

The gas products from the hydrazine decomposition chamber are taken as fully reacted. The resultant inlet temperature to the augments is taken to be 886.5°K for the purposes of the analysis. This is the coolest transfer temperature condition between the separate decomposition chamber and augments stages, hence has least interstage heat loss potential.



a) Temperature distribution operating on fully decomposed hydrazine at an inlet temperature of 866.5°K and design heater maximum temperature of 2073°K (1800°C).



b) Thermal node diagram

Figure 36. - Results of analysis of Concept 5, Configuration E

This represents a different design choice than for the non-augmented monopropellant hydrazine thruster. An intermediate degree of NH_3 decomposition for non-augmented designs is generally employed.

The effect of degree of dissociation of the inlet gas on augmentor thermal performance wasn't studied here. Only the complete dissociation case is treated. It is the easiest to analyze because the gas composition is specified and no finite chemical kinetic considerations are involved within the augmentor.

Experience with resistojets operating on ammonia has shown (ref. 4) that, at the design temperatures here, the gas is fully dissociated at the throat of the nozzle. In a hydrazine augmentor thruster full dissociation ($x=1$) of the NH_3 at the nozzle throat may be expected as well because of the high temperature created there.

The electric power required is essentially independent of degree of dissociation of the inlet gas providing the gas temperature shown is not degraded due to the loss..

The energy to dissociate the ammonia further, to its equilibrium state, is contained thermally within the gas. Only the time to complete the reaction is missing. No further electric energy is required.

The design philosophy chosen for the first stage decomposition chamber is full reaction resulting in the lowest temperature for one stage coupling. The condition at the nozzle throat of the augmentor would be full decomposition regardless of the inlet gas state. Only the temperature distribution within the thruster would be different. The overall power input would be the same.

A series of iterative designs were undertaken. The alternatives considered in making the final selection are reviewed.

The exact geometry of Concept 3, with the substitution of rhenium for platinum and identified as Concept 5, was thermally analyzed by means of its existing node diagram and found to have attractive performance in that the maximum augmented gas temperature of the decomposed hydrazine of 2060°K is close to the limiting heater wall temperature prescribed for the design of 2073°K . The thermal efficiency is low, however, - less than 60%.

Concept 3 was described as an inverted design earlier. By inverted is meant the radial order of components as previously described. Because hydrogen has such an outstanding thermal conductivity as compared to the biowaste gases, the use of the wide regenerator passages typical of Concept 3 with decomposed hydrazine resulted in high radial losses. Further, the insulation is immersed in the expellant gas as the pressure case in

this design is the exterior member. The thermal conductivity of the insulation is increased greatly. While this value is not serious for the lower temperature inlet biowaste gas, it certainly is for ones rich in a hydrogen constituent at high inlet temperatures such as an augments.

Further, from reference 31 it was verified that the hydrazine readily chemically attacks zirconia, the high temperature material used for thermal insulation which further negates the use of the inverted design here.

The net effect of this was to return to the philosophy of an inner pressure case and exterior thermal insulation in a vacuum for decomposed hydrazine as is shown in the balance of the Concept 5 configurations presented here.

In a series of design iterations Concept 5E evolved as shown in figure 35. The considerations in arriving at this design are described as follows:

1) Because the inlet gas is hot, extra care must be exercised in designing an acceptable cool mount end where the power feedthrough is located. The inlet gases cannot be used to cool this region as they are already above the maximum allowable metal to ceramic seal temperature (-13) of 623°K. Careful thermal damping is required in the entrance section of the case. Short inlet sections can be achieved with due regard to the fact that the power feed terminal clamp provides a thermal sink. Comparing the terminal temperature without and with this sink results in a temperature decrease from 856°K to 583°K. Only 12 additional watts loss are required to affect this protection of the metal to ceramic seal joint, meaning a reduction in heater efficiency of only 0.8% for this assurance.

2) The effect of the use of a regenerator in otherwise identical cases is compared in table 30 for Configuration 5B with regenerator against 5A without. The regenerator is thermally more efficient, giving a net ≈1% increase in overall efficiency and a cooler pressure case by 23°C.

3) The propellant feed inlet to the regenerator, being located at the nozzle or mount end, is found to be inconsequential with regard to heater efficiency. The nozzle end configuration was selected for simplicity of design and is shown in figure 35.

4) The finally selected Concept 5E is 2.5 cm shorter than the initial Configuration 5A, shown on the same table, which has a significantly improved efficiency. Overall length reduction has much more benefit than including a regenerator. A lower heater voltage results by the reduction. This voltage decrease

can be offset by increasing the coil and pressure case diameter, but is not shown here.

5) It is found that the heat exchanger design and ohmic heater design considerations are reasonably independent in that the bicoil is immersed in the pressure cavity and is not itself under any serious pressure vessel design constraint. A higher voltage design could readily be achieved. It is not shown here.

The scaled drawing of Concept 5E is shown in figure 35 which is modeled for the mathematical computational model in figure 36b. The thermal profiles at design are shown in figure 36a. The design has a favorable temperature profile with mount at 643°K maximum and the power feedthrough ceramic seal at 583°K, increasing in temperature to the maximum heater temperature just before the nozzle throat. The gas temperature follows this same trend, closely approaching the heater wall temperature to within 13°K and leaving the throat about 66°K below the maximum heater wall temperature. Only a small segment of the thruster, the heater bicoil hot end, is operated at the temperature limits. Because of the higher resistivity coefficient with temperature of rhenium, the heater tube walls can even be made thicker in this region for further reliability. It satisfies the life requirement of >10,000 hours with uniform wall thickness. Since the heater is immersed in the expellant gases, sublimation is suppressed. Chances of metallic vapors migrating to the seal area against the general flow are minimized in the design.

Conclusions with regard to starting.- The specific impulse response of the Concept 5 design is expected to be high in that the heating element mass of the bicoil is small. The gas temperature is primarily influenced by this element since it is the last heat transfer surface seen. There is little time for much thermal loss to the nozzle. The specific impulse will approach its steady state value quickly as compared to Concept 6, described following, which must have its pressure case heated as well to reach this value which takes approximately 10 times longer.

Reliability.- Because of the small pressure drop across the bicoil walls, any long term leakage of the bicoil merely allows small flows into the exchanger from a zone already at very high temperature. This leakage can only escape through the nozzle and is ohmically heated in the process, not compromising the thruster's performance significantly. Since two heating elements are involved, the bicoils, a complete severance of one of the heater tubes does not shut down the thruster. The heat exchanger has great structural integrity laterally and the wall cross sections are generous compared to a wire type design, hence should be more reliable than the latter.

Gas Dynamic Analysis

A summary of the parameters is shown in table 31 for a design heater temperature of 2073°K and a mass flow of .07 grams per second of decomposed hydrazine.

TABLE 31
SUMMARY OF FLUID FLOW PARAMETERS

| Parameter | Propellant inlet | Bicoil entrance | Bicoil exit | Nozzle throat |
|---|---------------------|--------------------|----------------|------------------|
| Flow area, (cm ²)x10 ³ | 28.5 | 7.71 | 7.71 | 4.58 |
| Total pressure, atm | 4.08 | 3.97 | 3.00 | 3.00 |
| Total pressure, psia | 60.0 | 58.41 | 44.09 | 44.09 |
| Static pressure, atm | 4.08 | 3.95 | 2.94 | 1.59 |
| Static pressure, psia | 60.0 | 58.05 | 43.20 | 23.43 |
| Total gas temp., °K | 866.5 | 1193.3 | 2058.7 | 2007.5 |
| Wall temp., °K | - | 1138.7 | 2073.1 | 1645.0 |
| Mach number | .01 | .09 | .17 | 1.0 |
| Reynolds number | 39,300 | 1120 | 787 | 2356 |

The static pressure within pressure case cavity is 59.0 psia. The critical flows within the augments are everywhere laminar. The favorably low mach number of the design in the heat exchanger promotes a relatively low pressure drop. Further, the static pressure at the bicoil exit is only slightly suppressed below the total pressure. This reduces the wall delta pressure, and, hence, stress at this critical section.

Mechanical Design

Pressure envelope.- The critical stress region is at the hemispherical end of the pressure case where the nozzle penetrates it. Using the area replacement rule of the ASME pressure vessel code for this penetration (ref. 32), the hemispherical thin shell equation is used. The membrane stress given by $PR/2t$ is 2.05 MPa (297 psi) based upon the pressure p within the case of .4 MPa (59.0 psia) and a radius of curvature, R of 7.6 mm (.30 inches) with a wall, $t = .08$ mm (.030 inches). There the temperature is 1758°K from the thermal analysis.

The stress rupture endurance capability based on the 10,000 hour rhenium design line is projected to be 26.5 MPa (3,845 psi).

In figure 35 the balance of the envelope is seen from the thermal analysis to decrease in temperature toward the hermetic power feedthrough. As a result, the wall thicknesses are tapered

thinner to reduce the axial heat conduction and are still able to provide generous structural allowance primarily because of the lower temperatures. The feedthrough, because of its metal to ceramic construction, is a critical member reviewed below.

Metal to ceramic seal.- The power feedthrough shown is a metal to ceramic seal very much like that demonstrated in extended resistojet life tests of 8,000 hours on NH_3 at 2 atmospheres nozzle pressures without failure (ref. 5). This type design, as reviewed for use by its manufacturer, is suitable for use at the 3 atmosphere condition under a continuous rating of 350°C (623°K).

Heating Element.- The bicoil heater is critical near its exit where the temperature is the maximum value for the thruster of 2073°K . The pressure across the tube wall from the gas dynamic study is the difference between the cavity of .4 MPa (59.0 psia) less the internal static pressure at the maximum wall temperature point of .3 MPa (43.2 psia) or .1 MPa (15.8 psi). The hoop stress, is $pD/2t$ giving a value of .48 MPa (69.5 psi) where the mean diameter is 1.1 mm (.044 inches) and the thickness, t , is .1 mm (.005 inches). The stress rupture endurance from the 10,000 hour rhenium design line is 12.4 MPa (1802 psi).

The structural integrity of the bicoil heater under the maximum expected operating conditions warrant more detailed explanation since the concept is new.

The bicoil is seen to be constrained at each end by its mounts. Under the thermal profile these mounting points move away from each other due to the thermal expansion of the pressure envelope. However, the thermal expansion of the bicoil between these two points is greater putting it into compression. Of particular interest is whether the coil buckles sideways and possibly comes into electrical contact with the insulated side walls of the enclosure.

An over design operating condition of twice the mass flow and a temperature of 2600°K was analyzed by the ANSYS (1) finite element model computer program. Based upon the results of these analyses, it is concluded that the bicoil design provides a very stable, strong, yet flexible, component which is capable of withstanding the loads produced by the operating environment. The results of the analysis indicated that the load factor against buckling is 475. The resistance of the bicoil to side deflections is very impressive in light of its axial flexibility. The low stresses of 3.1 MPa (450 psi) developed in the coils at this over design operating condition should result in a high tolerance to thermal cycling and good component reliability at design.

The bicoil was found to exert negligible reaction loads on the components to which it is attached, particularly the hermetic seal.

Chemical Corrosion, Sublimation and Deposition

Chemical.- Operation on decomposed hydrazine exposes the rhenium primarily to hydrogen, ammonia and nitrogen. All of these represent no problem. The 8000 hour resistojet life tests (ref. 5) on ammonia exposed rhenium to the same species.

Hydrazine contains other trace compounds from its manufacture and small amounts of water are added for stabilization. The particulates are not believed to be a problem. Extensive bench tests on simulated sample systems are ultimately required. Rhenium's resistance to water vapor is the best of all of the refractory metals (ref. 33). The long term effect of water on rhenium, while favorable, needs to be more thoroughly evaluated. Very high temperature tests at 2400°K with rhenium and 1% water vapor would not pose a serious loss mechanism. Lower temperatures, however, might and should be verified by further experimental testing for extended periods and temperature range in bench tests. Hydrazine propellant with minimum water content of the order of .1% and/or an erosion rate less than 2.5×10^{-8} (10^{-7} inches) per hour would be required. Values greater than this might represent a problem over 10,000 hours on the thin bicoil heater wall.

Sublimation.- A maximum sublimation rate occurs on the pressure case exterior at its high temperature hemispherical end where it is also subjected to vacuum. The temperature there from the thermal analysis is 1758°K. The estimated erosion rate is 10^{-11} inches per hour and inconsequential.

With regard to the heating element at 2073°K, an erosion is estimated. By means of reference 23, where the influence of sublimation and the combined effects of pressure and a main gas velocity over the surface, the following loss rate is estimated within the tube. The velocity from the gas dynamics analysis is 450 m/s (1480 feet per second) and the pressure is .3 MPa (44.09 psia). From the data presented by Zima (ref. 23), the total erosion for 10,000 hours is 1.42 picometers (5.6×10^{-8} inches) on the interior of the tube. Sublimation, then, is not of consequence on the design.

Deposition.- Since the general gas flow is from the entrance into the cavity towards the nozzle at increasing temperature, back-streaming of metallic vapors is not anticipated. The life test of reference 5 experienced minimal deposition of rhenium in the nozzle throat at these same temperature levels.

Rating

The benefits of the bicoil enumerated under the discussion of Concept 3 apply also to Concept 5. The major differences between the two designs are the use of biowaste and hydrazine resistant materials, respectively, and the inverted versus normal radial order configuration.

Advantages.- 1) The gas approaches the limiting wall temperature very closely, therefore, is the highest specific impulse augments design of the study.

2) Because the bicoil is immersed in its own gas, the pressure drop, hence stress, across the wall is low compared to a coil acting as its own pressure vessel and sublimation is less.

3) The design requires no pressure balancing internally to avoid creep.

4) The bicoil design relieves differential thermal expansion stresses by ready axial compression by readily compressing axially at a low spring constant.

5) The heater is structurally sturdy and stable from buckling transversely because the coils are metallurgically bonded along the transverse length about every half turn at equipotential points.

6) Any pinhole leak in the coil is not catastrophic. There is not any propellant lost. Any specific impulse degradation is minimal.

Disadvantages.- 1) It is naturally higher current - lower voltage design of 29.1 amperes and 10.1 volts than Concept 6. Some increase can be safely included if this is serious.

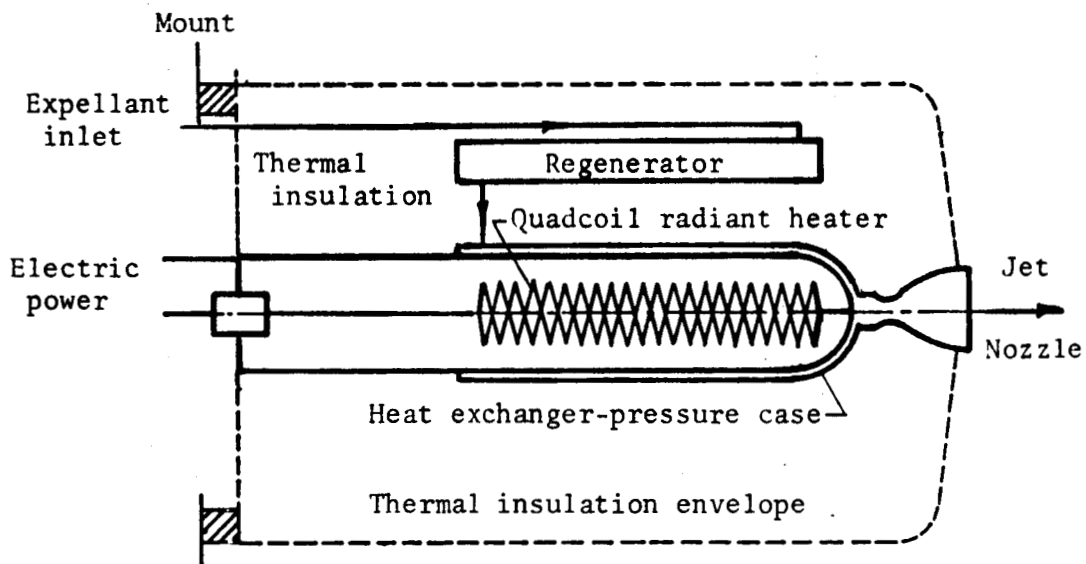
2) The thinner walled heat exchanger tube is more sensitive to any long term erosion attack.

APPENDIX F

CONCEPT 6 - NONEXPOSED RADIANT HEATER WITH FLOW IN SURROUNDING CASE SPIRAL PASSAGE - (HYDRAZINE)

Concept 6 physically separates the heat exchanger function from that of the ohmic heater. The heater and exchanger may thus be each made of different materials, each favorable to its own design. The figure below illustrates the concept schematically. Because of the decoupling of the designs, the voltage of the heater may be made higher and the walls of the gas exchanger thicker than if the design were an integral one. The design here as a hydrazine augments has all high temperature parts fabricated of the same material, grain stabilized rhenium.

A unique feature of the design here is the use of a sturdy quad coil, described herein, to give more reliability against touching and electrical continuity in the event of breakage for increased reliability. A variation from that of the original design (ref. 31) is introduced. The detailed results in performance through use of the pressurized cavity are shown compared to the original.



Description

The final preliminary design of Concept 6B, is shown in figure 37. Table 32 identifies the components and materials. The supporting geometries of 5 and 6 are nearly identical. The only differences occur within the pressure case. This was done primarily for consistency in comparison. The designs were appropriate as well.

TABLE 32
CONCEPT 6 - COMPONENT PARTS, MATERIALS OF CONSTRUCTION

| <u>Item</u> | <u>Component</u> | <u>Material</u> |
|-------------|-------------------------------------|--|
| 1. | Nozzle | Grain stabilized rhenium |
| 2. | High temperature thermal insulation | Fibrous zirconia ¹ |
| 3. | Heat exchanger pressure case | Grain stabilized rhenium |
| 4. | Heater exit support terminal | Grain stabilized rhenium |
| 5. | Quadcoil ohmic heater | Grain stabilized rhenium |
| 6. | Low k thermal insulation | Min-K 2000, |
| 7. | Regenerator | Grain stabilized rhenium |
| 8. | Heater entrance, terminal support | Grain stabilized rhenium |
| 9. | Heater electric insulator, support | Alumina 99.5% |
| 10. | Pressure case entrance | Grain stabilized rhenium |
| 11. | Thermal-electric, standoff, support | AISI 304L |
| 12. | Mount | AISI 304L |
| 13. | Power feedthrough | Metal to ceramic seal materials ² |
| 14. | Power ground | AISI 304L |
| 15. | Regenerator support | AISI 304L |
| 16. | Electric insulator | Alumina 99.5% |
| 17. | Electric insulator | Alumina 99.5% |
| 18. | Expellant inlet | Grain stabilized rhenium |
| 19. | Insulation container | AISI 304L |
| 20. | Electric insulator | Alumina 99.5% |
| 21. | Transfer lines (3) | Grain stabilized rhenium |
| 22. | Heater cavity pressurization inlet | Grain stabilized rhenium |

1. Data from Zircar, Florida, NY.

2. Data for Min-K 2000, Johns-Mansville Aerospace Products, N.Y., NY.

3. Typical materials: nickel A conductors; glazed high alumina ceramic (85% min. Al₂O₃) insulators; vacuum tube grade brazing alloys and nickel-iron caps. Data from Ceramaseal, Inc., New Lebanon Center, NY.

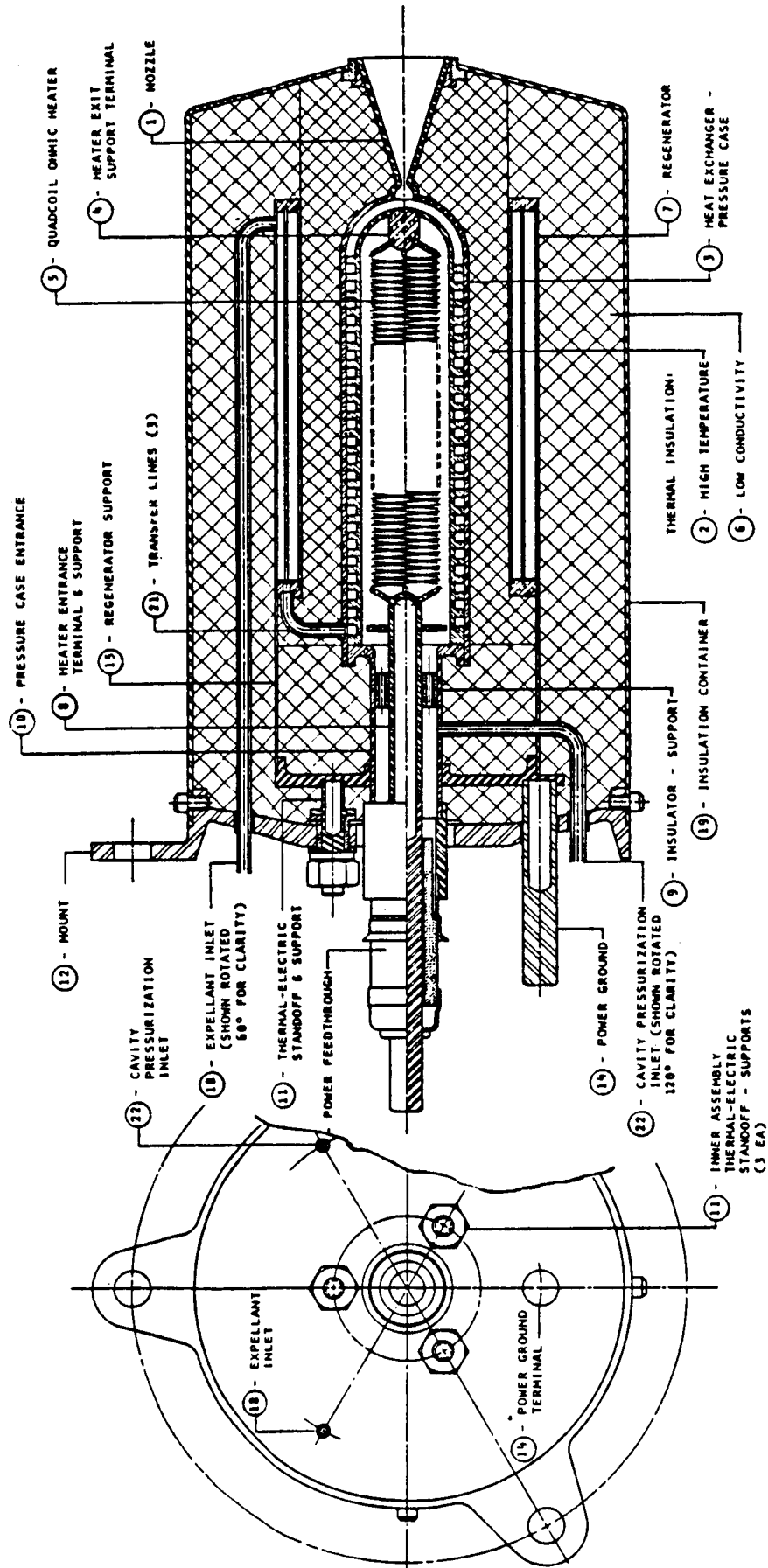


Figure 37. - Concept 6, a hydrazine augments heater with nonexposed radiant rhenium heater with flow in the surrounding case passage of grain stabilized rhenium.

The key features of this concept are the radiant wire heater within the central cavity, separated from but surrounded by an annular spiral heat exchanger to capture the heat in the gas as it moves to the nozzle. The heater is mounted within the pressure case (-3) supported by the feedthrough hermetic seal at the mount end, similarly to Concept 5. The hermetic seal may be either of the double terminal type or the single one with the power return utilizing the case itself. The former has the advantage of isolating the rest of the system from the power source; the latter, simplicity and possibly reliability. The latter is shown. The heat exchanger - pressure case is double walled and the flow is down a thin annular passage or a spiral passage as modeled here.

The thruster assembly is shown thermally and electrically stood off from the mount by means of the three (-11) assemblies. The power terminals (-13) and (-4) accept the spacecraft cable connectors using the single hermetic seal terminal approach. The thruster is designed to be mounted to the spacecraft at three points by equally spaced attachment holes to the mount as shown. The thermal analysis presented did not utilize the thermal stand-offs from the mount.

The power ground side of the power supply line is connected to the terminal (-14) where it connects to the case. The circuit is completed through the power feed-through to the high side of the power line.

The expellant feed line enters the thruster at the nozzle end of the concentric counterflow regenerator (-7). Three lines exiting from the regenerator enter the pressure case at the beginning of the wire wound central heater, again passing toward the nozzle and the annular heat exchanger, hence out the central nozzle.

The heater geometry consists of four parallel electric coils made of rhenium wire .36 mm (.014 in.) in diameter. Two coils are clockwise, the other two counterclockwise wound. Like the bicoil, this quadcoil is bonded at the crossover points. These points are at the same electric potential on each wire by the principle of symmetry. The pitch diameter of the set is 10 mm. The overall axial length is 47 mm.

The exchanger consists of spiral passages for the model. The cross section of the flow passage is 1.5 mm x 1.5 mm. The pitch is 2.5 mm. The pitch diameter is 16.7 mm and the axial length is 56.5 mm.

Performance

The projected performance of the radiant heater type hydrazine augmenters studied are shown in table 33 for heating element temperature of 2073°K. Two type designs were considered. The first operates the heater in a vacuum cavity; the second in a hermetically sealed cavity with a suppressant gas. The purpose of the latter is to provide an additional heat transfer mode conduction to that of the radiation and to supply a suppressing effect on heating element sublimation. The latter requires a hermetic seal. The performance is based upon the thermal analysis of the next section and that of the nozzle that was discussed earlier. The design with the suppressant gas achieves a higher specific impulse because it is able to achieve a higher gas temperature through better coupling. The life and reliability of the heating element is enhanced. The question of a hermetic seal is a complexity but has been successfully tested (ref. 5). The overall efficiency of the design with the suppressant gas is 2.7 points less, expectedly, because of the higher temperature (and specific impulse) performance.

TABLE 33
CONCEPT 6 PERFORMANCE SUMMARY
FOR AUGMENTED HYDRAZINE

| Configuration | Projected Performance | |
|----------------------------------|-----------------------|--------|
| | 6A | 6B |
| Specific impulse, s | 278.2 | 295.2 |
| Maximum heater temp., °K | 2073 | 2073 |
| Electric input | | |
| Voltage, V | 21.77 | 24.70 |
| Current, A | 8.33 | 9.71 |
| Power, W | 181.32 | 239.91 |
| Power/thrust. W/mlb _r | 4.23 | 5.27 |
| Nozzle chamber | | |
| Total pressure, Atm | 3.0 | 3.0 |
| Total temperature, °K | 1512.8 | 1726.7 |
| Expellants inlet | | |
| Total temperature, °K | 866.5 | 866.5 |
| Mass flow, gms/sec | .070 | .070 |
| Initial gas power, W | 166.84 | 166.84 |
| Power lost from heater, W | 42.65 | 54.17 |
| Total input power, W | 347.69 | 406.27 |
| Maximum gas temp., °K | 1551.8 | 1773.9 |
| Max. case temp., °K | 1557.0 | 1780.9 |
| Power efficiencies | | |
| Overall, η_o | .749 | .722 |
| Overall electric, η^* | 1.437 | 1.223 |
| Heater, η_h | .877 | .866 |
| Nozzle, η_n | .854 | .834 |
| Thrust check, lb _r | .0429 | .0455 |

The performance with a high emissivity coating on the interior of the heater cavity wall was not evaluated for hydrazine operation. Concept 4, the biowaste equivalent of Concept 6, the last to be evaluated, did determine the benefits of emissivity enhanced walls. The effect was found significant.

Thermal Analysis

Analysis by the generalized mathematical computational model; the node diagram for Concept 6 which may be utilized for Configuration A or B is shown in figure 38. The resultant temperature distributions for the study are shown for the heater design condition of 2073°K for hydrazine at nominally 50 millipounds thrust. Because the resultant gas temperature was lower than that anticipated, the mass flow initially selected for the run was less. The actual thrust level check as shown on the performance table is for a 43 to 46 millipounds class engine because of this.

As with Concept 5, the same inlet assumptions were used for the decomposed hydrazine, specifically that of fully decomposed hydrazine with an inlet temperature of 866°K.

Configuration A assumes strictly radiative heat transfer from the central cavity to the heat exchanger in order to avoid the use of the metal to ceramic seal. This configuration is currently used to avoid the deposition problems which could cause short circuits. Figure 39a shows the resultant temperature distribution. Note that the gas temperature is 1513°K, approximately 557°C lower than the heater temperature.

This analysis recognizes that the free molecule conductive transfer is essentially zero under applicable space conditions. Yet to simulate this condition in a test cell, a cell pressure of approximately 10 microns Hg is required! If a pressure much greater than this is used, which unfortunately has been the case, specific impulses erroneously high will be reported. These values will not be realized in space by the actual Configuration A. The results obtained under these conditions will be those of Configuration B presented below.

Configuration B, which employs a metal to ceramic seal and nitrogen gas for sublimation suppression and heat transfer enhancement to improve the outlet temperature to be realized in space. See figure 39b. The gas temperature at the nozzle is 1727°K resulting in an improvement in specific impulse as a result from 278 to 298 seconds with the same heater temperature. Because of the higher temperature, the heater efficiency is approximately 1 percentage point less than that of A for the same maximum heater wall temperature. The temperature difference for B is 347°K below heater temperature.

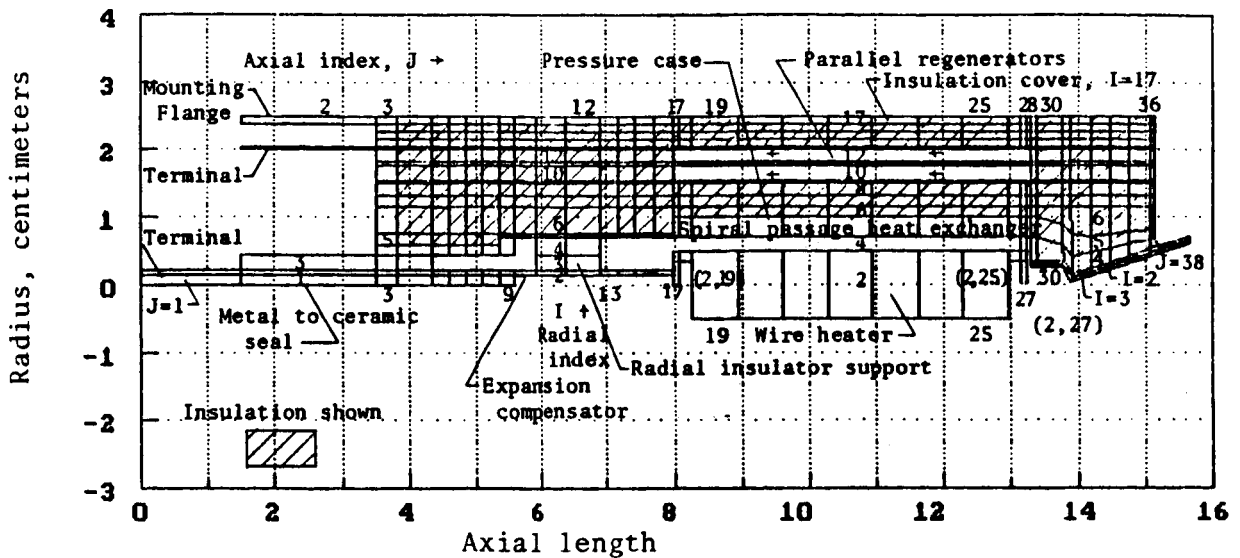


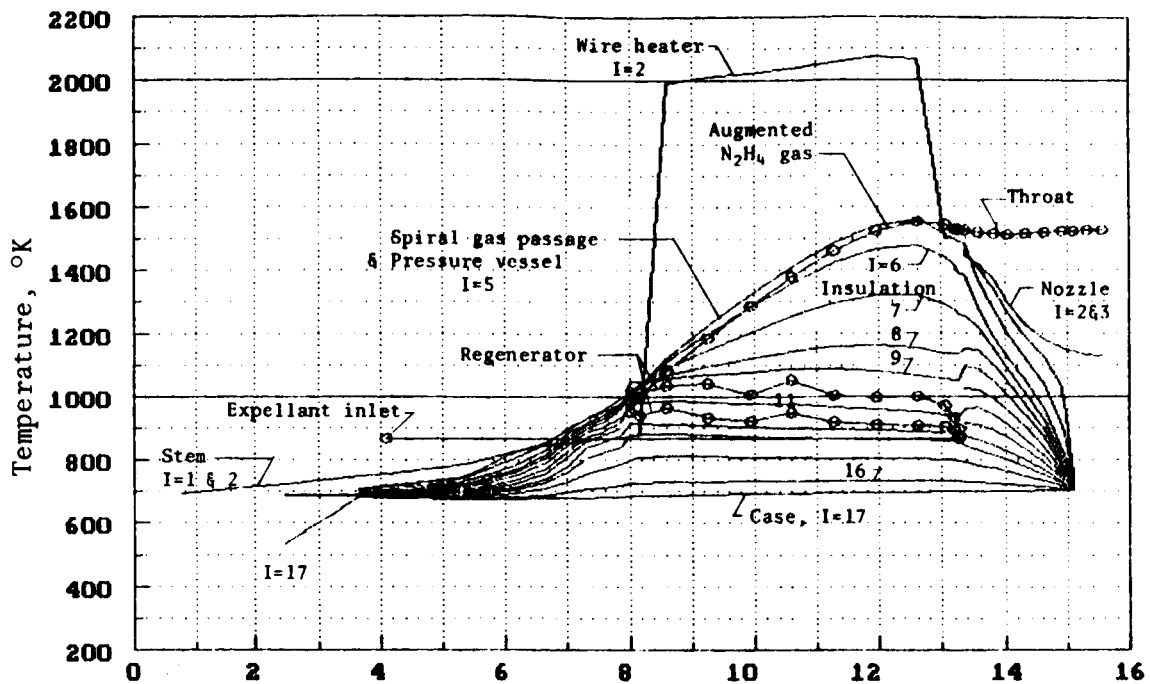
Figure 38. - Thermal node diagram used in Concept 6.

The temperature distribution and results here are based upon the heat exchanger geometry and heater configuration described by figure 36. The thermal nodal model, figure 38, is rectilinearized for convenience. The the actual hardware represented is believed closely approximated.

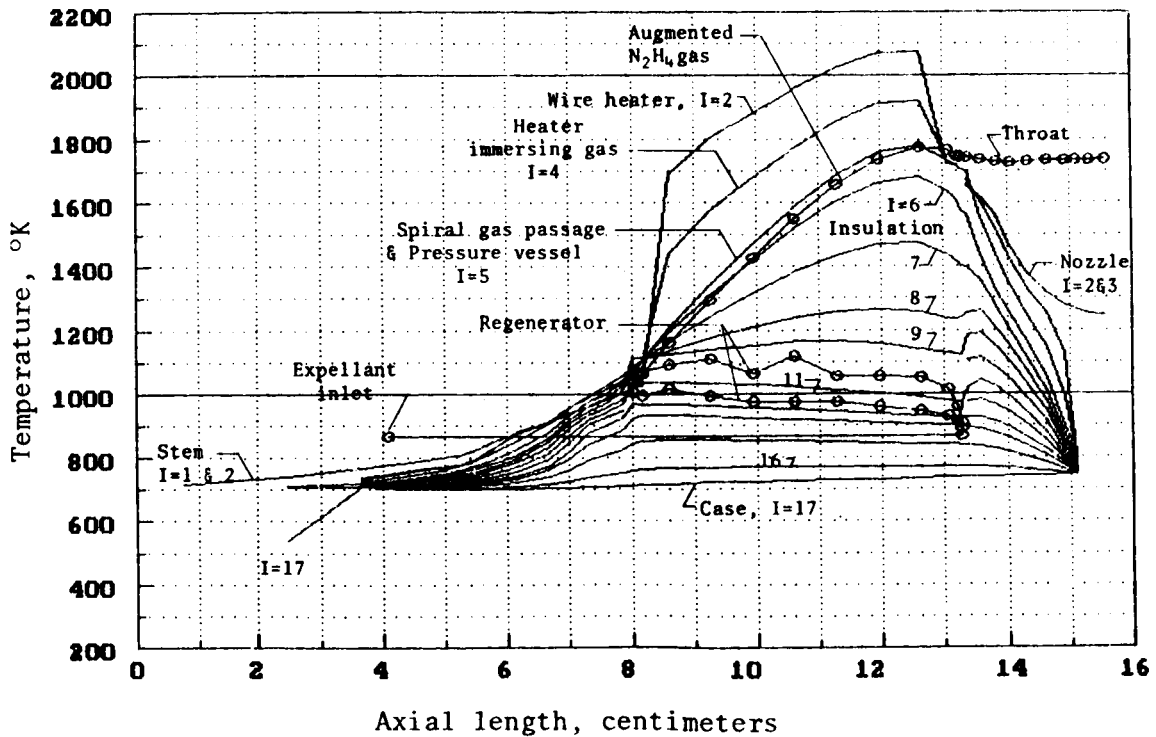
Because the flow is laminar, a straight annular exchanger could have been used equally well to the one used here. A spiral design was suggested by reference 31.

In examining, in a preliminary way, other gases, such as hydrogen, with this same type geometry, lower gas temperatures resulted. The configuration tends to be a constant power output device because of its independent heater. Gases with high specific heats, such as hydrogen, in the same design do not achieve as high a temperature. Putting it another way, the thruster has to be designed for each propellant and is not as universal a thruster with regard to multipropellant usage as is a convective design. It does not work the propellants to the same gas temperature for a given heater temperature.

Starting.- The relative mass of the heat exchanger of Concept 6 as compared to the tubular bicoil exchanger of Concept 5 is larger by a factor of over 10. This could have implications on short term firing attitude control applications as differentiated from long term drag makeup functions.



a) Concept 6A - Heater cavity at space vacuum.



b) Concept 6B - Heater cavity at 3 atmospheres of nitrogen.

Figure 39. - Temperature distribution at a maximum heater temperature of 2073°K for fully decomposed hydrazine. (Inlet temperature 866.5°K).

Gas Dynamic Analysis

A summary of the parameters is shown in the following table for the temperatures of the heat exchanger with hydrazine at a mass flow of .07 grams per second for Configuration B.

TABLE 34
SUMMARY OF FLUID FLOW PARAMETERS

| Parameter | Propellant inlet | Exchanger entrance | Exchanger exit | Nozzle throat |
|---|---------------------|-----------------------|-------------------|------------------|
| Flow area, (cm ²)x10 ³ | 28.5 | 22.5 | 22.5 | 4.58 |
| Total pressure, atm | 3.25 | 3.18 | 3.0 | 3.0 |
| Total pressure, psia | 47.7 | 46.75 | 44.09 | 44.09 |
| Static pressure, atm | 3.25 | 3.17 | 2.97 | 1.61 |
| Static pressure, psia | 47.7 | 46.62 | 43.71 | 23.82 |
| Total gas temp., °K | 866.5 | 1012 | 1745.0 | 1726.7 |
| Wall temp., °K | - | - | 1703 | 1511.1 |
| Mach number | .01 | .074 | .114 | 1.0 |
| Reynolds number | 39,300 | 1429 | 907 | 2423 |

The nitrogen gas pressure in the heater cavity is taken as 3 atmospheres in Configuration B. The flow is laminar. The low mach number chosen for the heat exchanger promotes a low pressure drop.

Mechanical Design

Pressure envelope.- The critical stress region and maximum temperature of the pressure case (-3) is in the hemispherical end where the nozzle joins it. Like Concept 5, its stress is about about 2.07 MPa (300 psi). The temperature is now 1655°K. The stress rupture endurance for 10,000 hours from the rhenium design line is 33.9 MPa (4925 psi), an adequate factor of safety.

The heater has been designed as a quadcoil (four parallel heater wires - two CW and two CCW) for transverse stability. A single terminal feedthrough is used. Little stress is induced in thermal expansion adjustments under temperature conditions either within itself or its attached hermetic seal.

The hermetic seal is of the same design as Concept 5.

Chemical Corrosion, Sublimation and Deposition

Chemical.- The chemical exposure as discussed under Concept 5 possesses the same problems, if any, with the trace contaminants in hydrazine. The one notable difference may be the water in the hydrazine. The more robust heat exchanger of the radiant design is more insensitive to erosion caused possibly by heavy water vapor content in the 10,000 hours than the bicoil heater. The latter will definitely require the special grades of hydrazine low water content which are available, such as the so-called Viking grade.

TABLE 35
COMPARISON OF HYDRAZINE GRADES

| | Standard hydrazine | Viking grade |
|------------------|--------------------|--------------|
| Hydrazine w/o | 98 - 98.5 | 99.9 |
| Water w/o | 1.5 - 1.0 | >.02 |
| Particulates | | |
| Milligrams/liter | 10 - 1 | <.2 |

Sublimation: The maximum evaporation rate occurs on the hemispherical end where temperature is 1655°K. The estimated surface erosion rate is 5×10^{-12} inches per hour or 5×10^{-8} inches total in 10,000 hours, or inconsequential. The .014 inch diameter heating element wire is at 2073°K is expected to sublime 2×10^{-8} inches, an inconsequential amount in a vacuum.

The suppressing effect of the nitrogen on sublimation is desirable to prevent subsequent deposition in insulators. This is a serious problem as there is no sweeping gas flow toward the high temperature zone around the heater and away from the hermetic seal. A serious alternative would be having elected a hermetic cavity to introduce a small leakage flow from thruster inlet through the heater cavity out a small orifice at the nozzle chamber to perform this function of sweeping vapors. The better heat transfer capabilities of the decomposed hydrazine compared to nitrogen (Configuration B suppressant gas) for instance, would further increase the specific impulse.

Rating

The pros and cons of the radiation type augments such as Concept 6 are described here. These are essentially the same as those of its biowaste resistojet version, Concept 4. The two thrusters, geometrically identical, differ primarily in materials of construction, propellants and operating temperatures.

Advantages.- 1) Higher voltages are possible than with integral convective ones, or 24.7 versus 8.9 volts for Concept 5E. The reason is that the radiant electric heater and gas heat exchanger designs are more independent than are these functions in an integral heater - convective heat exchanger one.

2) The heat exchanger of Concept 6 is more massive by a factor of ten that of the direct convective Concept 5, hence, is less sensitive to erosion due to any abnormal water level content in the hydrazine.

Disadvantages.- 1) Radiant designs produce lower specific impulse for the same maximum heater temperature. The maximum specific impulse for 6B is 295 seconds and 317 seconds for 5E. The integral heater - convective exchanger (bicoil) design was overall power efficiency, of .737 versus .722 for the radiative.

2) The thermal mass of the Concept 6 gas exchanger (32,400 joules) is ten times more than that of the Concept 5 convective exchanger (3390 joules) and, therefore, is less responsive in specific impulse on short firings.

3) The radiant heater must be specifically sized with regard to power required by a specific propellant. It has a narrow range. In this regard, it is less general purpose for various compatible propellants and thrust levels with a given propellant.

APPENDIX G

DEFINITION OF PERFORMANCE PARAMETERS

Specific impulse, I_{sp} , seconds

$$I_{sp} = F/\dot{m} \quad (G1)$$

where F = measured thrust by dynamometer, g,
 \dot{m} = propellant mass flow, g-sec⁻¹

Electric power to terminals, P_E , watts

$$P_E = E_t \times I_t \quad (G2)$$

E_t = electric voltage difference between
 thruster terminals, V
 I_t = electric current through terminals

Heater Resistance, R , ohms

$$R = E_t/I_t \quad (G3)$$

Efficiency - total power overall, η_o

$$\eta_o = F \times I_{sp} / (20.8 (P_E + P_z)) \quad (G4)$$

Efficiency - electrical power overall, η_o^*

$$\eta_o^* = F \times I_{sp} / (20.8 P_E) \quad (G5)$$

Initial power in gas, P_z , watts

$$P_z = \dot{m} h \ 4.186 \quad (G6)$$

h = absolute enthalpy, ideal gas, cal/gm

Power in the jet, P_J , watts

$$P_J = P_E + P_z - P_L \quad (G7)$$

P_L = heat lost from the thruster prior to
 the exhaust jet, W

Heater efficiency, η_H

$$\eta_H = P_J / (P_E + P_z) \quad (G8)$$

Nozzle efficiency, η_N

$$\eta_N = F \times I_{sp} / (20.8 P_J) \quad (G9)$$

$$\eta_N = \eta_E \eta_D \eta_V \eta_F \quad (G10)$$

where the component efficiencies are

- η_E = expansion efficiency
- η_D = divergence efficiency
- η_V = viscous efficiency optimized with Reynolds No.
- η_F = frozen flow efficiency

All of the above considerations are included in the nozzle efficiencies reported here.

APPENDIX H

BASIS OF MATHEMATICAL COMPUTATIONAL MODEL

By L. Barker

An IBM P.C. running a compiled BASIC was used to model the resistojet. The compiler uses up to 128 K bytes of memory and then requires about 192K to run. This permitted a node model with about 500 to 600 nodes. Because the total program was too large to be run at once, the BASIC chain command was used to combine two or three subprograms.

The Model

The model basis for the thermal analysis is a generalized system of orthogonal elements in cylindrical coordinates. The elements dimensions are dr , $r d\theta$ and dz and are considered finite. The model is treated as axisymmetric. The elements, called nodes here, are treated as a matrix and are numbered with the first index, I , radially outward, and the second index, J , axially positive toward the nozzle.

A specific thruster is studied by assigning dimensional specifiers to the corners of the elements (nodes) so as to represent the geometry. This shaping gives a physical character to the model approximating the physical description of the thruster. See figures 35 and 36b for example. The material identifiers of each element are next assigned, which allows access to the needed material properties subroutine banks as required, e.g., electrical conductivity with temperature, emissivity, etc. The properties are summarized in Appendix I. The various heat transfer linkages between the various adjacent elements are embodied in the program and are activated as required to model the specific thruster. Heat transfer procedures for treating nonadjacent nodes and nonaxisymmetric components are provided on an individual basis. The net heat flow into an element can be determined for its assumed temperature and that of its adjacent elements. When the net heat flux into each node is zero, the equilibrium temperature throughout the model is found. The method for determining this temperature distribution is next described.

The Method

To solve for a steady-state temperature distribution, the detailed procedure outlined in figure 38 was used. In summary, heat flows between all nodes are calculated using assumed values for temperatures and then are summed for each node. If the sums are not sufficiently small, the temperatures are adjusted and the

calculations repeated. The systematic temperature correction used is a fraction (usually .7) of the following expression:

$$\Delta T_i = \frac{-\sum_{j=1}^N q_{i,j}}{\sum_{j=1}^N \frac{\partial q_{i,j}}{\partial T_i}}$$

where $q_{i,j}$ = the heat flow into node i from node j .

There is a test for convergence. This section requires that the heat balance error be no more than 0.1 watt for any node and that the maximum heater temperature at any station differs from the prescribed values by no more than 0.1°K. If the conditions for convergence are met, the procedure leaves the main loop and jumps to the printout section, and if not, the iterative process continues.

In the next approximation equation for temperatures above, it has been found that the fraction (.7 used here) must be less than unity to stabilize the convergence process. Too high a value can result in increasing errors of alternate sign, while too low a value will reduce the rate of convergence.

When the temperatures have converged, values of heat flows and temperatures are printed out and the temperatures are plotted on a dot matrix printer. For a transient solution, the above approach is used except instead of using the above temperature correction, mass and specific heat data for each node are used with a maximum allowable time interval to adjust temperatures. The models used for various heat flow mechanisms follow.

Conduction

The equation used is the Fourier equation:

$$q = -kA \frac{\partial T}{\partial x}$$

Heat flow towards increasing x is positive. In the program the opposite sign is used.

For a given geometry one can assume that q is a constant and that A is a function of x .

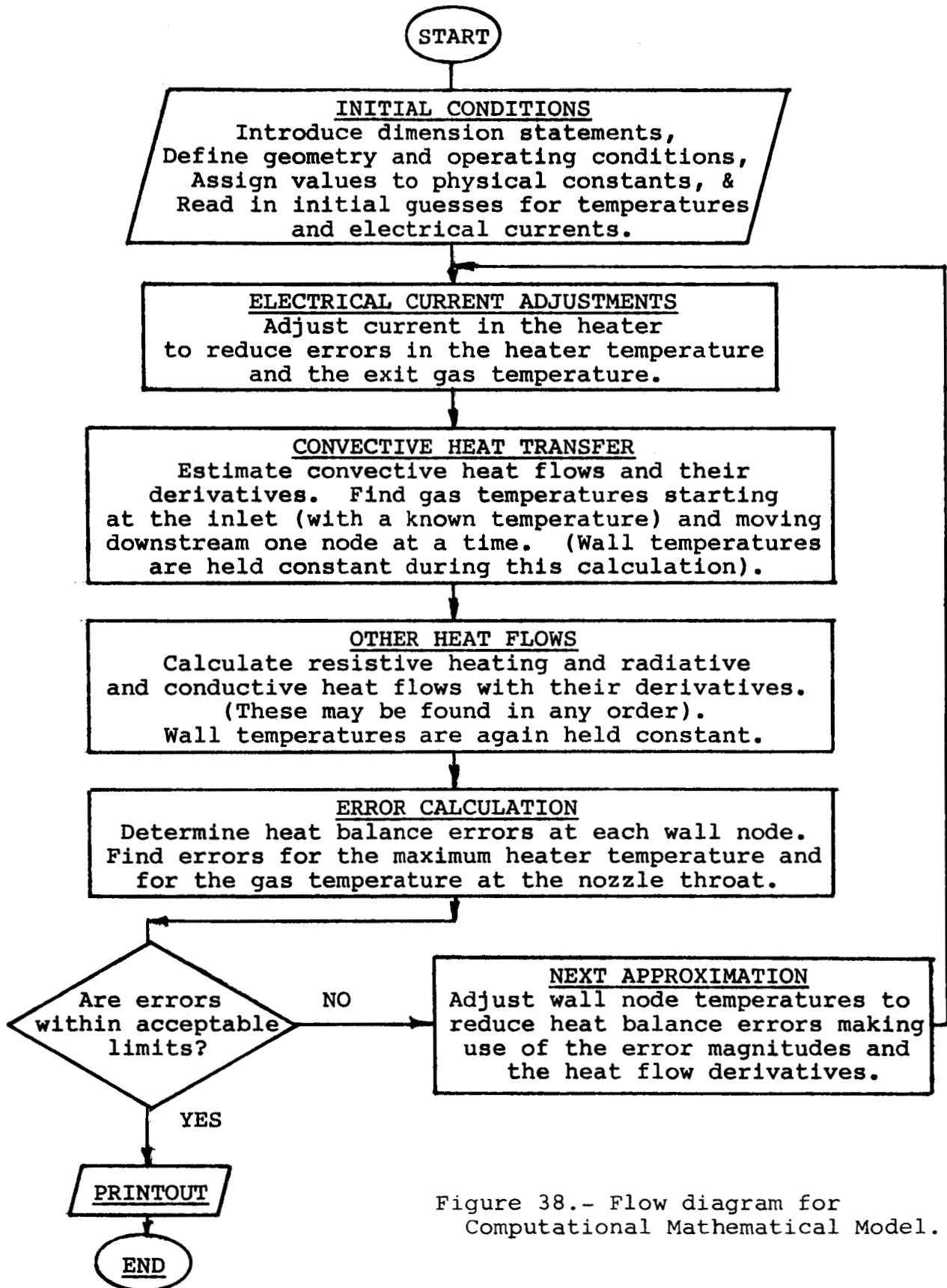


Figure 38.- Flow diagram for Computational Mathematical Model.

Or, rearranging terms:

$$\frac{q}{A(x)} = -k(T) \frac{dT}{dx}$$

For axial conduction $A = A(x)$

$$\text{and } q = \frac{A}{(x_2 - x_1)} \int_{T_2}^{T_1} k(T) dT$$

For radial conduction $A(r) = 2\pi r dx$

$$\text{and } q = \frac{2 dx}{\ln \left(\frac{r_o}{r_i} \right)} \int_{T_2}^{T_1} k(T) dT$$

where,

$$\begin{aligned} r_o &= r_{\text{outer}} \\ r_i &= r_{\text{inner}} \end{aligned}$$

For nodes that are neither axial nor radial, a linear area variation is assumed approximately orthogonal to flow path.

Thus, $A(L) = aL$

$$\text{and } q = \frac{a}{\ln(L_2/L_1)} \int_{T_2}^{T_1} k(T) dt$$

To simplify the problem, when adjacent nodes are not of the same material, a heat flow resistance approach is used.

$$\text{In the program, } q_1 = \frac{2(T_2 - T_1)}{(R_1 + R_2)}$$

Where $R_{ax} = dx / (Ak(T))$

$R_{rad} = \ln(r_o/r_i) / (2\pi x k(T))$

and $R_{len} = \ln(L_2/L_1) / (ak(T))$

Convection

The equation used for tubes is:

$$q = (ANuk / D_h) (T_w - T_m)$$

Where D_h = hydraulic diameter = $4(\text{flow area}/\text{flow perimeter})$

The approach for annual passages is described in Kays (Ref. 29).

$$\text{Where } q_i = \frac{A_i}{D_h(1-\theta_i, \theta_o)} (K_i Nu_{i,i} (T_i - T_m) + \theta_i K_o Nu_{o,o} (T_o - T_m))$$

$$q_o = \frac{A_o}{D_h(1-\theta_i, \theta_o)} (\theta_o k_i Nu_{i,i} (T_i - T_m) + k_o Nu_{o,o} (T_o - T_m))$$

In the nozzle high velocity region, the approach used is described in Eckert and Drake. The equation used is:

$$q = (ANuk / D_h) (T_w - T_{aw})$$

where k and Nu are determined for the reference temperature

$$T^* = T_m + .5(T_w - T_m) + .22(T_{aw} - T_m)$$

where $T_o = T_m (1 + \frac{\gamma-1}{2} M_m^2)$ = stagnation temperature

$$T_{aw} = T_m (1+r \frac{\gamma-1}{2} M_m^2) = \text{adiabatic wall temperature}$$

and the recovery factor $r = Pr^{1/2}$ for laminar flow and $r = Pr^{1/3}$ for turbulent flow. M_m = the mach number input to the program as a constant for each node in the nozzle which is calculated as a function of gamma (γ) and the ratio of cross-sectional area to throat area.

Radiation

Given two surfaces, the equation used is

$$q_1 = \frac{A_1 (e_{b2} - e_{b1})}{\frac{1}{\epsilon_1} + \left[\frac{1}{F_{12}} - 1 \right] + \frac{A_1}{A_2} \left[\frac{1}{\epsilon_2} - 1 \right]}$$

where $e_{b2} = \sigma T_2^4$

Usually $F_{12} = 1$ and this equation reduces to Christianson's equation. For radiation to ambient $A_2 \rightarrow \infty$ and the equation becomes

$$q_1 = A_1 \epsilon_1 (e_{b2} - e_{b1}) \quad \text{where } e_{b2} = \sigma T_{amb}^4$$

For more than two surfaces simultaneous equations are used to solve for the heat transfer.

For each node, adapting the terminology of Eckert and Drake (Ref. 34).

$$Q = q/A \quad \text{heat transfer per area per time}$$

$$e_b = \sigma T^4 \quad \text{the emissive power, net radiation per area per time}$$

time

$$M = \text{net heat flux arriving at node}$$

$$B = \text{net heat flux leaving the node}$$

$$e_m = (B/e_b) \quad \text{the apparent emissivity}$$

$$\epsilon M = \quad \text{the absorbed part of } M$$

$$\text{Then, } Q_i = \epsilon_i M_i - \epsilon_i e_{b1}$$

$$\text{where } M_i = \frac{1}{A_i} \sum_{k=1}^N (A_k F_{ki} \epsilon_m e_{bk})$$

$$\text{or } M_i = \sum_{k=1}^N (F_{ik} \epsilon_{mk} e_{bk})$$

Thus, for each node i

$$Q_i = -\epsilon_i e_{b1} + \epsilon_i \sum_{k=1}^N (F_{ik} \epsilon_{mk} e_{bk})$$

This set of equations can be solved for the ϵ_m 's and by substituting into the equation q_i can be found. Or, when $\epsilon_i \ll 1$, the equation can be reduced to

$$Q_i = \frac{\epsilon_i}{1 - \epsilon_i} e_{b1} (e_{m1} - 1)$$

APPENDIX I

THERMOPHYSICAL PROPERTIES USED IN MATHEMATICAL MODELING PROGRAMS

The material properties used are based primarily upon recommended values selected in reference 13 and data sheets of key material suppliers.

The bases for the appropriate propellant properties are presented in the main body of the report. Polynomial representations to the necessary degrees were generated to match these data within 1% for use in the study. The values presented in the tables below were generated primarily by the polynomials used.

List of Tables

Table Number

- | | |
|----|---|
| 36 | Propellants a) Steam b) Carbon dioxide c) Decomposed hydrazine |
| 37 | Heaters, Pressure Vessels and Structures a) Platinum b) Zirconia c) Rhenium d) Stainless steel e) Nickel |
| 38 | Electric Insulation a) Alumina |
| 39 | Thermal Insulations a) Min-K 2000 b) Fibrous zirconia |

TABLE 36
EXPELLANT PHYSICAL PROPERTIES

a) Steam

| Temperature °K | Specific heat, Cp $\frac{\text{cal}}{\text{g}^\circ\text{K}}$ | Viscosity $\times 10^4$ poise | Thermal conduct- ivity $\times 10^4$ $\frac{\text{cal}}{\text{s cm}^\circ\text{K}}$ | Molecular weight g mole |
|-------------------|---|-------------------------------------|--|-------------------------------|
| 300 | .4453 | 1.096 | 0.699 | 18.016 |
| 400 | .4541 | 1.432 | 0.930 | 18.016 |
| 500 | .4669 | 1.786 | 1.190 | 18.016 |
| 600 | .4815 | 2.149 | 1.473 | 18.016 |
| 700 | .4969 | 2.515 | 1.775 | 18.016 |
| 800 | .5132 | 2.879 | 2.094 | 18.016 |
| 900 | .5300 | 3.235 | 2.425 | 18.016 |
| 1000 | .5471 | 3.587 | 2.768 | 18.016 |
| 1100 | .5637 | 3.932 | 3.122 | 18.016 |
| 1200 | .5800 | 4.267 | 3.481 | 18.016 |
| 1300 | .5957 | 4.593 | 3.841 | 18.016 |
| 1400 | .6104 | 4.910 | 4.201 | 18.014 |
| 1500 | .6242 | 5.217 | 4.560 | 18.015 |
| 1600 | .6372 | 5.516 | 4.915 | 18.012 |
| 1800 | .6600 | 6.090 | 5.617 | 18.002 |
| 2000 | .6795 | 6.638 | 6.304 | 17.972 |
| 2200 | .6962 | 7.160 | 6.987 | 17.899 |
| 2400 | .7105 | 7.659 | 7.683 | 17.747 |
| 2600 | .7229 | 8.132 | 8.417 | 17.465 |

b) Carbon dioxide

| | | | | |
|------|-------|-------|-------|--------|
| 300 | .2012 | 1.520 | 0.435 | 44.011 |
| 400 | .2234 | 1.960 | 0.618 | 44.011 |
| 500 | .2412 | 2.354 | 0.798 | 44.011 |
| 600 | .2558 | 2.714 | 0.973 | 44.011 |
| 700 | .2679 | 3.048 | 1.140 | 44.011 |
| 800 | .2781 | 3.359 | 1.302 | 44.011 |
| 900 | .2866 | 3.653 | 1.457 | 44.011 |
| 1000 | .2937 | 3.931 | 1.605 | 44.011 |
| 1100 | .2997 | 4.197 | 1.747 | 44.011 |
| 1200 | .3048 | 4.454 | 1.884 | 44.011 |
| 1300 | .3092 | 4.702 | 2.016 | 44.011 |
| 1400 | .3129 | 4.942 | 2.143 | 44.009 |
| 1500 | .3160 | 5.176 | 2.265 | 44.007 |
| 1600 | .3188 | 5.402 | 2.385 | 43.998 |
| 1800 | .3232 | 5.839 | 2.611 | 43.945 |
| 2000 | .3265 | 6.258 | 2.826 | 43.784 |
| 2200 | .3287 | 6.666 | 3.032 | 43.392 |
| 2400 | .3300 | 7.076 | 3.233 | 42.618 |
| 2600 | .3302 | 7.498 | 3.431 | 41.322 |

TABLE 36 (Concluded)

c) Dissociated hydrazine

| Temperature °K | Specific heat, Cp $\frac{\text{cal}}{\text{g}^\circ\text{K}}$ | Viscosity $\times 10^4$ poise | Thermal conduct- ivity $\times 10^4$ $\frac{\text{cal}}{\text{s cm}^\circ\text{K}}$ | Molecular weight g mole |
|-------------------|---|-------------------------------------|--|-------------------------------|
| 300 | .6486 | 1.60 | 2.45 | 10.684 |
| 400 | .6514 | 1.95 | 3.00 | 10.684 |
| 500 | .6558 | 2.27 | 3.50 | 10.684 |
| 600 | .6616 | 2.57 | 3.98 | 10.684 |
| 700 | .6686 | 2.84 | 4.43 | 10.684 |
| 800 | .6764 | 3.10 | 4.88 | 10.684 |
| 900 | .6850 | 3.34 | 5.31 | 10.684 |
| 1000 | .6939 | 3.58 | 5.75 | 10.684 |
| 1100 | .7032 | 3.80 | 6.19 | 10.684 |
| 1200 | .7126 | 4.02 | 6.64 | 10.684 |
| 1300 | .7220 | 4.24 | 7.08 | 10.684 |
| 1400 | .7312 | 4.45 | 7.53 | 10.684 |
| 1500 | .7401 | 4.65 | 7.98 | 10.684 |
| 1600 | .7486 | 4.86 | 8.44 | 10.684 |
| 1700 | .7567 | 5.05 | 8.88 | 10.683 |
| 1800 | .7643 | 5.25 | 9.32 | 10.683 |
| 1900 | .7714 | 5.43 | 9.76 | 10.683 |
| 2000 | .7779 | 5.62 | 10.18 | 10.680 |
| 2100 | .7839 | 5.80 | 10.60 | 10.676 |
| 2200 | .7895 | 5.97 | 11.00 | 10.670 |
| 2300 | .7945 | 6.14 | 11.39 | 10.660 |
| 2400 | .7993 | 6.31 | 11.78 | 10.644 |
| 2500 | .8037 | 6.48 | 12.17 | 10.622 |
| 2600 | .8081 | 6.64 | 12.56 | 10.590 |

TABLE 37
THERMOPHYSICAL PROPERTIES OF HEATERS,
PRESSURE VESSELS AND STRUCTURES

a) Platinum

| Temperature °K | Specific heat, C _p $\frac{\text{cal}}{\text{g}^\circ\text{K}}$ | Thermal conduct ivity $\frac{\text{cal}}{\text{s cm}^\circ\text{K}}$ | Total hemi- spherical emittance | Electric resist- ivity $\mu\Omega\text{-cm}$ | Linear thermal expansion % |
|-------------------|---|---|--|---|-------------------------------------|
| 300 | .0317 | .1662 | .1154 | 10.56 | 0.000 |
| 400 | .0324 | .1707 | .1230 | 13.71 | 0.096 |
| 500 | .0330 | .1735 | .1306 | 16.86 | 0.189 |
| 600 | .0336 | .1754 | .1382 | 20.01 | 0.288 |
| 700 | .0343 | .1768 | .1459 | 23.16 | 0.388 |
| 800 | .0349 | .1779 | .1535 | 26.31 | 0.490 |
| 900 | .0356 | .1788 | .1611 | 29.46 | 0.593 |
| 1000 | .0362 | .1794 | .1687 | 32.61 | 0.699 |
| 1100 | .0369 | .1803 | .1764 | 35.71 | 0.810 |
| 1200 | .0375 | .1815 | .1840 | 38.69 | 0.920 |
| 1300 | .0381 | .1830 | .1916 | 41.56 | 1.039 |
| 1400 | .0388 | .1848 | .1992 | 44.32 | 1.157 |
| 1500 | .0394 | .1869 | .2069 | 46.97 | 1.286 |
| 1600 | .0401 | .1891 | .2145 | 49.50 | 1.414 |
| 1700 | .0407 | .1916 | .2221 | 51.93 | 1.552 |
| 1800 | .0414 | .1942 | .2297 | 54.24 | 1.690 |
| 1900 | .0420 | .1970 | .2374 | 56.44 | 1.837 |

b) Cubic phase stabilized zirconia

| | | | | | |
|------|-------|--------|-------|-----------------------|------|
| 300 | .1139 | .00425 | .7892 | 1.55×10^{12} | .00 |
| 400 | .1240 | .00426 | .7200 | 879.3×10^7 | .09 |
| 500 | .1323 | .00428 | .6569 | 140.6 | .18 |
| 600 | .1391 | .00430 | .5999 | 22.23 | .27 |
| 700 | .1444 | .00432 | .5492 | 4.39 | .38 |
| 800 | .1485 | .00435 | .5050 | 1.10 | .49 |
| 900 | .1514 | .00438 | .4672 | 340×10^6 | .60 |
| 1000 | .1533 | .00441 | .4361 | 125 | .73 |
| 1100 | .1544 | .00445 | .4117 | 52.7 | .85 |
| 1200 | .1550 | .00449 | .3942 | 25.0 | .99 |
| 1300 | .1556 | .00455 | .3836 | 13.2 | 1.13 |
| 1400 | .1561 | .00462 | .3800 | 7.63 | 1.27 |
| 1500 | .1567 | .00469 | .3846 | 4.75 | 1.42 |
| 1600 | .1572 | .00478 | .4078 | 3.13 | 1.57 |
| 1700 | .1578 | .00487 | .4578 | 2.17 | 1.73 |
| 1800 | .1584 | .00497 | .5350 | 1.57 | 1.90 |
| 1900 | .1589 | .00509 | .6322 | 1.17 | 2.06 |
| 2000 | .1595 | .00521 | .7344 | 900×10^3 | 2.23 |
| 2100 | .1600 | .00534 | .8189 | 710 | 2.41 |

TABLE 37 (Continued)

c) Rhenium (Specific gravity 21.04)

| Temperature °K | Specific heat, $\frac{\text{cal}}{\text{g}\cdot\text{K}}$ | Thermal conduct ivity $\frac{\text{cal}}{\text{s cm}\cdot\text{K}}$ | Total hemi- spherical emittance | Electric resist- ivity $\mu\Omega\text{-cm}$ | Linear thermal expansion % |
|-------------------|--|--|--|---|-------------------------------------|
| 300 | .0326 | .1149 | .1332 | 19.86 | 0.000 |
| 400 | .0333 | .1106 | .1338 | 27.80 | 0.067 |
| 500 | .0340 | .1076 | .1362 | 35.15 | 0.130 |
| 600 | .0347 | .1058 | .1403 | 41.96 | 0.194 |
| 700 | .0353 | .1049 | .1460 | 48.27 | 0.259 |
| 800 | .0360 | .1048 | .1530 | 54.13 | 0.325 |
| 900 | .0366 | .1053 | .1613 | 59.57 | 0.392 |
| 1000 | .0371 | .1063 | .1705 | 64.61 | 0.460 |
| 1100 | .0376 | .1076 | .1807 | 69.30 | 0.530 |
| 1200 | .0380 | .1091 | .1917 | 73.66 | 0.599 |
| 1300 | .0383 | .1108 | .2031 | 77.71 | 0.672 |
| 1400 | .0387 | .1126 | .2151 | 81.49 | 0.744 |
| 1500 | .0390 | .1144 | .2272 | 85.00 | 0.820 |
| 1600 | .0393 | .1162 | .2395 | 88.26 | 0.896 |
| 1700 | .0396 | .1181 | .2516 | 91.30 | 0.975 |
| 1800 | .0399 | .1199 | .2636 | 94.12 | 1.053 |
| 1900 | .0403 | .1218 | .2752 | 96.72 | 1.135 |
| 2000 | .0408 | .1237 | .2862 | 99.13 | 1.216 |
| 2100 | .0414 | .1258 | .2965 | 101.33 | 1.301 |
| 2200 | .0421 | .1281 | .3059 | 103.34 | 1.386 |
| 2300 | .0430 | .1308 | .3143 | 105.14 | 1.475 |
| 2400 | .0442 | .1339 | .3216 | 106.74 | 1.563 |
| 2600 | .0474 | .1420 | .3318 | 109.29 | 1.748 |
| 2800 | .0521 | .1485 | .3354 | 110.89 | 1.941 |

d) Stainless steel (AISI 304L) (Specific gravity 7.81)

| | | | | | |
|------|------|-------|-----|-------|-------|
| 300 | .090 | .0317 | .55 | 55.32 | .000 |
| 400 | .091 | .0355 | .62 | 65.89 | .166 |
| 500 | .092 | .0399 | .66 | 73.36 | .336 |
| 600 | .094 | .0447 | .68 | 78.48 | .517 |
| 700 | .095 | .0500 | .70 | 81.92 | .708 |
| 800 | .098 | .0556 | .71 | 84.20 | .907 |
| 900 | .104 | .0614 | .73 | 85.71 | 1.112 |
| 1000 | .109 | .0675 | .74 | 86.75 | 1.322 |
| 1100 | .110 | .0736 | .75 | 87.51 | 1.535 |
| 1200 | .110 | .0797 | .76 | 88.14 | 1.749 |
| 1300 | .110 | .0857 | .77 | 88.77 | 1.962 |
| 1400 | .110 | .0916 | .78 | 89.46 | 2.171 |

TABLE 37 (Concluded)

e) Nickel (Specific Gravity = 8.9)

| Temperature °K | Specific heat, C_p $\frac{\text{cal}}{\text{g}^\circ\text{K}}$ | Thermal conduct ivity $\frac{\text{cal}}{\text{s cm}^\circ\text{K}}$ | Total hemi- spherical emittance | Electric resist- ivity $\mu\Omega\text{-cm}$ | Linear thermal expansion % |
|-------------------|--|---|--|---|-------------------------------------|
| 300 | .1067 | .216 | .0243 | 12.54 | 0.000 |
| 400 | .1140 | .196 | .0375 | 16.72 | 0.150 |
| 500 | .1258 | .172 | .0560 | 20.90 | 0.299 |
| 600 | .1408 | .156 | .0772 | 25.08 | 0.455 |
| 700 | .1248 | .156 | .0992 | 29.26 | 0.617 |
| 800 | .127 | .161 | .1206 | 33.44 | 0.783 |
| 900 | .129 | .166 | .1408 | 37.62 | 0.953 |
| 1000 | .131 | .172 | .1598 | 41.80 | 1.126 |
| 1100 | .134 | .176 | .1781 | 45.98 | 1.302 |
| 1200 | .138 | .182 | .1972 | 50.16 | 1.483 |
| 1300 | .142 | .187 | .2188 | 54.34 | 1.669 |
| 1400 | .146 | .192 | .2456 | 58.52 | 1.861 |
| 1500 | .156 | .197 | .2808 | 62.70 | 2.060 |

TABLE 38
PROPERTIES OF ELECTRIC INSULATION USED

Alumina (Specific gravity = 3.7)

| | | | | | |
|------|-------|-------|-------|-----------------|-------|
| 300 | .1871 | .0779 | .7896 | - | 0.000 |
| 400 | .2237 | .0629 | .7508 | - | 0.075 |
| 500 | .2487 | .0503 | .7122 | 10^{14} | 0.148 |
| 600 | .2650 | .0394 | .6739 | - | 0.225 |
| 700 | .2754 | .0309 | .6358 | - | 0.305 |
| 800 | .2820 | .0247 | .5979 | - | 0.388 |
| 900 | .2865 | .0204 | .5602 | - | 0.476 |
| 1000 | .2902 | .0176 | .5228 | 5×10^8 | 0.565 |
| 1100 | .2941 | .0158 | .4871 | - | 0.658 |
| 1200 | .2984 | .0147 | .4545 | 4×10^7 | 0.754 |
| 1300 | .3032 | .0141 | .4262 | - | 0.852 |
| 1400 | .3080 | .0138 | .4030 | - | 0.952 |
| 1500 | .3118 | .0137 | .3854 | 10^7 | 1.054 |
| 1600 | .3134 | .0138 | .3735 | - | 1.158 |
| 1700 | .3109 | .0141 | .3668 | - | 1.263 |
| 1800 | .3021 | .0147 | .3647 | - | 1.370 |
| 1900 | .2843 | .0158 | .3659 | - | 1.480 |
| 2000 | .2544 | .0178 | .3688 | - | 1.480 |
| 2100 | .2087 | .0210 | .3715 | - | - |
| 2200 | .1434 | .0258 | .3715 | - | - |
| 2300 | .0539 | .0328 | .3661 | - | - |

TABLE 39
 PROPERTIES OF THERMAL INSULATIONS USED

a) Min-K 2000 ^(*) (Specific gravity = .32)

| Temperature °K | Specific heat, C_p $\frac{\text{cal}}{\text{g } ^\circ\text{K}}$ | Thermal conduct- ivity $\times 10^4$ $\frac{\text{cal}}{\text{s cm } ^\circ\text{K}}$ |
|-------------------|--|--|
| 300 | .1760 | .33 |
| 400 | .2007 | .34 |
| 500 | .2199 | .37 |
| 600 | .2347 | .42 |
| 700 | .2459 | .50 |
| 800 | .2545 | .61 |
| 900 | .2612 | .74 |
| 1000 | .2671 | .90 |
| 1100 | .2728 | .09 |

^(*) T.M. Johns-Mansville, NY, NY.

b) Zircar ^(*) (Specific gravity = .48)

| | | |
|------|-------|-----|
| 300 | .1139 | .47 |
| 400 | .1240 | .53 |
| 500 | .1323 | .61 |
| 600 | .1391 | .71 |
| 700 | .1441 | .81 |
| 800 | .1485 | .91 |
| 900 | .1514 | .02 |
| 1000 | .1533 | .13 |
| 1100 | .1544 | .24 |
| 1200 | .1550 | .35 |
| 1300 | .1556 | .46 |
| 1400 | .1561 | .57 |
| 1500 | .1567 | .68 |
| 1600 | .1572 | .78 |
| 1700 | .1578 | .89 |
| 1800 | .1584 | .98 |
| 1900 | .1589 | .12 |
| 2000 | .1595 | .49 |
| 2100 | .1600 | .86 |

^(*) T.M. Zircar, Florida, NY.

REFERENCES

1. Jack, J.R.: Theoretical Performance of Propellants Suitable for Electrothermal Jet Engines. ARS J., Vol 31, 1961, pp 1685 - 1689.
2. Howard, J.M.: The Resistojet. ARS J., Vol 32, 1962, pp 961-962.
3. Page, R.J.; Halbach, C.R.; and Short, R.A.: 3 kW Concentric Tubular Resistojet Performance. J. Spacecraft, Vol. 3, No. 11, Nov. 1966, pp. 1669-1674.
4. Page, R.J.; and Short, R.A.: Definition of a Resistojet Control System for the Manned Orbital Research Laboratory. Vol. V Resistojet Design and Development. Final Report prepared under Contract NAS1-6702 by the Marquardt Corporation, VanNuys, CA, May 1968.
5. Yoshida, R.Y.; Halbach, C.R.; Page, R.J.; Short, R.A.; and Hill, C.S.: Resistojet Thruster Life Tests and High Vacuum Performance. NASA CR-66970, 1970.
6. Pisciotta, A., Jr.; and Eusanio, E.N.: Definition of a Resistojet Control System for the Manned Orbital Research Laboratory. Final Report. Vol 1 Summary. NASA CR-66600, May 1968.
7. Pisciotta, A., Jr.; and Eusanio, E.N.: Definition of a Resistojet Control System for the Manned Orbital Research Laboratory. Final Report - Vol. 2 Resistojet Control System Analysis. Appendix, by Halbach, C.R., - Optimized Resistojet Performance Predictions. NASA CR-66601.
8. Smith, J.M.; and VanNess, H.C.: Introduction to Chemical Engineering Thermodynamics, Third Edition, McGraw-Hill Book Co., 1975, pp. 424-428.
9. Stull, D.R.; and Prophet, H.: Program Director, JANAF Thermochemical Tables, Second Edition, 1971.
10. Svehla, Roger: Estimated Viscosities and Thermal Conductivities of Gases at High Temperatures. NASA Technical Report R-132, 1963.
11. Fishender, M.; and Saunders, O.A.: Introduction to Heat Transfer, Oxford University Press, 1950.

PRECEDING PAGE BLANK NOT FILMED

PRECEDING PAGE BLANK NOT FILMED

12. Brokaw, R.S.: Alignment Charts for Transport Properties, Viscosity, Thermal Conductivity and Diffusion Coefficients for Nonpolar Gases and Gas Mixtures at Low Density. NASA Technical Report R-81, 1981.
13. Page, R.J.; Halbach, C.R.; McCaughey, O.J.; and Short, R.A.: Investigation of Biowaste Resistojets for Space Station Application. NASA CR-112159, July 1972.
14. Phillips, D.G.: Technology Development of a Biowaste Resistojet, Vols I and II. NASA CR-112149 and CR-112150, June 1972.
15. Albert, H.J.; and Hill, J.S.: Development of a Platinum-Thorium Oxide Alloy for Resistojet Thruster Use. NASA CR-111959, 1971.
16. Selman, G.L.; Day, J.G.; and Bourne, A.A.: Dispersion Strengthened Platinum Properties and Characteristics of a New High Temperature Material. Research Laboratories, Johnson Matthey & Co., Limited, Westchester, PA. 1984.
17. Halbach, C.R.; Ozawa, T.; Page, R.J.; Stoner, W.A.; and Todd, J.P.: Design and Prototype Development of a High Temperature Materials Processing Facility for Sounding Rockets. NAS8-31512, June, 1978.
18. Herbell, Thomas P.; Weeton, John W.; and Quantinetz, Max: Structure and Properties of Tungsten-Base Powder Metallurgy Composites. NASA TN D-3610, 1966.
19. King, George W: An Investigation of the Yield Strength of a Dispersion Hardened W-3.8 Vol % ThO₂ Alloy. Trans. AIME. Vol. 245. January 1969, pp.83-89.
20. Conway, J.B.; and Flagella, P.N.: Creep-Rupture Data for the Refractory Metals to High Temperatures. Gordon and Breach Science Publishers, New York, NY. 1971.
21. Barr, F.A.; and Page, R.J.: Slip Casting and Extruding Shapes of Rhenium with Metal Oxide Additives. Part 1 - Feasibility Demonstration. NASA CR-174970, 1985.
22. Touloukian, Y.S., et al: Thermophysical Properties of Matter, Thermophysical Properties Research Center (TPRC). Purdue University, Lafayette, Indiana. In 13 Volumes. IFI/Plenum. New York, beginning 1970-1976
23. Dushman, S.: Scientific Foundations of Vacuum Technique. John Wiley & Sons, Inc., New York, 1962.

24. Hoch, M.; Nakata, M.; and Johnston, H.L.: Vapor Pressures of Inorganic Substances XII. Zirconium Dioxide. J. Am. Chem. Soc. 76 2651, 1954.
25. Zima, G.E.: Vaporization of Advanced Powerplant Metals Under Vacuum and Forced Convection Conditions. Lawrence Radiation Laboratory, University of California, Publication No. UCRL-14274, 1965.
26. Phillips, W.L.: Oxidation of the Platinum Metals in Air. Trans Am. Soc. Metals, Vol 57, 1964, pp 33-37.
27. Stanley, R.G.; and Wilson, F.G.: ODS Platinum - a Unique High Temperature Material for the Most Demanding Applications. Metal Power Report, Englehard Minerals, Vol. 37, No. 4, April 1982.
28. Bussard, R.W.; and Delauer, R.D.: Fundamentals of Nuclear Flight. McGraw-Hill Book Company, 1965, pp. 142-148.
29. Kays, William, M.; and London, A.L.: Compact Heat Exchangers. Third Ed., McGraw-Hill Book Co., Inc. 1980.
30. Hoerner, Dr.-Ing.S.F.: Fluid Dynamic Drag. Published by the Author, Midland Park, New Jersey. 1965.
31. Bruun, E.R.; and Kingsley, T.C.: Monopropellant Thruster Performance Augmentation Heater Development Program. Final Report AFRPL-TR-80-73. Hamilton Standard., February 1981.
32. ASME Boiler and Pressure Vessel Code. Section VIII Division 1 and 2. ASME 1985.
33. Kilpatrick, M.; and Lott, S.: Reaction of Flowing Steam with Refractory Metals II Rhenium (850° - 1700°C). J Electrochem. Soc. January 1966. pp. 15-16.
34. Eckert, E.R.G.; and Drake, R.M.: Analysis of Heat and Mass Transfer. McGraw-Hill Book Co., 1972.

| | | | | | |
|---|--|--|--|---|-------------------|
| 1. Report No. NASA CR-179510 | | 2. Government Accession No. | | 3. Recipient's Catalog No. | |
| 4. Title and Subtitle A Design Study of Hydrazine and Biowaste Resistojets | | | | 5. Report Date September 1986 | |
| | | | | 6. Performing Organization Code | |
| 7. Author(s) Russell J. Page, Willis A. Stoner and Larry Barker | | | | 8. Performing Organization Report No. None | |
| | | | | 10. Work Unit No. 481-02-02 | |
| 9. Performing Organization Name and Address The R. J. Page Company 18792 Dodge Avenue Santa Ana, CA 92705 | | | | 11. Contract or Grant No. NAS3-23863 | |
| | | | | 13. Type of Report and Period Covered Contractor Report Final | |
| 12. Sponsoring Agency Name and Address National Aeronautics and Space Administration Lewis Research Center Cleveland, Ohio 44135 | | | | 14. Sponsoring Agency Code 506-55-22 | |
| | | | | | |
| 15. Supplementary Notes Project Manager, James S. Sovey, Space Propulsion Technology Division, NASA Lewis Research Center. | | | | | |
| 16. Abstract A generalized modeling program was adapted in BASIC on a personal computer to compare the performance of four types of biowaste resistojets and two types of hydrazine augmenters. Analyzed biowaste design types were: 1) an electrically conductive ceramic heater-exchanger of zirconia; 2) a truss heater of platinum in cross flow; 3) an immersed bicoiled tubular heater-exchanger; and 4) a nonexposed, refractory metal, radiant heater in a central cavity within a heat exchanger case. Concepts 2 and 3 are designed to have an efficient, stainless steel outer pressure case. The hydrazine design types are: 5) an immersed bicoil heater exchanger and 6) a nonexposed radiant heater now with a refractory metal case. The ceramic biowaste resistojet has the highest specific impulse growth potential at 2000°K of 192.5 (CO ₂) and 269 s (H ₂ O). The bicoil produces the highest augmentor temperature of 1994°K for a 2073°K heater giving 317 s at .73 overall efficiency. Detailed temperature profiles of each of the designs are shown. The scaled layout drawings of each are presented with recommended materials and fabrication methods. | | | | | |
| 17. Key Words (Suggested by Author(s)) Biowaste resistojets Hydrazine augmenters | | | 18. Distribution Statement Unclassified - unlimited STAR Category 20 | | |
| 19. Security Classif. (of this report) Unclassified | | 20. Security Classif. (of this page) Unclassified | | 21. No. of pages 149 | 22. Price* A07 |